ASPECTS OF WAVE PROPAGATION IN ANISOTROPIC ELASTIC HALF-SPACES AND PLATES

WENFEI WANG

Submitted in Partial Fulfillment of the Requirements

of the Degree of Doctor of Philosophy in Applied Mathematics,

Keele University,

February 2013

Acknowledgements

I would like to thank my lead supervisor Prof. Graham Rogerson for providing me with scientific and moral support, encouraging me to make progress and being very patient. Also I would like to thank my second supervisor Prof. Yibin Fu for introducing me into the field of solid mechanics, sharing many ideas and giving out advices. The PhD studentship jointly provided by China Scholarship Council and Keele University is very gratefully appreciated. I would like to thank Joe for our interesting talks and my oral English has been improved a lot. Finally I would like to thank my parents for rasing me up and supporting me through hard times in my life.

Abstract

The propagation of waves along elastic half-spaces and plates has long been an active research area with lots of applications in seismology and modern industries. Much attention has been paid to the study of wave propagation in a linear isotropic solid with traction-free or fixed boundary conditions. However, much more investigation is deserved for anisotropic solids under other type of boundary conditions, or even a solid with a hump on its surface.

The purpose of the thesis is to investigate the influence of the elastic property and profile of propagation media and boundary conditions on wave speeds, and predict the wave speed in various situations. Chapter 1 is devoted to introducing the governing equations and several specific materials used as examples in subsequent analysis. Chapter 2 is concerned with the propagation of free surface waves on an elastic half-space that has a localized geometric inhomogeneity perpendicular to the direction of wave propagation (such waves are known as topography-guided surface waves). We use the Stroh formalism to examine how such hump modifies the surface wave speed slightly on an anisotropic elastic half-space. In Chapter 3, an asymptotic model

is constructed to predict the speed of waves propagating along a thin elastic plate with elastically restrained boundary conditions (ERBC). The Stroh formalism is again applied to deal with general anisotropy, which can be specified later to analyze the case of linear isotropy and the transverse isotropy. Chapter 4 deals again with the case of a thin plate with ERBC as in the previous chapter, but the effects of pre-stress and the condition of incompressibility are also considered.

Keywords: Trapped modes; guided waves; anisotropic; Stroh formalism; surface waves; elastic half-space; thin plate; elastically restrained boundary conditions; pre-stress.

Contents

List of Figures

Introduction

Surface waves

A surface wave is a wave propagating along a free surface, for which the associated displacement and traction decay away from the surface. Surface waves were first investigated within the context of seismology, but have more recently found application in signal processing, non-destructive testing (NDT) and many high-tech devices.

Within seismology, a seismic wave travels through the Earth, often as the result of an earthquake or explosion. When seismic waves are generated at or near the surface of the Earth, both body (P and S) and surface (e.g. Rayleigh, Love) waves are generated. Body waves propagate through the whole solid body of the Earth, whereas surface waves only propagate along (or near) the surface of the Earth. Love waves have transverse motion (movement perpendicular to the direction of travel), whereas Rayleigh waves have both longitudinal (movement parallel to the direction of travel) and transverse motions. The velocity of the Rayleigh wave is strictly smaller

than the speed of either body wave. For isotropic materials the P - wave always has a larger speed than the S - wave and this is the first arrival detected for earthquakes. The existence of real body wave speeds is guaranteed by the strong convexity condition and strong ellipticity condition, as demonstrated in Chapter 1. Seismic surface waves span a wide frequency range, and the period of waves that are most damaging is usually 10 seconds or longer. Seismic surface waves can travel around the globe many times during the largest earthquakes.

In signal processing, a surface acoustic wave (SAW) can be generated by SAW devices, which are composed of two transducers with interdigital transducers (IDT) of thin metal electrodes placed on a piezoelectric substrate, such as quartz or lithium tantalite. One of these acts as the device input and converts signal voltage variations into mechanical surface acoustic waves. The other IDT acts as an output receiver to convert mechanical SAW vibrations back into output voltages.

SAW devices have been used previously as sensors for temperature, pressure (in intelligent tyres), force, electric voltage, humidity and gases. Most of these devices are based on detecting the change in the phase velocity of the SAW caused by the fluctuations of the above factors. They have also been used in gyroscopes to stabilize vehicles and camcorders. SAW convolvers find their application in indoor/outdoor spread-spectrum wireless for packet-data and packet-voice communications. They are also well suited to combat multi-path interference due to spurious reflections in indoor environments.

In many non-destructive evaluation (NDE) problems, people use Rayleigh surface waves

in the ultrasonic frequency range to help detect cracks and other material imperfections. The advantages of using Rayleigh waves for non-destructive testing, over other types of wave, are considered to be their high sensitivity to surface flaws and their longer propagation distance.

Literature review on the surface wave problem

Lord Rayleigh (1885) was the first to show that the plane traction-free surface of an elastic isotropic half-space could support a surface wave, for which displacement and traction decay exponentially, for harmonic time dependence, with depth below the surface. Synge (1956) studied the case for elastic waves in anisotropic media, but concluded incorrectly that surface waves could only propagate in some exceptional directions. The main problem in the linear theory of surface waves lies in existence and uniqueness, namely whether a half-space can support a surface wave and, if it does, whether the surface-wave solution is unique. With the help of the Stroh formalism (Stroh 1958,1962), Barnett *et al*. (1973) firstly proved uniqueness; Barnett and Lothe (1974) provided a first existence proof, and Lothe and Barnett (1976) provided an alternative existence proof. These results were later polished and presented in terms of the surface impedance matrix in their later paper (Barnett and Lothe, 1985). The review article by Chadwick and Smith (1977) and the book by Ting (1996) give detailed descriptions of the subject. A discussion on a new identity satisfied by the surface impedance matrix is given by Fu and Mielke (2002), and with the use of this identity, Mielke and Fu (2003) gave a more direct proof of uniqueness that

is independent of the Stroh Formalism.

Other related localization phenomena have also recently been investigated. Zernov *et al.* (2006) studied the problem of elastic waves trapped at the edges of a semi-infinite strip to provide a semi-analytical proof for the existence of edge resonance. Gridin *et al.* (2005 a,b) and Kaplunov *et al.* (2005) studied trapped elastic waves in elastic plates, shells and rods. They showed that modes can be trapped in regions of either high local curvature or thickness variation. Burridge and Sabina (1972 a,b), using the finite element method, considered three kinds of ridge-like defects on the surface: a tall square plate, a tall rectangular plate, and a dovetail plate. Numerical simulations indicate that a wave seems to be trapped within the plate on the surface, propagate along it and is unattenuated in the direction of propagation. Bonnet-Ben Dhia *et al.* (1999) and Duterte and Joly (1999) proved the existence of the topographically trapped Rayleigh waves in an isotropic homogeneous elastic half-space.

Guided waves are traveling waves whose transverse energy is concentrated essentially in the disturbed zone of the half-space. Much research has been carried out concerning the guiding of surface waves by topography, curved surface or material inhomogeneities in isotropic materials. However there is very little work on such problems associated with generally anisotropic elastic materials. The problem that we consider in Chapter 2 is that of guided waves in a generally anisotropic elastic half-space whose free surface is not flat, but has a localized hump in the direction transverse to that of wave propagation. The traction-free surface condition is applied on the entire humped surface. Our objective is to develop an asymptotic method to capture this

trapping effect, not for plates of high aspect ratio attached to a semi-infinite half-space, but for smooth perturbations to the semi-infinite half-space, and then to present a convenient way to calculate the perturbed wave speed. The work outlined in Chapter 2 formed the basis of a recent publication, see Fu *et al.* (2012).

A surface wave solution is very closely related to a trapped mode, in the sense that propagation energy is confined to within a few wavelengths of the free surface. At the same time as the extension of Rayleigh's classical surface wave solution was made to anisotropic elastic and/or viscoelastic materials, much interest was also shown in trapped modes around thin rectangular plates, wedges, or similar structures attached to a half-space. There are two important limits corresponding to this geometrical set-up. When the rectangular plates are thin and long, the trapped modes are expected to be localized near the free edge and the associated modes are also known as edge waves. Edge wave propagation forms an important branch of applied mathematics and was seemingly first studied by Konenkov (1960). When the extrusions are flat and small, we expect the trapped modes to be the classical surface wave mode slightly modified by the geometrical inhomogeneity. It is the latter scenario that we are studying in this thesis.

Topography guided surface waves

In Chapter 2 we investigate topography guided surface waves. This work is partly motivated by the recent series of studies by Kaplunov *et al.* (2005), Gridin *et al.* (2005a, b), Adams *et al.*

(2007), Postnova and Craster (2007, 2008), in which a multiple-scale approach was fruitfully used to study trapped modes in a variety of problems, but with attention invariably focussed on isotropic materials. We however demonstrate that the same methodology, coupled with the Stroh formalism, can be used to extend these studies to their anisotropic counterparts.

In Chapter 2, after formulating our problem of surface wave propagation, we present and solve the leading-order and second-order problems in the subsequent two sections, respectively. In Section 2.4, we write down the third-order problem and obtain the amplitude equation by imposing a solvability condition. After demonstrating in Section 2.5 that our formulation can recover the isotropic results of Adams *et al.* (2007), we solve our amplitude equation in Section 2.6 numerically. Illustrative examples are given which demonstrate a rich variety of behaviour associated with anisotropy: we may have zero, a single or multiple topography-guided solutions, and the associated speed may be higher or lower than the speed corresponding to that of a flat surface.

In carrying out our research we have extended Adams *et al.* 's (2007) research to anisotropic materials using Stroh formalism. Inspired by Song and Fu (2007) and Adams *et al.* (2007), we introduce an infinitesimal quantity ε within the equations of motion and boundary conditions and establish problems at the first three orders. The amplitude equation is derived, and we confirm that our equation is equivalent to that of Adams *et al.* (2007) when specialised to the isotropic case. We establish that for anisotropic materials the amplitude equation is in the form of a Schrödinger equation, thus with the help of previous research the value of the asso-

ciated eigenvalue is analytically given. Additionally, the existence, the number and sign of the eigenvalues can be deduced, again extending the work of Adams *et al.* (2007). We are able to draw the same conclusion as Adams *et al.* (2007), namely that the eigenvalue is dependent on the wave number, which means that on a given wave number, the eigenvalue can be solved numerically.

Layered media

Layered media occur frequently in both Nature and high technology industry. The Grand Canyon in America, a magnificent geological museum, shows the life of the Earth vividly through layers of sedimentary rocks of different ages on the cliff walls, see Figure 1. The rock layers are usually referred to as stratum, which, interestingly enough, share the same structure (transverse isotropy) with annual rings of tree trunks. In transverse isotropy, each layer has the same properties in-plane but different properties in direction normal to plane. The plane of each layer is the plane of isotropy and the vertical axis is the axis of symmetry. The Grand Canyon gives people a chance to see a slice of real Earth structure, and in research, the stratum can be modelled as layers of infinite elastic plates possessing different physical properties. Petroleum and natural gas may exist in the ancient forest layers. In petroleum exploration, some scientists use surface waves (Rayleigh waves) to investigate surface layer structures. Researchers first study wave propagation in single layered materials before they extend their research to multi-

layered composites. Rayleigh (1889) and Lamb (1917) were the first to study wave propagation in a linear isotropic elastic plate with traction-free surfaces.

Figure 1: Grand Canyon, source: `http://en.wikipedia.org/wiki/File:USA_10052_Grand_Canyon_Luca_Galuzzi_2007.jpg`

Layered media finds applications in high technology industry. Some layered composite membranes receive wide attention as biomaterials. In architecture, some multi-layer composite makes a very stiff and stable material that provides excellent erosion resistance and insulation of sound or heat. There are also other applications in thermo insulation. With the help of Layered Composite Insulation (LCI) technology, not only the transportation of fluids such as liquefied natural gas, refrigerants, chilled water, crude oil, or low-pressure steam, but also that of food, medicine, and other perishable commodities, has been made ever easier through advanced re-

frigerated containers. One can also find layered composite in both military and civil aircrafts, such as wing and tail sections, propellers and rotor blades.

Literature review on Elastically Restrained Boundary Conditions and dispersion

In real world problems, most layers interact with their surroundings. For example, the wall of a human artery is supported by tissue. It is difficult to model the interaction between a layer and its surroundings, but in theory it is helpful to consider two extremes first: elastic bodies in vacuum (or air) and soft body in a stiff enclosure. The former is essentially the stress-free (Neumann) boundary condition: by setting the surface traction to be zero, the problem is greatly simplified, see Rayleigh (1889) and Lamb (1917). The second scenario is the fixed (Dirichlet) boundary condition which implies vanishing of the displacements at the boundary. For instance, a coal seam can be modelled as fixed faces because it is surrounded by much stiffer rocks, see Liang et al. (1993). In reality, a lot of scenarios fall in between these two and may therefore be regarded as somewhere between these two extremes.

Much work have been carried out in respect of these two limiting cases mentioned above, with relatively little attention paid to the transitional case. Intuitively a good approximation of the transition can be obtained by assuming that the layer boundaries are subject to a Hooke-type

law, meaning that the boundaries are elastically restrained. With this idea in mind, Mindlin (1960) extended Rayleigh and Lamb's research to an isotropic elastic plate with elastically restrained boundary conditions (ERBC) in the normal direction. However his study is limited to the analysis of a grid of bounds for dispersion curves. Achenbach (1969) applied an iterative procedure to study free and forced vibrations of elastic layer. Graff (1991) called it the mixed boundary condition, which enabled him to separate the vector problem into two scalar problems and obtain the Rayleigh-Lamb spectrum.

When boundary conditions are applied, an implicit relationship between phase speed (or frequency) and wave number, usually termed as the dispersion relation, is derived. Dispersion relations are typically transcendental equations and can generally be transformed to be either real or pure imaginary. Thus, it is convenient to use numerical analysis to obtain an infinite number of solutions arising from such dispersion relations at each wave number. The branches with a finite wave speed in the long wave (low wave number) region are termed fundamental modes, with all other higher branches termed harmonics. Long wave motion in elastic layers are thus separated into two types: low frequency and high frequency.

The long wave low frequency asymptotics describe the fundamental mode, which is the feature of a single layer with free faces and corresponds to classical approximate theories of rods, plates and shells, see e.g. Kaplunov et al. (2000b); Shuvalov (2000); Poncelet et al. (2006). The long wave high frequency asymptotics describe thickness variations and are of great importance for layers with fixed faces, where the classical long wave low frequency modes do not exist,

indicating that energy will propagate only with higher modes, see Kaplunov (1995). This is how the waveguides of Dirichlet boundary conditions, known as high-pass filters, work. Lamb (1917) first considered wave propagation in an isotropic plate with higher (non-fundamental) modes. In static problems, only long wave motion of the fundamental mode exists; in the dynamic case, there are long wave low frequency, long wave high frequency and short wave high frequency aspects. To simplify the subsequent analysis, the dispersion relation may be decomposed into symmetric and anti-symmetric components, provided that the material symmetry and the symmetry of boundary conditions are ensured. Connor and Ogden (1995, 1996) studied wave propagation in an incompressible elastic layer subject to a simple shear deformation, for which it is impossible to decouple the dispersion relation into symmetric and anti-symmetric parts. Fu (2007) studied the case of one fixed and one free face boundary condition, a problem which again did not allow the decomposition into symmetric and anti-symmetric parts is not possible.

The effect of anisotropy and pre-stress on long wave high frequency motion has previously been analyzed by a number of researchers; for example, Kaplunov et al. (2000a) studied a three dimensional transversely isotropic elastic plate. In long wave high frequency motion, it is worth noting that the cut-off frequencies of two different modes may coincide with each other, see Werby and Uberall (2002). As a result, special quasi-linear expansions need to be developed, see Nolde et al. (2004); Shuvalov and Poncelet (2008). But these asymptotics are not uniform with respect to parameters that affect long wave frequency limits. Moukhomodiarov *et al.* (2010)

presented uniform asymtotics to overcome this problem.

Outline and contribution to the ERBC problem for anisotropic plates

Chapter 3 deals with wave propagation in an anisotropic plate with ERBC. In Section 3.1, ERBC in the two dimensional case is formulated and with the help of the Stroh formalism, the dispersion relation is derived. After adjusting the parameters to make sure that the boundary conditions are the same on both the top and bottom faces, and we are able to separate the dispersion relation into anti-symmetric and symmetric modes. In the subsequent analysis, in order to reduce the parameter space, we consider particular types of ERBC which depend on a single parameter. In Section 3.2, by taking the long wave limit of the dispersion relation, we obtain two families of solution branches associated with different cut-off frequencies: thickness shear resonance frequencies and thickness stretch resonance frequencies. After correlating the magnitudes of the single boundary parameter with the scaled wave number, the asymptotic expansions of the frequencies or the speeds are obtained. Section 3.3 involves the behavior of anti-symmetric and symmetric fundamental modes and the derivation of the asymptotic expansion of wave speed in the short wave limit. In Sections 3.4 and 3.5 we consider a numerical analysis for linear isotropic materials and transversely isotropic materials, respectively.

The asymptotic expansions derived in Chapter 3 are shown to give an excellent approximation to the numerical solutions. The results for a linear isotropic material are successfully recovered and shown to agree with those of Moukhomodiarov *et al.* (2010). In Section 3.5, the cut-off frequencies of two different families, which coincide, are investigated. A uniform asymptotic expansion is developed, providing much better approximation to numerical results than that of classical asymptotic expansion. Within Chapter 3 we have extended Moukhomodiarov *et al.* (2010) to anisotropic materials using Stroh formalism. The dispersion relation and subsequent asymptotic expansions are derived for a more general case.

Literature review on rubber-like materials and pre-stress

Rubber and rubber-like materials find some of their popular industrial applications in modern construction, due to their ability to withstand large strains and then recover elastically. For example, in transport suspensions, bridge bearings and spring mountings, rubber and rubber-like materials are widely used, see Hirst (1969), Torr (1969) and Crawford (1985). Also, rubber and rubber-like materials play a key role in base isolation, which is a cost effective technique for protecting buildings and bridges from earthquakes using highly elastic bearings, see Tyler (1991), Sheridan et al. (1992) and Prendergast (1995). Thus, it is of inrerest to study the mechanical properties and behaviour of rubber and rubber-like materials.

The elastic response of rubber is usually treated as homogeneous and isotropic. Rubber-like

materials are often regarded as slightly compressible or fully incompressible, because volume changes are very small for most deformations, see Ogden (1984, p.488). The constraint of incompressibility largely simplifies the analysis. Ogden and Roxburgh (1993) and Roxburgh and Ogden (1994) considered plane incremental waves and vibrations in incompressible and compressible elastic plates with free faces, respectively. Rogerson (1997), Sandiford and Rogerson (2000) and Nolde et al. (2004) investigated two dimensional motion for a plane wave travelling along principle axes of deformation for incompressible, nearly incompressible and compressible plates, respectively. Pichugin and Rogerson (2002) extended these results to three dimensional motions parallel to the faces of the layer. Nolde and Rogerson (2002) and Kaplunov and Nolde (2002) studied incompressible and nearly incompressible plates with fixed faces, respectively.

The term pre-stress is used to describe an initial deformation and suggests the presence of stress prior to wave propagation. The term pre-stress usually indicates that the media is subject to high external loads. In non-linear theory, Green and Adkins (1960) and Green and Zerna (1954) proposed a complete theory for finite deformations, but their approach made dynamic analysis very algebraically complicated. To simplify analysis of structure under large initial stress, the incremental deformation theory was introduced by Biot (1965) to describe infinitesimal incremental motion of finitely and statically deformed bodies. To linearize the equations of motion, it is necessary to separate the large static homogeneous deformation from the infinitesimal time-dependent motions. This is done by expanding the stress as a Taylor series about the initial deformed state. Biot (1965) derived incremental governing equations for both initially

isotropic and orthotropic media. Green et al. (1952) also developed the static framework of incremental deformations superimposed on finite strains.

There are several papers dealing with the asymptotic modeling of the effects of pre-stress on the plane strain dynamic response of an incompressible initially isotropic layer with free faces, see Kaplunov et al. (2000b) (2001a) (2001b) and with fixed faces, also see Nodle and Rogerson (2002). In this thesis, we will focus on the effects of pre-stress on an incompressible layer with elastically restrained boundary conditions. Ogden and Roxburgh (1993) studied wave propagation in a pre-stressed incompressible plate finite in all directions, derived the dispersion relation and discussed the influence of pre-stress on the dynamic stability of the plate. However they did not discuss the asymptotic behaviour of the dispersion relation in the long wave and short wave regimes. Rogerson and Fu (1995) derived long and short wave asymptotic expansions for the dispersion relation up to third order, and the expansions were shown to be in good agreement with numerical solutions.

Outline and contribution to the ERBC problem for a pre-stressed incompressible elastic plate

In Chapter 4, we study wave propagation in a pre-stressed incompressible plate with ERBC, using a similar procedure to that employed in Chapter 3. The difference is that the elastic

moduli are modified by the effect of pre-stress, and the use of a neo-Hookean strain energy largely simplifies the subsequent analysis. We present the derivation of dispersion relation in Section 4.1 and long wave analysis in Section 4.2. In Section 4.3, we additionally present results of harmonics in short wave analysis. We use the Stroh formalism, deviation from Rogerson and Fu (1995), to study a pre-stressed incompressible plate. The investigation in respect of ERBC in our analysis extends the previous work carried out by Edmondson and Fu (2009).

Chapter 1

Basic equations and preliminaries

In this chapter, we derive equations of motion for both linear elasticity and pre-stressed incompressible elasticity and introduce some specific materials which are used as examples in our subsequent numerical analysis: the linear isotropic material, the transversely isotropic material, the cubic material, neo-Hookean material and Mooney-Rivlin material. In the first part of this chapter, stemming from different strain energy functions, we arrive at different constitutive relations. In linear elasticity, with the use of the corresponding constitutive relation and linear momentum principle, the equations of motion are derived. In pre-stressed incompressible elasticity, the configuration of a pre-stressed body is first presented, and then an incremental stress tensor is introduced. As we expand the corresponding constitutive component of the stress tensor into a Taylor series, the first order instantaneous elastic moduli $\mathcal{A}_{jilk}$ are obtained, which, together with the linearized incompressibility constraint, facilitate the process of deriving a linearized

form of equations of motion. We consider the neo-Hookean strain energy function as a model for rubber-like materials. In the two dimensional plate problem, the first order instantaneous elastic moduli, and thus the equations of motion, are significantly simplified for neo-Hookean materials. In the derivation of the linearized boundary condition, Nanson's formula is introduced to convert the incremental surface traction into the form required. In the second part of this chapter, we present the classical Rayleigh wave problem for an isotropic elastic half-space with flat surface. We also present three models which will be used for numerical calculations and comparisons of numerical and asymptotic results throughout the thesis.

1.1 Governing equations

1.1.1 Linear elasticity

We begin by reviewing the governing dynamic equations of linear elasticity. For a more detailed discussion of the derivation, the reader is referred to Love (1944). For a linear elastic material, the strain energy function W may be presented as a quadratic function of the strain components, taking the general form

$$W = \frac{1}{2} c_{ijkl} e_{ij} e_{kl}, \tag{1.1}$$

where the c_{ijkl} are the Cartesian components of fourth order elasticity tensor and e_{ij} components of the infinitesimal strain tensor, defined by

$$e_{ij} = \frac{1}{2}\left(\frac{\partial u_i}{\partial x_j} + \frac{\partial u_j}{\partial x_i}\right) \equiv \frac{1}{2}(u_{i,j} + u_{j,i}). \tag{1.2}$$

Here, and hereafter, we use the summation convention on repeated suffices, a comma indicates differentiation with respect to the associated spatial components and u_i are the components of infinitesimal displacement, relative to a fixed rectangular Cartesian system $(x_1,\, x_2,\, x_3)$.

We assume that the elastic moduli obey the symmetry relations

$$c_{jikl} = c_{klij} = c_{ijkl} = c_{ijlk}, \tag{1.3}$$

and also satisfy the strong convexity condition

$$c_{pqrs}S_{pq}S_{rs} > 0, \forall \text{ non-zero real symmetric tensors } S. \tag{1.4}$$

We note that the strong convexity condition implies the weaker strong ellipticity condition

$$c_{pqrs}a_p b_q a_r b_s > 0, \forall \text{ non-zero real vectors } \boldsymbol{a},\ \boldsymbol{b}. \tag{1.5}$$

Using these symmetries, together with the relation

$$\sigma_{ij} = \frac{\partial W}{\partial e_{ij}}, \tag{1.6}$$

where σ_{ij} are components of the stress tensor, enables us to establish the constitutive relation

$$\sigma_{ij} = c_{ijkl} e_{kl} = c_{ijkl} u_{k,l}. \tag{1.7}$$

To obtain the equation of motion, we use the linear momentum principle

$$\int_S \boldsymbol{T}^{(\boldsymbol{n})} dS + \int_V \rho \boldsymbol{b} dV = \int_V \rho \ddot{\boldsymbol{u}} dV, \tag{1.8}$$

where $\boldsymbol{T}^{(\boldsymbol{n})}$ is the surface traction vector, defining the force per unit area across a plane with outward unit normal in the direction $\boldsymbol{n}$, $\boldsymbol{b}$ is the body force per unit mass, ρ is the mass density, a superimposed dot indicates differentiation with respect to time and dS and dV denote elements of area and volume, respectively.

The surface traction may be expressed as

$$\boldsymbol{T}_i^{(\boldsymbol{n})} = \sigma_{ij} n_j. \tag{1.9}$$

Substitution of (1.9) into (1.8), together with use of the divergence theorem, reveals that

$$\int_V \sigma_{ij,j} dV + \int_V \rho b_i dV = \int_V \rho \ddot{u}_i dV. \tag{1.10}$$

This equation is satisfied in respect of any arbitrary volume V, and therefore the local equation of motion is

$$\sigma_{ij,j} + \rho b_i = \rho \ddot{u}_i. \tag{1.11}$$

In the absence of body forces, by using equation (1.7), the equations of motion (1.11) reduce to

$$c_{ijkl} u_{k,lj} = \rho \ddot{u}_i. \tag{1.12}$$

1.1.2 Pre-stressed incompressible elasticity

Configuration of a pre-stressed body

The following part of this chapter deals with non-linear elastic deformations, and the reader is referred to Ogden (1984) for a more detailed account of the underlying theory. Consider a homogeneous elastic body $\mathbb{B}$, composed of a non-heat-conducting hyper-elastic material. A purely homogeneous static deformation is then imposed upon an initial unstressed state B_0, to produce a finitely stressed equilibrium configuration denoted by B_e. Finally, a small time-dependent motion is superimposed upon B_e, resulting in the final current configuration B_t. The position

vectors of a representative particle are denoted by their Cartesian components X_A, $\bar{x}_i(X_A)$ and $x_i(X_A, t)$ in B_0, B_e and B_t, respectively. The position vector $x_i(X_A, t)$ may therefore be represented in the form

$$x_i(X_A, t) = \bar{x}_i(X_A) + u_i(\bar{\boldsymbol{x}}, t), \tag{1.13}$$

within which $\boldsymbol{u}(\bar{\boldsymbol{x}}, t)$ is a small time-dependent displacement associated with the deformation $B_e \to B_t$.

The deformation gradients arising from the deformations $B_0 \to B_t$ and $B_0 \to B_e$ are denoted by F and $\bar{F}$ and defined by

$$F_{iA} = \frac{\partial x_i}{\partial X_A}, \quad \bar{F}_{iA} = \frac{\partial \bar{x}_i}{\partial X_A}, \tag{1.14}$$

respectively. Equations (1.13) and (1.14) may now be employed to deduce that these two deformation gradients are related through

$$F_{iA} = \frac{\partial x_i}{\partial X_A} = \frac{\partial \bar{x}_i}{\partial X_A} + \frac{\partial u_i}{\partial \bar{x}_j}\frac{\partial \bar{x}_j}{\partial X_A} = \delta_{ij}\frac{\partial \bar{x}_j}{\partial X_A} + u_{i,j}\frac{\partial \bar{x}_j}{\partial X_A} = (\delta_{ij} + u_{i,j})\bar{F}_{jA}, \tag{1.15}$$

where the comma indicates differentiation with respect to the implied spatial coordinate in B_e.

Motion of a pre-stressed incompressible elastic body

The incompressibility constraint, which is usually referred to as an internal constraint, is imposed and thus every possible material deformation must be isochoric. This in turn may be shown to imply that

$$J - 1 = 0, \;\; J = \det F, \tag{1.16}$$

throughout every possible material motion. A pseudo strain energy function is usually introduced for problems involving internal constraints. In the case of incompressibility this function is of the form

$$W(F) = W_0(F) - p(J - 1). \tag{1.17}$$

In equation (1.17), W_0 generates the constitutive part of the stress, whilst the other term, constrained to be zero throughout all material deformations, generates a workless reaction stress. Furthermore, in (1.17), p is a Lagrangian multiplier and is independent of F. For incompressibility, p may be interpreted as a hydro-static pressure. If we use $\bar{p}$ to denote the pressure in B_e and p^* to denote its time dependent incremental pressure, then

$$p = \bar{p} + p^*. \tag{1.18}$$

In the absence of body forces, the equations of motion are given by

$$\pi_{iA,A} = \rho_0 \ddot{u}_i, \tag{1.19}$$

where π is the first Piola-Kirchhoff stress which, in component form, is given by

$$\pi_{iA} = \frac{\partial W}{\partial F_{iA}}, \tag{1.20}$$

ρ_0 is the material mass density relative to B_0 and a superimposed dot indicates differentiation with respect to time.

Upon invoking equation (1.16), we obtain

$$\frac{\partial \text{det}F}{\partial F_{iA}} = \text{det}F \cdot \text{tr}\left(\frac{\partial F}{\partial F_{iA}} F^{-1}\right) = \left(\frac{\partial F}{\partial F_{iA}}\right)_{jB} F^{-1}_{Bj} = \delta_{ij}\delta_{AB} F^{-1}_{Bj} = F^{-1}_{Ai}. \tag{1.21}$$

The first Piola-Kirchhoff stress tensor π may now be decomposed into its constitutive and reaction components, as

$$\pi_{iA} = \frac{\partial W_0}{\partial F_{iA}} - pF^{-1}_{Ai}. \tag{1.22}$$

Because the Cauchy stress and the first Piola-Kirchhoff stress tensors are related through

$$\sigma_{ij} = J^{-1}\pi_{iA}F_{jA}, \tag{1.23}$$

it is convenient to introduce an incremental Cauchy stress tensor with components χ_{ij} through $(\bar{J}^{-1} = 1)$

$$\chi_{ij} = \pi_{iA}\bar{J}^{-1}\bar{F}_{jA} - \bar{\pi}_{iA}\bar{J}^{-1}\bar{F}_{jA} = \frac{\partial W_0}{\partial F_{iA}}\bar{F}_{jA} - pF^{-1}_{Ai}\bar{F}_{jA} - \bar{\pi}_{iA}\bar{F}_{jA}, \tag{1.24}$$

where $\bar{\pi}_{iA}$ is the value of π_{iA} calculated from (1.22) with F replaced by $\bar{F}$ and p by $\bar{p}$.

We now prove that

$$\chi_{ij,j} = \pi_{iA,A}, \tag{1.25}$$

so that equations of motion (1.19) can be written as

$$\chi_{ij,j} = \rho_0\ddot{u}_i. \tag{1.26}$$

Proof

Firstly, we have

$$\frac{\partial \bar{J}}{\partial X_r} = \bar{J}\cdot \text{tr}\left(\frac{\partial \bar{F}}{\partial X_r}\bar{F}^{-1}\right) = \bar{J}\frac{\partial \bar{F}_{qp}}{\partial X_r}\bar{F}^{-1}_{pq} = \bar{J}\frac{\partial^2 \bar{x}_q}{\partial X_p \partial X_r}\bar{F}^{-1}_{pq}. \tag{1.27}$$

From this we deduce that

$$\frac{\partial}{\partial \bar{x}_j}(\bar{J}^{-1}\bar{F}_{jA}) = \frac{\partial}{\partial X_r}(\bar{J}^{-1}\bar{F}_{jA})\frac{\partial X_r}{\partial x_j} = \left(\bar{J}^{-1}\frac{\partial^2 \bar{x}_j}{\partial X_A \partial X_r} - \bar{J}^{-2}\frac{\partial \bar{J}}{\partial X_r}\bar{F}_{jA}\right)\bar{F}^{-1}_{rj}$$

$$= \bar{J}^{-1}\frac{\partial^2 \bar{x}_q}{\partial X_A \partial X_p}\bar{F}^{-1}_{pq} - \bar{J}^{-1}\frac{\partial^2 \bar{x}_q}{\partial X_r \partial X_p}\bar{F}^{-1}_{pq}\delta_{rA} = 0. \tag{1.28}$$

Due to the equilibrium equations $\bar{\pi}_{iA,A} = 0$ in B_e, we finally arrive at

$$\chi_{ij,j} = (\pi_{iA}(\bar{J}^{-1}\bar{F}_{jA}))_{,j} - (\bar{\pi}_{iA}(\bar{J}^{-1}\bar{F}_{jA}))_{,j}$$

$$= \pi_{iA,j}(\bar{J}^{-1}\bar{F}_{jA}) + \pi_{iA}(\bar{J}^{-1}\bar{F}_{jA})_{,j} - \bar{\pi}_{iA,j}(\bar{J}^{-1}\bar{F}_{jA}) - \bar{\pi}_{iA}(\bar{J}^{-1}\bar{F}_{jA})_{,j}$$

$$= \frac{\partial \pi_{iA}}{\partial \bar{x}_j}\frac{\partial \bar{x}_j}{\partial X_A} + 0 - \frac{\partial \bar{\pi}_{iA}}{\partial \bar{x}_j}\frac{\partial \bar{x}_j}{\partial X_A} - 0 = \pi_{iA,A}. \tag{1.29}$$

We assume that the deformation $B_e \to B_t$ is small. It is then appropriate to obtain a linearized equation of motion by expanding everything as a Taylor series about the pre-stressed equilibrium state B_e. We remark that in the two dimensional plate problem to be discussed later, we have $k, l, i, A, k, B \in \{1, 2\}$, so that $\frac{\partial W_0}{\partial F_{iA}}$ has four variables.

We also note that

$$F_{kB} - \bar{F}_{kB} = (\delta_{kl} + u_{k,l})\bar{F}_{lB} - \bar{F}_{kB} = \delta_{kl}\bar{F}_{lB} - \bar{F}_{kB} + u_{k,l}\bar{F}_{lB} = u_{k,l}\bar{F}_{lB}, \tag{1.30}$$

from which we obtain

$$\frac{\partial W_0}{\partial F_{iA}}\bar{F}_{jA} = \frac{\partial W_0}{\partial F_{iA}}\,|_{F=\bar{F}}\,\bar{F}_{jA} + \frac{\partial^2 W_0}{\partial F_{iA}\partial F_{kB}}\,|_{F=\bar{F}}\,(F_{kB} - \bar{F}_{kB})\bar{F}_{jA} + O(\epsilon^2)$$

$$= \frac{\partial W_0}{\partial F_{iA}} \mid_{F=\bar{F}} \bar{F}_{jA} + \mathcal{A}_{jilk} u_{k,l} + O(\epsilon^2), \tag{1.31}$$

where ϵ is a small parameter measuring the magnitude of $u_{i,j}$ and the tensor $\mathcal{A}$ is the first order instantaneous elastic moduli tensor in B_e defined by its components as follows

$$\mathcal{A}_{jilk} = \bar{F}_{jA}\bar{F}_{lB}\frac{\partial^2 W_0}{\partial F_{iA}\partial F_{kB}} \mid_{F=\bar{F}} . \tag{1.32}$$

We note that the moduli $\mathcal{A}_{jilk}$ have a pairwise symmetry property such as

$$\mathcal{A}_{jilk} = \mathcal{A}_{lkji}, \tag{1.33}$$

and satisfy the strong ellipticity condition

$$\mathcal{A}_{jilk} c_j d_i c_l d_k > 0 \tag{1.34}$$

for all non-zero vectors $\boldsymbol{c}$ and $\boldsymbol{d}$ satisfying $\boldsymbol{c} \cdot \boldsymbol{d} = 0$.

Next, denoting the displacement gradient tensor $(u_{i,j})$ by d and making use of the matrix form of equation (1.15) $F = (I + d)\bar{F}$, we obtain

$$F^{-1}_{Ai}\bar{F}_{jA} = (\bar{F}F^{-1})_{ji} = ((I+d)^{-1})_{ji} = (I - d + d^2 - d^3 + \cdots)_{ji} = \delta_{ji} - u_{j,i} + O(\epsilon^2). \tag{1.35}$$

On substituting (1.18), (1.31) and (1.35) into (1.24), we obtain

$$\chi_{ij} = \frac{\partial W_0}{\partial F_{iA}} \mid_{F=\bar{F}} \bar{F}_{jA} + \mathcal{A}_{jilk} u_{k,l} - (\bar{p} + p^*)(\delta_{ji} - u_{j,i}) - (\frac{\partial W_0}{\partial \bar{F}_{iA}} \bar{F}_{jA} - \bar{p} \bar{F}^{-1}_{Ai} \bar{F}_{jA}) + O(\epsilon^2)$$

$$= \mathcal{A}_{jilk} u_{k,l} + \bar{p} u_{j,i} - p^*(\delta_{ji} - u_{j,i}) + O(\epsilon^2). \tag{1.36}$$

In view of the incompressibility constraint $\det F = 1 = \det \bar{F}$, we have

$$\det F = 1 = \det[(I + d)\bar{F}] = \det(I + d) \det \bar{F} = \det(I + d). \tag{1.37}$$

For arbitrary scalar Λ, we note that

$$\det(d - \Lambda I) = -\Lambda^3 + I_d \Lambda^2 - II_d \Lambda + III_d, \tag{1.38}$$

where I_d, II_d, III_d are the first, second and third principal invariants of the matrix d, respectively, given by

$$I_d = \mathrm{Tr} d, \qquad II_d = \frac{1}{2}(I_d^2 - \mathrm{Tr}(d^2)), \qquad III_d = \det d. \tag{1.39}$$

If we now let $\Lambda = -1$, we establish that

$$I_d + II_d + III_d = 0, \tag{1.40}$$

which implies

$$u_{i,i} = \frac{1}{2}u_{m,n}u_{n,m} - \frac{1}{2}(u_{i,i})^2 - \text{det}(u_{m,n}). \tag{1.41}$$

The linearized form of the incompressibility constraint is thus given by

$$u_{i,i} = 0. \tag{1.42}$$

With the use of (1.42), the equations of motion $\chi_{ij,j} = \rho_0 \ddot{u}_i$ can be written in their linearized form as

$$\mathcal{A}_{jilk}u_{k,lj} - p^*_{,i} = \rho_0 \ddot{u}_i. \tag{1.43}$$

We consider a hyperelastic material or Green elastic material. The most common example is rubber, whose stress-strain relationship is usually modeled as non-linearly elastic, isotropic, incompressible and generally independent of strain rate. Elastomers and biological tissues are often modeled as hyperelastic materials, which are special cases of Cauchy elastic materials. There are some well-known hyperelastic models, such as the neo-Hookean materials, Mooney-Rivlin materials and Varga materials.

On substituting (1.74) into (1.32), we obtain

$$\mathcal{A}_{jilk} = \mu\delta_{ik}\bar{B}_{jl}, \tag{1.44}$$

where $\bar{B}$ is the value of B in B_e. Thus, as far as incremental deformations are concerned, a neo-Hookean material behaves as a linear material. We now provide proof of (1.44).

It is known that

$$I_1 = B_{ii} = (FF^T)_{ii} = F_{iA}F_{iA}. \tag{1.45}$$

It follows from (1.45) that

$$\frac{\partial^2 W_0}{\partial F_{iA}\partial F_{kB}} \mid_{F=\bar{F}} = \mu\delta_{ik}\delta_{AB}. \tag{1.46}$$

Because

$$\bar{F}_{jA}\bar{F}_{lB}\delta_{AB} = (\bar{F}\bar{F}^T)_{jl} = \bar{B}_{jl}, \tag{1.47}$$

we conclude that for neo-Hookean materials, the fourth order elasticity tensor $\mathcal{A}$ is simply

$$\mathcal{A}_{jilk} = \mu\delta_{ik}\bar{B}_{jl}. \tag{1.48}$$

We assume that the axes of the (x_1, x_2, x_3) coordinate system are aligned with the principal directions,

$$x_1 = \lambda_1 X_1,\ \ x_2 = \lambda_2 X_2,\ \ x_3 = \lambda_3 X_3, \tag{1.49}$$

where λ_i is the stretch in the x_i-direction. When

$$\lambda_1 = \bar{\lambda}, \qquad \lambda_2 = \bar{\lambda}^{-1}, \qquad \lambda_3 = 1, \tag{1.50}$$

we have

$$x_1 = \bar{\lambda} X_1, \ x_2 = \bar{\lambda}^{-1} X_2, \ x_3 = X_3. \tag{1.51}$$

We then readily establish that

$$\bar{F} = \begin{pmatrix} \bar{\lambda} & 0 & 0 \\ 0 & \bar{\lambda}^{-1} & 0 \\ 0 & 0 & 1 \end{pmatrix}, \ \bar{B} = \bar{F}\bar{F}^T = \begin{pmatrix} \bar{\lambda}^2 & 0 & 0 \\ 0 & \bar{\lambda}^{-2} & 0 \\ 0 & 0 & 1 \end{pmatrix}. \tag{1.52}$$

It follows that the normal stresses are the principal stresses and the stress tensor is represented by a diagonal matrix, with principal stress on diagonal components. From now on, we non-dimensionalize the governing equations and boundary conditions using μ as the stress scale.

For incompressible materials, the principle Cauchy stresses σ_i along x_i-axis are given by

$$\sigma_i = \lambda_i \frac{\partial W_0}{\partial \lambda_i} - p. \tag{1.53}$$

For the plane strain problem, the Cauchy stress tensor σ is given by

$$\sigma = 2\frac{\partial W_0}{\partial I_1}B - pI = \mu B - pI = \begin{pmatrix} \sigma_1 & 0 & 0 \\ 0 & \sigma_2 & 0 \\ 0 & 0 & \sigma_3 \end{pmatrix} = \begin{pmatrix} \bar{\lambda}^2 - p & 0 & 0 \\ 0 & \bar{\lambda}^{-2} - p & 0 \\ 0 & 0 & 1 - p \end{pmatrix}. \quad (1.54)$$

It follows that in B_e the pressure $\bar{p}$ is related to the 22-component of σ by

$$\bar{p} = \mu \bar{B}_{22} - \bar{\sigma}_2 = \bar{\lambda}^{-2} - \bar{\sigma}_2. \quad (1.55)$$

Measure of incremental surface traction

We now proceed to derive the linearized boundary conditions. Let an infinitesimal area element in B_e be given as $\boldsymbol{n}da$, where *da* is the area, and $\boldsymbol{n}$ is the unit outward normal to the surface. Similarly, let the same differential area element in B_0 be given by $\boldsymbol{n}dA$, where dA is the area and $\boldsymbol{n}$ is the unit outward normal to the surface.

Now, we can form a differential volume element dv in B_e by using a differential length vector dx and taking $dv = dx \cdot (\boldsymbol{n}da)$. Let this length vector be mapped into dX in B_0, which means

$$dx = \bar{F}dX. \quad (1.56)$$

Since we know that volume between the two configurations is related by

$$dv = JdV, \tag{1.57}$$

we can then form the relation

$$dx(\boldsymbol{n}da) = dv = JdV = JdX\boldsymbol{n}dA. \tag{1.58}$$

Using (1.56) and rearranging, we find

$$dX(F^T\boldsymbol{n}da) = dX(J\boldsymbol{n}dA). \tag{1.59}$$

After eliminating dX from both sides, and applying the incompressibility constraint $J = 1$, we obtain

$$F^T\boldsymbol{n}da = \boldsymbol{n}dA, \tag{1.60}$$

which is known as *Nanson's formula* in incompressible media.

During the incremental deformation $B_e \rightarrow B_t$, the plates we consider in later chapters are subjected to the so-called Elastically Restrained Boundary Condition (ERBC). The incremental surface traction represented by $(\pi_{iA} - \bar{\pi}_{iA})\boldsymbol{n}_A$ is equivalent to $\chi_{ij}n_j$ with the help of *Nanson's formula*.

1.2 Specific materials to be studied in numerical analysis

1.2.1 Linear isotropic elastic material

We note that for a linear isotropic material, for which

$$c_{ijkl} = \lambda\delta_{ij}\delta_{kl} + \mu(\delta_{ik}\delta_{jl} + \delta_{il}\delta_{jk}), \tag{1.61}$$

where λ and μ are Lame constants, δ_{ij} is the Kronecker delta, (1.4) and (1.5) yield

$$\lambda + \frac{2}{3}\mu > 0,\ \mu > 0, \quad \text{and} \quad \lambda + 2\mu > 0,\ \mu > 0. \tag{1.62}$$

Now we show that the classical Rayleigh wave speed $v_R(=\sqrt{X_0/\rho})$, which is based on isotropic elastic half-space with flat traction-free surface, is determined by solving the cubic

$$X_0^3 - 8\mu X_0^2 + \frac{8\mu^2(3\lambda+4\mu)}{\lambda+2\mu}X_0 - 16\mu^3\frac{\lambda+\mu}{\lambda+2\mu} = 0. \tag{1.63}$$

According to (1.12) and (1.61), the two dimensional problem is governed by

$$(\lambda+\mu)(u_{1,11} + u_{2,21}) + \mu(u_{1,11} + u_{1,22}) = \rho\ddot{u}_1, \tag{1.64}$$

$$(\lambda+\mu)(u_{1,12} + u_{2,22}) + \mu(u_{2,11} + u_{2,22}) = \rho\ddot{u}_2. \tag{1.65}$$

The traction-free boundary condition is

$$t_1 = c_{12kl}u_{k,l} = u_{1,2} + u_{2,1} = 0, \quad \text{on} \;\; x_2 = 0,$$

$$t_2 = c_{22kl}u_{k,l} = \lambda u_{1,1} + (\lambda + 2\mu)u_{2,2} = 0, \quad \text{on} \;\; x_2 = 0, \tag{1.66}$$

where t_i is the traction along x_i axis. The surface wave propagates along the x_1 axis, so we assume that

$$\boldsymbol{u} = \begin{pmatrix} u_1 \\ \\ u_2 \end{pmatrix} = \begin{pmatrix} U \\ \\ V \end{pmatrix} e^{ikpx_2} e^{ik(x_1 - vt)}, \tag{1.67}$$

where k is the wave number and p is the eigenvalue, and by substituting (1.67) into (1.64) and (1.65), we obtain

$$p_1 = \mathrm{i}\sqrt{1 - \frac{X_0}{\mu}}, \qquad \begin{pmatrix} U_1 \\ \\ V_1 \end{pmatrix} = \begin{pmatrix} -p_1 \\ \\ 1 \end{pmatrix}, \tag{1.68}$$

$$p_2 = \mathrm{i}\sqrt{1 - \frac{X_0}{\lambda + 2\mu}}, \qquad \begin{pmatrix} U_2 \\ \\ V_2 \end{pmatrix} = \begin{pmatrix} 1 \\ \\ p_2 \end{pmatrix}. \tag{1.69}$$

As a result, the displacement $\boldsymbol{u}$ takes the form

$$\boldsymbol{u} = j_1 \begin{pmatrix} U_1 \\ \\ V_1 \end{pmatrix} e^{ip_1x_2} e^{ik(x_1 - vt)} + j_2 \begin{pmatrix} U_2 \\ \\ V_2 \end{pmatrix} e^{ip_2x_2} e^{ik(x_1 - vt)}.$$

By substituting into $(1.66)_1$, we obtain $j_1 = 2p_2,\ j_2 = p_1^2 - 1$.

Now substituting the new form of $\boldsymbol{u}$ into the traction-free boundary condition $(1.66)_2$, we obtain

$$\lambda(1-p_1^2) + (\lambda+2\mu)p_2^2(1-p_1^2) - 4\mu p_1 p_2 = 0, \tag{1.70}$$

which after simplification, squaring and factorization, yields the given equation (1.63). We remark that p_1, p_2 and their associated vectors can also be obtained by solving the Stroh matrix for its eigenvalues and eigenvectors as we do in Section 2.2 for the leading order problem.

1.2.2 Transversely isotropic material

The moduli for a linear transversely isotropic elastic material are given by

$$c_{ijkl} = \lambda\delta_{ij}\delta_{kl} + \mu_T(\delta_{ik}\delta_{jl} + \delta_{il}\delta_{jk}) + \alpha(\delta_{ij}m_k m_l + m_i m_j \delta_{kl})$$

$$+(\mu_L - \mu_T)(m_i m_k \delta_{jl} + m_i m_l \delta_{jk} + m_j m_k \delta_{il} + m_j m_l \delta_{ik}) + \beta m_i m_j m_k m_l, \tag{1.71}$$

within which $\alpha, \beta, \lambda, \mu_L$ and μ_T are material constants; the unit vector **m**, with components m_i, is along the fibre direction regarded as uniform, see e.g., Spencer (1984). These constants are related to the longitudinal and transverse Young's moduli E_l, E_t, respectively, and Poisson's

ratio ν_{lt} through

$$E_l = \hat{\beta} - \frac{(\alpha+\lambda)^2}{\lambda+\mu_T}, \quad E_t = \frac{4\mu_T\left(\hat{\beta}(\lambda+\mu_T) - (\alpha+\lambda)^2\right)}{\hat{\beta}(\lambda+2\mu_T) - (\alpha+\lambda)^2}, \quad \nu_{lt} = \frac{\alpha+\lambda}{2(\lambda+\mu_T)},$$

where $\hat{\beta} = \lambda + 2\alpha + 4\mu_L - 2\mu_T + \beta$. In later numerical calculations, we shall take $\rho = 1852\,\mathrm{kg/m^3}$, $\nu_{lt} = 0.324$ and

$$(E_l,\ E_t,\ \mu_L,\ \mu_T) = (42.7,\ 11.6,\ 4.69,\ 6.07) \times 10^9\,\mathrm{N/m^2}. \tag{1.72}$$

These numerical values were given by Rikards *et al.* (1999) for a typical Glass-Epoxy composite.

1.2.3 Cubic material

Crystals are categorized in accordance with their structures, like lattice systems, which consist of a set of three axes in a particular geometrical arrangement. There are seven lattice systems. The cubic (or isometric) system is the simplest and most symmetric system. The other six lattice systems are called hexagonal, tetragonal, rhombohedral, orthorhombic, monoclinic and triclinic. The final material model we use for numerical investigations is the cubic material silicon with

material constants taken from Farnell (1970):

$$(c_{1111},\ c_{1122},\ c_{2323}) = (165.7,\ 63.9,\ 79.913) \times 10^9\,\mathrm{N/m^2},\ \ \rho = 2340\,\mathrm{kg/m^3}. \tag{1.73}$$

1.2.4 Neo-Hookean material

The strain-energy function of a neo-Hookean material is given by

$$W_0 = \frac{1}{2}\mu(I_1 - 3) \equiv \frac{1}{2}\mu(\lambda_1^2 + \lambda_2^2 + \lambda_3^2 - 3), \tag{1.74}$$

where $\mu(> 0)$ is the shear modulus, $I_i\,(i = 1, 2, 3)$ is the ith principal invariant of the left Cauchy-Green deformation tensor $B(= FF^T)$ and $\lambda_i\,(i = 1, 2, 3)$ are the principal stretches. Under the incompressible constraint (1.16),

$$I_3 = \mathrm{det}B = (\mathrm{det}F)^2 = (\lambda_1\lambda_2\lambda_3)^2 = 1, \text{which means } \lambda_1\lambda_2\lambda_3 = 1. \tag{1.75}$$

1.2.5 Mooney-Rivlin material

The strain-energy function of a Mooney-Rivlin material is given by

$$W_0 = C_1(I_1 - 3) + C_2(I_2 - 3) \equiv C_1(\lambda_1^2 + \lambda_2^2 + \lambda_3^2 - 3) + C_2(\lambda_1^{-2} + \lambda_2^{-2} + \lambda_3^{-2} - 3)$$

$$\equiv C_1(\lambda_1^2+\lambda_2^2+\lambda_3^2-3)+C_2(\lambda_2^2\lambda_3^2+\lambda_1^2\lambda_3^2+\lambda_1^2\lambda_2^2-3), \tag{1.76}$$

where C_1, C_2 are constants.

For plane strain deformations such that $\lambda_3 = 1$,

$$\lambda_1^2+\lambda_2^2+\lambda_3^2=\lambda_2^2\lambda_3^2+\lambda_1^2\lambda_3^2+\lambda_1^2\lambda_2^2, \tag{1.77}$$

which means that in this case the Mooney-Rivlin strain-energy function coincides with that of the neo-Hookean form.

1.3 Stroh formalism

Stroh formalism is an elegant matrix method dealing with equations of motion in terms of displacement and surface traction vectors. The eigenvalues and eigenvectors of Stroh Matrix are solved and they constitute the solutions of Stroh formalism. By substituting the solutions into boundary conditions, the dispersion relations are derived.

The displacement $\boldsymbol{u}(x_1, x_2)$ is assumed to have the general form

$$\boldsymbol{u}(x_1, x_2) = \boldsymbol{z}(x_2)\mathrm{e}^{\mathrm{i}(x_1-vt)}, \tag{1.78}$$

with the traction on its surface given by

$$\boldsymbol{t} = \boldsymbol{\sigma}\boldsymbol{n}_1 = c_{i2kl}u_{k,l} = (\mathrm{i}R^T\boldsymbol{z}(h) + T\boldsymbol{z}'(h))\mathrm{e}^{\mathrm{i}(x_1-\upsilon t)}, \tag{1.79}$$

where $\boldsymbol{n}_1 = (0,1)$, and the matrices *T, R, Q* are defined by

$$T_{ik} = c_{i2k2},\ R_{ik} = c_{i1k2},\ Q_{ik} = c_{i1k1}. \tag{1.80}$$

We shall now define

$$\boldsymbol{t} = -\mathrm{i}\boldsymbol{l}(x_2)\mathrm{e}^{\mathrm{i}(x_1-\upsilon t)}, \tag{1.81}$$

so that

$$-\mathrm{i}\boldsymbol{l}(x_2) = \mathrm{i}R^T\boldsymbol{z}(x_2) + T\boldsymbol{z}'(x_2), \tag{1.82}$$

which implies that

$$-\mathrm{i}\boldsymbol{l}'(x_2) = \mathrm{i}R^T\boldsymbol{z}'(x_2) + T\boldsymbol{z}''(x_2). \tag{1.83}$$

Recalling the definitions (1.80), on substituting (1.78) into (1.12), we obtain

$$T\boldsymbol{z}''(x_2) + \mathrm{i}(R+R^T)\boldsymbol{z}'(x_2) - (Q-\rho\upsilon^2 I)\boldsymbol{z}(x_2) = \boldsymbol{0}. \tag{1.84}$$

It is now possible to substitute (1.83) into (1.84) to establish that

$$\mathrm{i}R\boldsymbol{z}'(x_2) - \mathrm{i}\boldsymbol{l}'(x_2) - (Q - \rho\upsilon^2 I)\boldsymbol{z}(x_2) = 0. \tag{1.85}$$

Equation (1.82) is now employed to establish that

$$\boldsymbol{z}'(x_2) = -\mathrm{i}T^{-1}R^T\boldsymbol{z}(x_2) - \mathrm{i}T^{-1}\boldsymbol{l}(x_2), \tag{1.86}$$

which on substituting into (1.85), enables us to conclude that

$$\boldsymbol{l}'(x_2) = -\mathrm{i}(RT^{-1}R^T - Q + \rho\upsilon^2 I)\boldsymbol{z}(x_2) - \mathrm{i}RT^{-1}\boldsymbol{l}(x_2). \tag{1.87}$$

These two equations, (1.86) and (1.87), may now be incorporated into the form

$$\mathrm{i}N\begin{pmatrix}\boldsymbol{z}(x_2)\\ \boldsymbol{l}(x_2)\end{pmatrix} = \begin{pmatrix}\boldsymbol{z}'(x_2)\\ \boldsymbol{l}'(x_2)\end{pmatrix}, N = \begin{pmatrix}N_1 & N_2\\ N_3 - \rho\upsilon^2 I & N_1^T\end{pmatrix}, \tag{1.88}$$

where

$$N_1 = -T^{-1}R^T, \qquad N_2 = -T^{-1} = N_2^T, \qquad N_3 = -RT^{-1}R^T + Q. \tag{1.89}$$

Equation (1.88), together with (1.89), is known as the Stroh formalism.

Chapter 2

Rayleigh waves guided by topography in an anisotropic elastic half-space

In this chapter, we study the influence of a localized inhomogeneity on the speed of a surface wave propagating along the surface of an anisotropic elastic half-space. Firstly, after a variable transformation, the humped surface becomes flat in terms of the new coordinates. By substituting a perturbation expansion of wave speed and displacement into the equations of motion and traction free boundary conditions, we obtain the first three orders of this system of equations. The leading order solution is the solution for a flat surface, and at the third order, we finally arrive at the amplitude equation, recognized as a Schrödinger equation, which has been much studied in quantum mechanics and soliton theory. For an isotropic elastic half-space, we recover previously known results of Adams *et al.* (2007) and find that topography-guided surface waves

always exist and travel slower than the classical Rayleigh wave. For an anisotropic elastic half-space, we demonstrate that it is possible to have zero, a single or multiple topography-guided solutions, and that their speed may be higher or lower than the speed corresponding to a flat surface.

2.1 Problem formulation

We consider surface wave propagation along a half-space whose surface is defined by

$$x_2 = -h(\varepsilon x_3), \quad h(\pm\infty) \to 0, \tag{2.1}$$

with x_i Cartesian coordinates, h a smooth localized function and ε a small positive parameter. The surface is of slowly varying thickness, localized in the x_3-direction, see Fig. 2.1. The

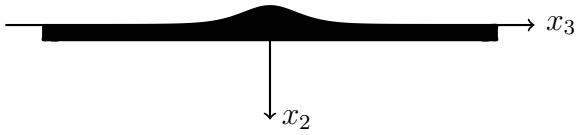

Figure 2.1: A half-space whose surface is not flat but is a localized and slowly varying perturbation. Surface waves propagate along the x_1-direction.

traction-free boundary and decay conditions are

$$\sigma_{ij} n_j = 0, \qquad \text{on } \; x_2 = -h(\varepsilon x_3), \qquad u_i \to 0 \quad \text{as } \; x_2 \to \infty, \tag{2.2}$$

where n_i is the unit normal to the free surface.

For a surface wave propagating in the x_1-direction with speed v, the dependence on x_1 and t is through $x_1 - vt$, and so equations (1.12) and $(2.2)_1$ may be written as

$$c_{ijkl}u_{k,lj} = \rho v^2 u_{i,11}, \quad -h(\varepsilon x_3) < x_2 < \infty, \tag{2.3}$$

$$c_{ijkl}u_{k,l}n_j = 0 \quad \text{on} \;\; x_2 = -h(\varepsilon x_3). \tag{2.4}$$

The free surface is defined by $x_2 + h(\varepsilon x_3) = 0$, and so its unit normal is in the direction $(0, 1, \varepsilon h'(\varepsilon x_3))$, where the prime indicates differentiation with respect to the argument εx_3. Thus, the traction-free boundary condition (2.4) may be written as

$$c_{i2kl}u_{k,l} + \varepsilon c_{i3kl}u_{k,l}h'(\varepsilon x_3) = 0 \quad \text{on} \;\; x_2 = -h(\varepsilon x_3). \tag{2.5}$$

We now introduce the variable transformation

$$x_1' = x_1, \quad x_2' = x_2 + h(\varepsilon x_3), \quad x_3' = \varepsilon x_3,$$

so that in terms of the new coordinates the free surface is given by $x_2' = 0$. We have

$$\frac{\partial}{\partial x_1} = \frac{\partial}{\partial x_1'}, \quad \frac{\partial}{\partial x_2} = \frac{\partial}{\partial x_2'}, \quad \frac{\partial}{\partial x_3} = \varepsilon\frac{\partial}{\partial x_3'} + \varepsilon h'(x_3')\frac{\partial}{\partial x_2'},$$

and in terms of the new coordinates, (2.3) and (2.5) become

$$c_{i\alpha k\beta}u_{k,\alpha\beta} + \varepsilon(c_{i\alpha k3} + c_{i3k\alpha})(u_{k,3\alpha} + h'u_{k,2\alpha})$$

$$+\varepsilon^2 c_{i3k3}(u_{k,33} + h''u_{k,2} + 2h'u_{k,23} + h'^2u_{k,22}) = \rho v^2 u_{i,11}, \quad 0 < x_2' < \infty, \tag{2.6}$$

$$c_{i2k\alpha}u_{k,\alpha} + \varepsilon c_{i3k\alpha}u_{k,\alpha}h'(\varepsilon x_3) + \varepsilon c_{i2k3}(u_{k,3} + h'u_{k,2})$$

$$+\varepsilon^2 c_{i3k3}(h'u_{k,3} + h'^2u_{k,2}) = 0 \quad \text{on} \;\; x_2' = 0, \tag{2.7}$$

where here and hereafter Greek subscripts range from 1 to 2, and a comma now signifies partial differentiation with respect to the primed coordinates. To simplify notation, we shall from now on drop the primes on the coordinates.

We now look for a perturbation solution of the form

$$\rho v^2 = X_0 + \varepsilon^2 X_1 + \cdots, \quad \boldsymbol{u} = \boldsymbol{u}^{(0)} + \varepsilon\boldsymbol{u}^{(1)} + \varepsilon^2\boldsymbol{u}^{(2)} + \cdots, \tag{2.8}$$

where X_0, X_1 are constants and $\boldsymbol{u}^{(k)}$ (k=1, 2, ...) are vector functions to be determined. Obviously, the solution $(X_0, \boldsymbol{u}^{(0)})$ describes a surface wave when the surface is flat. Our aim is to find the leading-order correction $\varepsilon^2 X_1$ when the surface is specified by (2.1). We observe that the speed correction is assumed to be of order ε^2. This is due to the fact that it will be determined at the third order of our successive approximations.

On substituting (2.8) into (2.6) and (2.7) and then equating coefficients of like powers of ε, we obtain, from the first three orders respectively, that

leading order:

$$c_{i\alpha k\beta}u^{(0)}_{k,\alpha\beta} - X_0 u^{(0)}_{i,11} = 0, \tag{2.9}$$

$$c_{i2k\alpha}u^{(0)}_{k,\alpha} = 0, \quad \text{on } \ x_2 = 0; \tag{2.10}$$

second order:

$$c_{i\alpha k\beta}u^{(1)}_{k,\alpha\beta} - X_0 u^{(1)}_{i,11} = -(c_{i\alpha k3} + c_{i3k\alpha})(u^{(0)}_{k,3\alpha} + h' u^{(0)}_{k,2\alpha}), \tag{2.11}$$

$$c_{i2k\alpha}u^{(1)}_{k,\alpha} = -h'(c_{i3k\alpha}u^{(0)}_{k,\alpha} + c_{i2k3}u^{(0)}_{k,2}) - c_{i2k3}u^{(0)}_{k,3}, \quad \text{on } \ x_2 = 0; \tag{2.12}$$

third order:

$$c_{i\alpha k\beta}u^{(2)}_{k,\alpha\beta} - X_0 u^{(2)}_{i,11} = X_1 u^{(0)}_{i,11} - (c_{i\alpha k3} + c_{i3k\alpha})(u^{(1)}_{k,3\alpha} + h' u^{(1)}_{k,2\alpha})$$

$$-c_{i3k3}(u^{(0)}_{k,33} + h'' u^{(0)}_{k,2} + 2h' u^{(0)}_{k,23} + h'^2 u^{(0)}_{k,22}), \tag{2.13}$$

$$c_{i2k\alpha}u^{(2)}_{k,\alpha} = -h'(c_{i3k\alpha}u^{(1)}_{k,\alpha} + c_{i2k3}u^{(1)}_{k,2}) - c_{i2k3}u^{(1)}_{k,3}$$

$$-c_{i3k3}(h' u^{(0)}_{k,3} + h'^{\,2} u^{(0)}_{k,2}), \quad \text{on } \ x_2 = 0. \tag{2.14}$$

2.2 The leading-order problem

The leading-order problem (2.9)-(2.10) is the classical surface-wave problem. The solution of the leading order surface wave problem may be written in the form

$$\boldsymbol{u}^{(0)} = f(kx_3)\boldsymbol{z}(kx_2)\mathrm{e}^{\mathrm{i}k(x_1-vt)} + \text{c.c.}, \tag{2.15}$$

where c.c. denotes the complex conjugate of the preceding term, k is the wave number and $f(kx_3)$ is a function to be determined. The depth variation $\boldsymbol{z}(kx_2)$ may be represented by

$$\boldsymbol{z}(kx_2) = \mathrm{e}^{-kx_2E}\boldsymbol{z}(0), \tag{2.16}$$

where E is a 3×3 matrix whose eigenvalues determine the decaying rate; see Fu and Mielke (2002). We shall initially set $k = 1$, and then show at a later stage (see the discussion leading to (2.70)) how to obtain the corresponding results when k is not unity.

On substituting (2.15) with $k = 1$ into (2.9) and (2.10), we find that the equations of motion reduce to

$$T\boldsymbol{z}''(x_2) + \mathrm{i}(R + R^T)\boldsymbol{z}'(x_2) - Q^{(v)}\boldsymbol{z}(x_2) = 0, \quad 0 < x_2 < \infty, \tag{2.17}$$

and the boundary conditions to $\boldsymbol{t}(0) = 0$, where the reduced traction vector $\boldsymbol{t}$ is given by

$$-\boldsymbol{t}(x_2) = T\boldsymbol{z}'(x_2) + \mathrm{i}R^T\boldsymbol{z}(x_2), \tag{2.18}$$

and the matrices $T, R, Q^{(v)}$ are defined by their components

$$T_{kl} = c_{k2l2}, \quad R_{kl} = c_{k1l2}, \quad Q^{(v)}_{kl} = c_{k1l1} - X_0\delta_{kl}. \tag{2.19}$$

On substituting a trial solution of the form $\boldsymbol{z} = \boldsymbol{a}\mathrm{e}^{\mathrm{i}px_2}$ into (2.17), we obtain

$$\left(p^2T + p(R + R^T) + Q^{(v)}\right)\boldsymbol{a} = 0, \tag{2.20}$$

so that the values of p are determined by setting the determinant of coefficient of $\boldsymbol{a}$ to zero. For v in the subsonic interval (Chadwick and Smith 1977), none of the values of p can be purely real. When the six values of p are distinct (as three pairs of complex conjugates), the surface wave solution can be written as

$$\boldsymbol{z}(x_2) = \sum_{k=1}^{3} \tilde{c}_k\boldsymbol{a}^{(k)}\mathrm{e}^{\mathrm{i}p_kx_2} = A\langle\mathrm{e}^{\mathrm{i}px_2}\rangle\boldsymbol{c} = A\langle\mathrm{e}^{\mathrm{i}px_2}\rangle A^{-1}\boldsymbol{z}(0) = \mathrm{e}^{\mathrm{i}A\langle p\rangle A^{-1}x_2}\boldsymbol{z}(0), \tag{2.21}$$

where p_1, p_2, p_3 are the eigenvalues of (2.20) with positive imaginary part, $\boldsymbol{a}^{(k)}$ $(k = 1, 2, 3)$ the associated eigenvectors, $\boldsymbol{c} = (\tilde{c}_1, \tilde{c}_2, \tilde{c}_3)^T$ is a constant vector, and

$$\langle\mathrm{e}^{\mathrm{i}px_2}\rangle = \mathrm{diag}\left\{\mathrm{e}^{\mathrm{i}p_1x_2}, \mathrm{e}^{\mathrm{i}p_2x_2}, \mathrm{e}^{\mathrm{i}p_3x_2}\right\}, \quad \langle p\rangle = \mathrm{diag}\left\{p_1, p_2, p_3\right\}, \quad A = [\boldsymbol{a}^{(1)}, \boldsymbol{a}^{(2)}, \boldsymbol{a}^{(3)}].$$

The last expression in (2.21) then shows that in this case the matrix E in (2.16) is equal to

$-\mathrm{i}A\langle p\rangle A^{-1}$.

When the six values of p are not distinct, the matrix E can be determined as follows. First, with the use of (2.17) and (2.18), the first order derivatives $\boldsymbol{z}'(x_2)$ and $\boldsymbol{t}'(x_2)$ can easily be written as a linear combination of $\boldsymbol{z}(x_2)$ and $\boldsymbol{t}(x_2)$, thus leading to

$$\begin{pmatrix} \boldsymbol{z}'(x_2) \\ \mathrm{i}\boldsymbol{t}'(x_2) \end{pmatrix} = \mathrm{i}N \begin{pmatrix} \boldsymbol{z}(x_2) \\ \mathrm{i}\boldsymbol{t}(x_2) \end{pmatrix}, \quad N = \begin{pmatrix} N_1 & N_2 \\ N_3 & N_1^T \end{pmatrix}, \tag{2.22}$$

the so-called Stroh formalism, with N_1, N_2 and N_3 given by

$$N_1 = -T^{-1}R^T, \;\; N_2 = T^{-1}, \;\; N_3 = RT^{-1}R^T - Q + X_0 I. \tag{2.23}$$

Next, we define the *surface-impedance matrix* M through

$$-\boldsymbol{t}(0) = M\boldsymbol{z}(0). \tag{2.24}$$

Since the half-space is homogeneous, the above relation implies that

$$-\boldsymbol{t}(x_2) = M\boldsymbol{z}(x_2) \quad \forall \;\; x_2 > 0. \tag{2.25}$$

On substituting (2.25) and (2.16) into (2.22), we find that the matrix *E* in (2.16) and the surface

impedance matrix are related by

$$E = T^{-1}(M + \mathrm{i}R^T), \tag{2.26}$$

and that M satisfies the Riccati matrix equation

$$(M - \mathrm{i}R)T^{-1}(M + \mathrm{i}R^T) - Q^{(v)} = 0. \tag{2.27}$$

It follows from the definition (2.24) of the impedance matrix that the traction-free boundary condition $\boldsymbol{t}(0) = \mathbf{0}$ can be satisfied only if

$$\det M = 0, \tag{2.28}$$

which is the secular equation determining X_0. When a root of this equation is found, a solution of $\boldsymbol{z}(0)$ can be obtained by solving $M\boldsymbol{z}(0) = 0$, and the corresponding surface wave solution is then given by (2.15) and (2.16).

Finally, we note that although (2.27) has multiple solutions, it has a unique solution for M that is positive definite for v less than the unique surface wave speed, and this unique solution is what should be selected in calculating the surface wave speed according to (2.28) and E according to (2.26) (Fu and Mielke 2002).

For an orthotropic elastic half-space whose axes of symmetry coincide with the coordinate

axes, the three matrices $T, R, Q^{(v)}$ take the simple forms

$$T = \begin{pmatrix} T_1 & 0 & 0 \\ 0 & T_2 & 0 \\ 0 & 0 & T_3 \end{pmatrix}, \quad R = \begin{pmatrix} 0 & R_1 & 0 \\ R_2 & 0 & 0 \\ 0 & 0 & 0 \end{pmatrix}, \quad Q^{(v)} = \begin{pmatrix} Q_1 & 0 & 0 \\ 0 & Q_2 & 0 \\ 0 & 0 & Q_3 \end{pmatrix}. \tag{2.29}$$

It can also be shown that the impedance matrix M then assumes the form

$$M = \begin{pmatrix} M_1 & M_3 + \mathrm{i}M_4 & 0 \\ M_3 - \mathrm{i}M_4 & M_2 & 0 \\ 0 & 0 & M_5 \end{pmatrix}, \quad M_i \in \mathbb{R}. \tag{2.30}$$

The Riccati matrix equation (2.27) can be solved exactly to give

$$M_1 = \sqrt{T_1 Q_1 - \frac{T_1}{T_2}\left(\frac{R_1 + R_2}{1+\gamma}\right)^2}, \quad M_2 = \gamma \frac{T_2}{T_1} M_1,$$

$$M_3 = 0, \quad M_4 = \frac{\gamma R_1 - R_2}{1+\gamma}, \quad M_5 = \sqrt{T_3 Q_3}, \tag{2.31}$$

where

$$\gamma = \sqrt{\frac{T_1 Q_2}{T_2 Q_1}}. \tag{2.32}$$

The secular equation (2.28) then takes the form

$$\sqrt{T_1 T_2 Q_1 Q_2} - \frac{\gamma R_1^2 + R_2^2}{1+\gamma} = 0. \tag{2.33}$$

For an isotropic elastic half-space, we have

$$T_1 = T_3 = \mu,\ T_2 = \lambda + 2\mu,\ Q_1 = \lambda + 2\mu - X_0,$$

$$Q_2 = Q_3 = \mu - X_0,\ R_1 = \lambda,\ R_2 = \mu,$$

and then the secular equation, once squared, reduces to the familiar classical form (1.63).

2.3 The second-order problem

We now assume that the $x_3 = 0$ plane is a plane of material symmetry, which is the case for monoclinic materials. In this case we may set $u_3^{(0)} = 0$. It can then readily be shown that $u_1^{(1)} = u_2^{(1)} = 0$, and the third component $u_3^{(1)}$ must take the form

$$u_3^{(1)} = (f' w_1 + f h' w_2) \mathrm{e}^{\mathrm{i}(x_1 - vt)} + \text{c.c.}, \tag{2.34}$$

where w_1 and w_2, both functions of x_2 only, (should not be confused with w_1 and w_2 in (3.31)) satisfy the following equations derived from (2.11) and (2.12):

$$c_{3232}w_1'' + 2\mathrm{i}c_{3132}w_1' - (c_{3131} - X_0)w_1 = -\mathrm{i}\boldsymbol{g}^{(1)} \cdot \boldsymbol{z} - \boldsymbol{g}^{(2)} \cdot \boldsymbol{z}', \tag{2.35}$$

$$\mathrm{i}c_{3231}w_1 + c_{3232}w_1' = -\boldsymbol{g}^{(4)} \cdot \boldsymbol{z}, \quad \text{on } \ x_2 = 0, \tag{2.36}$$

and

$$c_{3232}w_2'' + 2\mathrm{i}c_{3132}w_2' - (c_{3131} - X_0)w_2 = -\mathrm{i}\boldsymbol{g}^{(1)} \cdot \boldsymbol{z}' - \boldsymbol{g}^{(2)} \cdot \boldsymbol{z}'', \tag{2.37}$$

$$\mathrm{i}c_{3231}w_2 + c_{3232}w_2' = -(\mathrm{i}\boldsymbol{g}^{(3)} \cdot \boldsymbol{z} + \boldsymbol{g}^{(2)} \cdot \boldsymbol{z}'), \quad \text{on } \ x_2 = 0. \tag{2.38}$$

The four vectors $\boldsymbol{g}^{(1)}, \boldsymbol{g}^{(2)}, \boldsymbol{g}^{(3)}, \boldsymbol{g}^{(4)}$ in the above equations are defined by their components

$$g_\alpha^{(1)} = c_{31\alpha3} + c_{33\alpha1}, \quad g_\alpha^{(2)} = c_{32\alpha3} + c_{33\alpha2}, \quad g_\alpha^{(3)} = c_{33\alpha1}, \quad g_\alpha^{(4)} = c_{32\alpha3}. \tag{2.39}$$

To solve these two problems explicitly, we rewrite (2.21) in the form

$$z_\alpha = b_{\alpha\beta}\mathrm{e}^{\mathrm{i}p_\beta x_2}, \tag{2.40}$$

where the constants $b_{\alpha\beta}$ can in principle be obtained by comparing (2.40) with (2.16) and (2.21). For instance, when the half-space is isotropic, these constants are given, to within an multiplica-

tive constant, by

$$b_{11} = -2p_1p_2, \;\; b_{12} = p_1^2 - 1, \;\; b_{21} = 2p_2, \;\; b_{22} = p_2(p_1^2 - 1),$$

and

$$p_1 = p_3 = \mathrm{i}\sqrt{1 - X_0/\mu}, \quad p_2 = \mathrm{i}\sqrt{1 - X_0/(\lambda + 2\mu)}.$$

To solve the problem for w_1, we first note that a particular integral of (2.35) is given by

$$w_1 = s_1\mathrm{e}^{\mathrm{i}p_1x_2} + s_2\mathrm{e}^{\mathrm{i}p_2x_2} = s_\beta\mathrm{e}^{\mathrm{i}p_\beta x_2}, \tag{2.41}$$

where s_1 and s_2 are constants to be determined.

On substituting this into (2.35), making use of (2.40), and then comparing the coefficients of $\mathrm{e}^{\mathrm{i}p_\beta x_2}$, we obtain

$$s_\beta = \frac{\mathrm{i}g_\alpha^{(1)}b_{\alpha\beta} + \mathrm{i}g_\alpha^{(2)}b_{\alpha\beta}p_\beta}{c_{3232}p_\beta^2 + 2c_{3132}p_\beta + c_{3131} - X_0}, \quad \text{no summation on } \;\beta. \tag{2.42}$$

When the material is isotropic, the denominator of (2.42) becomes zero when $\beta = 1$. This is due to the fact that $p_1 = p_3$. In this case, (2.41) is modified to

$$w_1 = s_1x_2\mathrm{e}^{\mathrm{i}p_1x_2} + s_2\mathrm{e}^{\mathrm{i}p_2x_2}, \tag{2.43}$$

with the corresponding expressions for s_1 and s_2 given later in Section 2.5. Numerically, the case of isotropy can be dealt with by first considering a nearly isotropic material with e.g. moduli given by

$$c_{ijkl} = \lambda\delta_{ij}\delta_{kl} + \mu(\delta_{ik}\delta_{jl} + \delta_{il}\delta_{jk}) + \gamma\delta_{jl}\delta_{i2}\delta_{k2}, \tag{2.44}$$

and then taking the limit $\gamma \to 0$.

A general solution of (2.35) is then given by

$$w_1 = s_3 \mathrm{e}^{\mathrm{i}p_3 x_2} + s_\beta \mathrm{e}^{\mathrm{i}p_\beta x_2}, \tag{2.45}$$

where p_3 is the root of

$$c_{3232}p^2 + 2c_{3132}p + c_{3131} - X_0 = 0$$

with positive imaginary part, and s_3 is a disposable constant. We observe that such a p_3 exists only if $c_{3132}^2 - c_{3232}(c_{3131} - X_0) < 0$, that is if $X_0 < \rho v_t^2$, where v_t is the anti-plane shear body wave speed. In other words, the type of topography-guided surface wave solution under consideration only exists if the original surface wave on the associated flat half-space is subsonic. For the composites defined by (1.71) and (1.72) with $\boldsymbol{m} = (\cos\theta, \sin\theta, 0)^T$, Figure 2.2 shows the variation of $v_R(= \sqrt{X_0/\rho})$ and v_t with respect to the angle θ. It is seen that the subsonic condition is satisfied only for $0^\circ \le \theta < 24.37^\circ$, or $54.67^\circ < \theta \le 90^\circ$.

In Figure 2.3, we have shown the variation of $v_R(= \sqrt{X_0/\rho})$ and v_t with respect to the

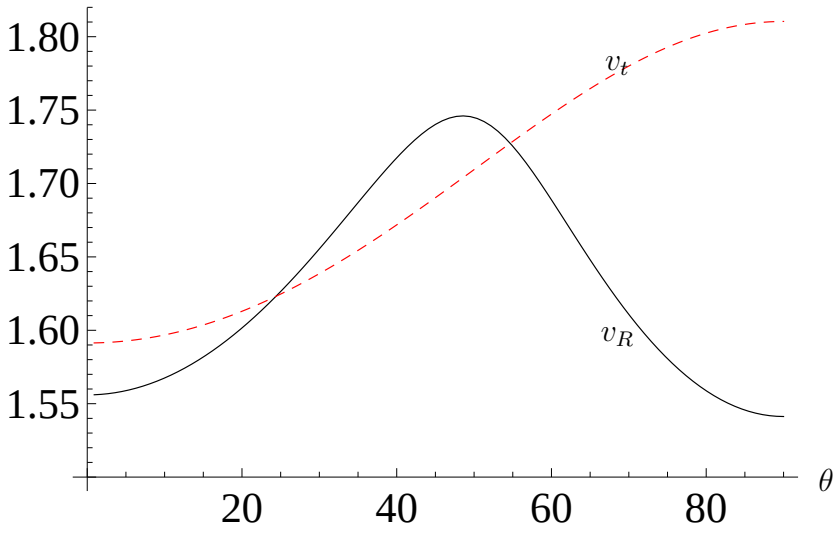

Figure 2.2: Variation of the leading-order surface wave speed v_R and anti-plane shear wave speed v_t against θ, showing that the 2D surface wave is subsonic only for $0^\circ \leq \theta < 24.37^\circ$, or $54.67^\circ < \theta \leq 90^\circ$. The unit of speed is km/s.

angle θ between the [100] direction and that of wave propagation, assuming that the surface waves propagates on the (001) plane of the silicon material described by (1.73). In this case the leading-order surface wave is subsonic for all the values of θ considered (Farnell 1970).

On substituting (2.45) into the boundary condition (2.36), we obtain

$$s_3 = \frac{\mathrm{i}g_\alpha^{(4)}(b_{\alpha 1} + b_{\alpha 2}) - c_{3231}(s_1 + s_2) - c_{3232}p_\beta s_\beta}{c_{3231} + c_{3232}p_3}. \tag{2.46}$$

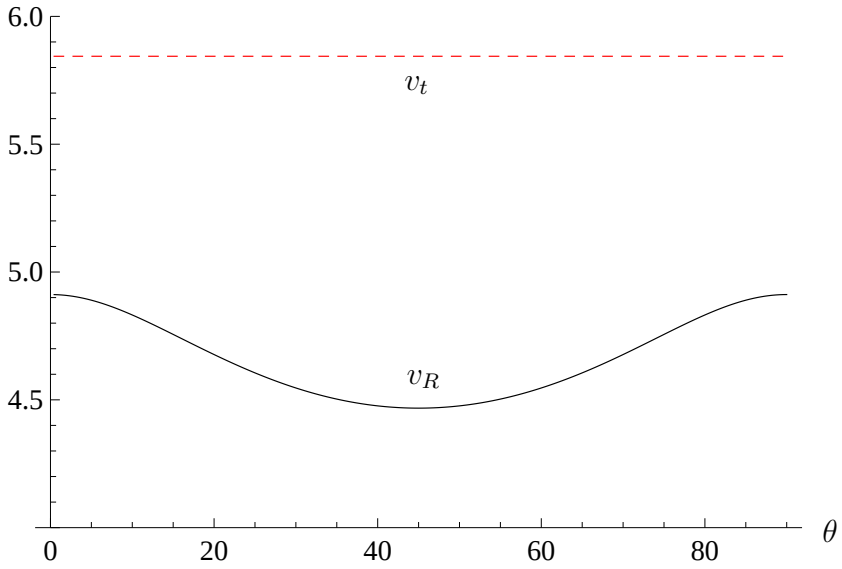

Figure 2.3: Variation of the leading-order surface wave speed v_R and anti-plane shear wave speed v_t against θ for a silicon material, showing that the 2D surface wave is subsonic for all values of θ.

Similarly, the problem for w_2 can be solved to yield

$$w_2 = t_3 \mathrm{e}^{\mathrm{i}p_3 x_2} + t_\beta \mathrm{e}^{\mathrm{i}p_\beta x_2}, \tag{2.47}$$

where

$$t_\beta = -\frac{g_\alpha^{(1)} b_{\alpha\beta} p_\beta + g_\alpha^{(2)} b_{\alpha\beta} p_\beta^2}{c_{3232} p_\beta^2 + 2c_{3132} p_\beta + c_{3131} - X_0}, \quad \text{no summation on } \beta. \tag{2.48}$$

and

$$t_3 = -\frac{g_\alpha^{(3)}(b_{\alpha 1} + b_{\alpha 2}) + g_\alpha^{(2)} b_{\alpha\beta} p_\beta + c_{3231}(t_1 + t_2) + c_{3232} p_\beta t_\beta}{c_{3231} + c_{3232} p_3}. \tag{2.49}$$

Thus, under the assumption that $x_3 = 0$ is a plane of material symmetry, the second order problem can be solved without having to impose any solvability conditions.

2.4 The third-order problem

If we write $\boldsymbol{u}^{(2)}$ as

$$\boldsymbol{u}^{(2)} = \boldsymbol{y}(x_2, x_3)\mathrm{e}^{\mathrm{i}(x_1 - vt)} + \text{c.c.}, \tag{2.50}$$

then the unknown vector function $\boldsymbol{y}(x_2, x_3)$ satisfies the following equations derived from (2.13) and (2.14)

$$T\boldsymbol{y}'' + \mathrm{i}(R + R^T)\boldsymbol{y}' - Q^{(v)}\boldsymbol{y} = \boldsymbol{h}^{(1)}, \tag{2.51}$$

$$T\boldsymbol{y}' + \mathrm{i}R^T\boldsymbol{y} = \boldsymbol{h}^{(2)}, \ \text{ on } x_2 = 0, \tag{2.52}$$

where a prime denotes partial differentiation with respect to x_2,

$$\boldsymbol{h}^{(1)} = -fX_1\boldsymbol{z} - \mathrm{i}\boldsymbol{g}^{(1)}\left\{f''w_1 + f'h'(w_2 + w_1') + f(h''w_2 + h'^2w_2')\right\}$$

$$-\boldsymbol{g}^{(2)}\left\{f''w_1' + f'h'(w_2' + w_1'') + f(h''w_2' + h'^2w_2'')\right\}$$

$$-f''S\boldsymbol{z} - 2f'h'S\boldsymbol{z}' - f(h''S\boldsymbol{z}' + h'^2S\boldsymbol{z}''), \tag{2.53}$$

$$\boldsymbol{h}^{(2)} = -\mathrm{i}\,(\boldsymbol{g}^{(1)} - \boldsymbol{g}^{(3)})(f'h'w_1 + fh'^2w_2) - (\boldsymbol{g}^{(2)} - \boldsymbol{g}^{(4)})[f''w_1 + (f'h' + fh'')w_2]$$

$$-\boldsymbol{g}^{(2)}(f'h'w_1' + fh'^2w_2') - f'h'S\boldsymbol{z} - fh'^2S\boldsymbol{z}', \tag{2.54}$$

and S is the matrix with components $c_{\alpha 3\beta 3}$.

It can easily be shown, by integrating by parts, that

$$\int_0^\infty \bar{\boldsymbol{z}} \cdot (T\boldsymbol{y}'' + \mathrm{i}(R + R^T)\boldsymbol{y}' - Q^{(v)}\boldsymbol{y})dx_2 = \bar{\boldsymbol{z}} \cdot (T\boldsymbol{y}' + \mathrm{i}R^T\boldsymbol{y})\big|_0^\infty .$$

Thus, the solvability condition for the inhomogeneous problem (2.51) and (2.52) is given by

$$\int_0^\infty \bar{\boldsymbol{z}} \cdot \boldsymbol{h}^{(1)}dx_2 = -\bar{\boldsymbol{z}} \cdot \boldsymbol{h}^{(2)}|_{x_2=0}. \tag{2.55}$$

We note that a similar solvability condition can be written down for the second order problem, but it can be shown to be automatically satisfied.

On substituting (2.53) and (2.54) into (2.55), we obtain

$$c_4 f''(x_3) + c_3 h' f'(x_3) + (c_2 h'^2 + c_1 h'' + c_0 X_1) f(x_3) = 0, \tag{2.56}$$

where

$$c_0 = \int_0^\infty |\boldsymbol{z}|^2 dx_2, \tag{2.57}$$

$$c_1 = \int_0^\infty \left\{ \mathrm{i}w_2 \bar{\boldsymbol{z}} \cdot \boldsymbol{g}^{(1)} - w_2 \bar{\boldsymbol{z}}' \cdot \boldsymbol{g}^{(2)} + \bar{\boldsymbol{z}} \cdot S\boldsymbol{z}' \right\} dx_2 - w_2(0)\bar{\boldsymbol{z}}(0) \cdot \boldsymbol{g}^{(4)}, \tag{2.58}$$

$$c_2 = \int_0^\infty \left\{ w_2(-\mathrm{i}\bar{\boldsymbol{z}}' \cdot \boldsymbol{g}^{(1)} + \bar{\boldsymbol{z}}'' \cdot \boldsymbol{g}^{(2)}) - \bar{\boldsymbol{z}}' \cdot S\boldsymbol{z}' \right\} dx_2$$

$$+ w_2(0)\boldsymbol{g}^{(2)} \cdot \bar{\boldsymbol{z}}'(0) - \mathrm{i}w_2(0)\boldsymbol{g}^{(3)} \cdot \bar{\boldsymbol{z}}(0), \tag{2.59}$$

$$c_3 = \int_0^\infty \left\{ \mathrm{i}(w_2 + w_1')\bar{\boldsymbol{z}} \cdot \boldsymbol{g}^{(1)} + (w_1'' + w_2')\bar{\boldsymbol{z}} \cdot \boldsymbol{g}^{(2)} + 2\bar{\boldsymbol{z}} \cdot S\boldsymbol{z}' \right\} dx_2$$

$$+ \mathrm{i}w_1(0)\bar{\boldsymbol{z}}(0) \cdot (\boldsymbol{g}^{(1)} - \boldsymbol{g}^{(3)}) + w_2(0)\bar{\boldsymbol{z}}(0) \cdot (\boldsymbol{g}^{(2)} - \boldsymbol{g}^{(4)})$$

$$+ w_1'(0)\bar{\boldsymbol{z}}(0) \cdot \boldsymbol{g}^{(2)} + \bar{\boldsymbol{z}}(0) \cdot S\boldsymbol{z}(0), \tag{2.60}$$

$$c_4 = \int_0^\infty \left\{ w_1(\mathrm{i}\bar{\boldsymbol{z}} \cdot \boldsymbol{g}^{(1)} - \bar{\boldsymbol{z}}' \cdot \boldsymbol{g}^{(2)}) + \bar{\boldsymbol{z}} \cdot S\boldsymbol{z} \right\} dx_2 - w_1(0)\bar{\boldsymbol{z}}(0) \cdot \boldsymbol{g}^{(4)}. \tag{2.61}$$

The coefficient c_0 is obviously real and positive. We now show that c_2 and c_4 are real, but c_3 is pure imaginary and is related to c_1 through $c_3 = 2\mathrm{i}\,\mathrm{Im}(c_1)$. We first define a differential operator $\mathcal{L}$ through

$$\mathcal{L}[w_1] = c_{3232}w_1'' + 2\mathrm{i}c_{3132}w_1' - (c_{3131} - X_0)w_1, \tag{2.62}$$

see (2.35). Then for any function $v(x_2)$, we have, by integrating by parts,

$$\int_0^\infty \bar{v}\mathcal{L}[w_1]dx_2 = \int_0^\infty \{c_{3232}[(w_1'\bar{v} - w_1\bar{v}')' + w_1\bar{v}'']$$

$$+ 2\mathrm{i}c_{3132}[(w_1\bar{v})' - w_1\bar{v}'] - (c_{3131} - X_0)w_1\bar{v}\}\, dx_2,$$

$$= \int_0^\infty w_1\overline{\mathcal{L}[v]}dx_2 - (\mathrm{i}c_{3132}w_1 + c_{3232}w_1')\bar{v}|_{x_2=0}$$

$$+\overline{(\mathrm{i}c_{3132}v+c_{3232}v')}w_1\Big|_{x_2=0}, \tag{2.63}$$

where an overbar signifies complex conjugation. With v replaced by w_1, the above identity shows that the expression

$$\int_0^\infty w_1\overline{\mathcal{L}[v]}dx_2+\overline{(\mathrm{i}c_{3132}v+c_{3232}v')}w_1\Big|_{x_2=0}$$

is real. With the further use of (2.34) and (2.35), we deduce that the expression

$$\int_0^\infty(\mathrm{i}w_1\bar{\boldsymbol{z}}\cdot\boldsymbol{g}^{(1)}-w_1\bar{\boldsymbol{z}}'\cdot\boldsymbol{g}^{(2)})dx_2-\boldsymbol{g}^{(4)}\cdot\bar{\boldsymbol{z}}(0)w_1(0)$$

is real. The reality of c_4 then follows from this result and the fact that S is a real symmetric matrix so that the extra term $\bar{\boldsymbol{z}}\cdot S\boldsymbol{z}$ is also real.

In a similar manner, on replacing v and w_1 in (2.63) by w_2 and making use of (2.36) and (2.37), we find that c_2 is also real. If, on the other hand, the v in (2.63) is replaced by w_2 and use is made of (2.34)–(2.37), we obtain

$$\int_0^\infty w_2(\mathrm{i}\bar{\boldsymbol{z}}\cdot\boldsymbol{g}^{(1)}-\bar{\boldsymbol{z}}'\cdot\boldsymbol{g}^{(2)})dx_2+\int_0^\infty\bar{w}_1(\mathrm{i}\bar{\boldsymbol{z}}'\cdot\boldsymbol{g}^{(1)}+\bar{\boldsymbol{z}}''\cdot\boldsymbol{g}^{(2)})dx_2$$

$$=w_2(0)\boldsymbol{g}^{(4)}\cdot\bar{\boldsymbol{z}}(0)-\bar{w}_1(0)[\mathrm{i}\boldsymbol{g}^{(3)}\cdot\bar{\boldsymbol{z}}(0)+\boldsymbol{g}^{(2)}\cdot\bar{\boldsymbol{z}}'(0)]. \tag{2.64}$$

The relation $c_3-c_1=-\bar{c}_1$ then follows from this result after straightforward manipulations.

Thus, on writing f in the polar form

$$f(x_3) = r(x_3)\mathrm{e}^{\mathrm{i}\theta(x_3)}, \tag{2.65}$$

where $r(x_3)$ and $\theta(x_3)$ are to be determined, the complex amplitude equation (2.56) provides the two real equations:

$$c_4(r'' - r\theta'^2) - 2c_1^{(i)}r\theta'h' + (c_2h'^2 + c_1^{(r)}h'' + c_0X_1)r = 0, \tag{2.66}$$

and

$$\left(c_4r^2\theta' + c_1^{(i)}r^2h'\right)' = 0, \tag{2.67}$$

where $c_1^{(r)}$ and $c_1^{(i)}$ are the real and imaginary parts of c_1, respectively. The second equation (2.67) can be integrated immediately, with the corresponding integration constant zero since both f and h decays to zero as $x_3 \to \pm\infty$. On substituting the resulting expression for θ' into (2.66), we obtain

$$r'' + (d_2h'^2 + d_1h'' + d_0X_1)r = 0, \tag{2.68}$$

where

$$d_0 = \frac{c_0}{c_4}, \quad d_1 = \frac{c_1^{(r)}}{c_4}, \quad d_2 = \frac{c_2}{c_4} + (\frac{c_1^{(i)}}{c_4})^2.$$

Thus, the problem of finding the speed correction X_1 is reduced to solving the eigenvalue prob-

lem (2.68) subject to the decay conditions $r(x_3) \to 0$ as $x_3 \to \pm\infty$. We recall, however, that the above eigenvalue problem as been derived under the assumption that the wave number k in (2.15) is unity. For the case when k is not unity, we may observe that under the substitutions $kx_1 \to x_1$, $kx_2 \to x_2$ and $kx_3 \to x_3$, equations (2.9)-(2.14) remain the same, except that $h'(x_3)$ and $h''(x_3)$ should be replaced by $h'(k^{-1}x_3)$ and $k^{-1}h''(k^{-1}x_3)$, respectively. Equations (2.68) is then replaced by

$$r''(x_3) + (d_2 h'^2(\frac{x_3}{k}) + \frac{d_1}{k}h''(\frac{x_3}{k}) + d_0 X_1)r(x_3) = 0, \tag{2.69}$$

or equivalently, with another substitution $x_3/k \to x_3$ followed by $r(kx_3) \to r(x_3)$,

$$r''(x_3) + (d_2 k^2 h'^2(x_3) + d_1 k h''(x_3) + d_0 k^2 X_1)r(x_3) = 0, \tag{2.70}$$

which shows that the speed correction is dependent on the wave number. This conclusion can also be verified analytically by (2.76) later.

The amplitude equation (2.68) is recognized as a special case of the so-called time-independent Schrödinger equation

$$r''(x_3) + (V(x_3) + E)r(x_3) = 0, \tag{2.71}$$

associated with the potential well $V(x_3)$ and energy level E (a constant, which should not be

confused with the E in (2.16)). Under the assumption that

$$\int_{-\infty}^{\infty}(1+|x_3|)|V(x_3)|dx_3<\infty$$

Simon (1976) and Klaus (1977) have established the following general results concerning its negative eigenvalues.

(i) If there exists an eigenvalue when the potential well $V(x_3)$ is of sufficiently small amplitude, then the eigenvalue is unique and is given by

$$\sqrt{-E}=\frac{1}{2}I-\frac{1}{4}\int_{-\infty}^{\infty}V(x_3)\left\{|x_3|*V(x_3)\right\}dx_3+O(\delta^3), \tag{2.72}$$

where the star denotes convolution, I is defined by

$$I=\int_{-\infty}^{\infty}V(x_3)dx_3,$$

and δ is a small positive parameter characterizing the amplitude of $V(x_3)$.

(ii) A necessary and sufficient condition for the existence of the above-mentioned single eigenvalue is that the right hand side of (2.72) is positive. Thus, under the assumption that the *second term on the right hand side of (2.72) is one order of magnitude smaller than the first term*, this condition is $I\geq 0$ (note that if $I=0$ the second term on the right

hand side of (2.72) is automatically positive; see Simon 1976, p284).

(iii) Since increasing the amplitude of a potential can only increase the number of eigenvalues (Simon 1976, p284), the condition $I \geq 0$ is also sufficient for the existence of at least one eigenvalue even when the amplitude of V is not small.

For the special form of V in (2.68), we have

$$I = d_2 k^2 \int_{-\infty}^{\infty} h'^2 dx_3,$$

and so $I \geq 0$ if and only if $d_2 \geq 0$. However, when h is of small amplitude, h' and h'' are of the same order as h, while h'^2 is of higher order which should be ignored. As a result,

$$\int_{-\infty}^{\infty} V(x_3) \left\{ |x_3| * V(x_3) \right\} dx_3 = \int_{-\infty}^{\infty} V(x_3) \left\{ \int_{-\infty}^{\infty} |x_3 - y| V(y) dy \right\} dx_3$$

$$= d_1^2 \int_{-\infty}^{\infty} h''(x_3) \left\{ \int_{-\infty}^{\infty} |x_3 - y| h''(y) dy \right\} dx_3 + O(\delta^3). \tag{2.73}$$

In view of

$$\int_{-\infty}^{\infty} |x_3 - y| h''(y) dy = \int_{-\infty}^{x_3} (x_3 - y) h''(y) dy + \int_{x_3}^{\infty} (y - x_3) h''(y) dy$$

$$= x_3 \int_{-\infty}^{x_3} h''(y) dy - \int_{-\infty}^{x_3} y h''(y) dy + \int_{x_3}^{\infty} y h''(y) dy - x_3 \int_{x_3}^{\infty} h''(y) dy$$

$$= 2x_3 h'(x_3) - \left[y h'(y) - h(y) \right] \Big|_{-\infty}^{x_3} + \left[y h'(y) - h(y) \right] \Big|_{x_3}^{\infty}$$

$$= 2h(x_3), \tag{2.74}$$

we have

$$\int_{-\infty}^{\infty} V(x_3)\left\{|x_3| * V(x_3)\right\} dx_3 = 2d_1^2 \int_{-\infty}^{\infty} h(x_3)h''(x_3)dx_3 + O(\delta^3)$$

$$= 2d_1^2 \int_{-\infty}^{\infty} [(h(x_3)h'(x_3))' - h'^2(x_3)]dx_3 + O(\delta^3)$$

$$= -2d_1^2 \int_{-\infty}^{\infty} h'^2(x_3)dx_3 + O(\delta^3). \tag{2.75}$$

The two terms in the asymptotic expansion (2.72) are of the same order of magnitude and they combine to give

$$\sqrt{-d_0 X_1} = \frac{1}{2}(d_2 + d_1^2)k \int_{-\infty}^{\infty} h'^2 dx_3 + O(\delta^3). \tag{2.76}$$

Thus, the existence condition is in fact given by

$$d_2 + d_1^2 > 0. \tag{2.77}$$

This special case of V serves to demonstrate the fact that eigenvalues may still exist even if $I < 0$ (whether V has small amplitude or not). We highlight this fact since some authors have previously claimed that $I \geq 0$ is also necessary for the existence of an eigenvalue. This claim is only valid if the condition in italics in (ii) above is satisfied and if the potential is of sufficiently small amplitude.

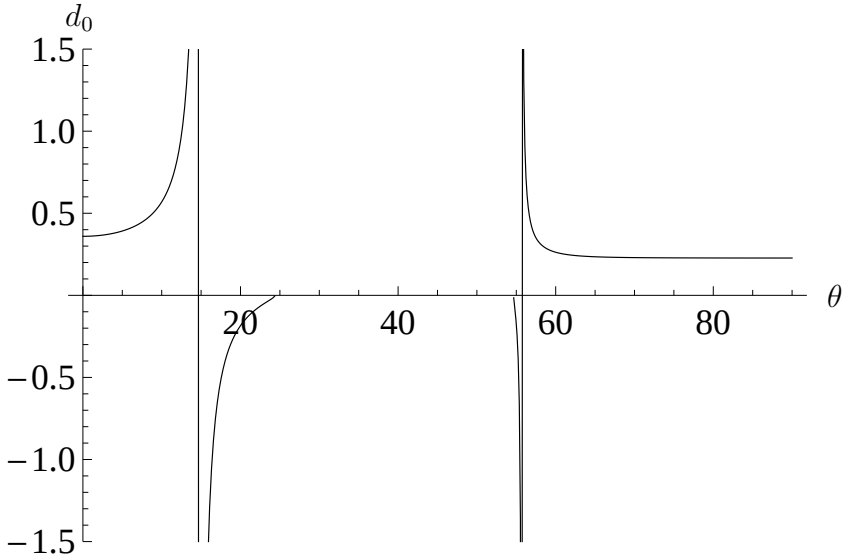

Figure 2.4: Variation of d_0 with respect to θ for the case considered in Fig.2.2

For the case corresponding to Fig.2.2, Figs.2.4-2.6 show the variations of the three coefficients for values of the angle θ for which the 2D surface wave is subsonic. The blow up behaviour corresponds to the fact that c_4 vanishes at $\theta = 14.8^\circ \text{ or } 55.7^\circ$ approximately. It is seen that d_2 is positive in both subsonic ranges (except at the two isolated values of θ where it blows up). It therefore follows immediately from the above general results that (2.68) has at least one eigenvalue. This fact is confirmed in our numerical calculations later. In contrast, for the silicon material defined by (1.73), Fig.2.7 shows that $d_2 + d_1^2$ is negative for all values of θ, and so the existence of eigenvalues cannot be established using the general results above.

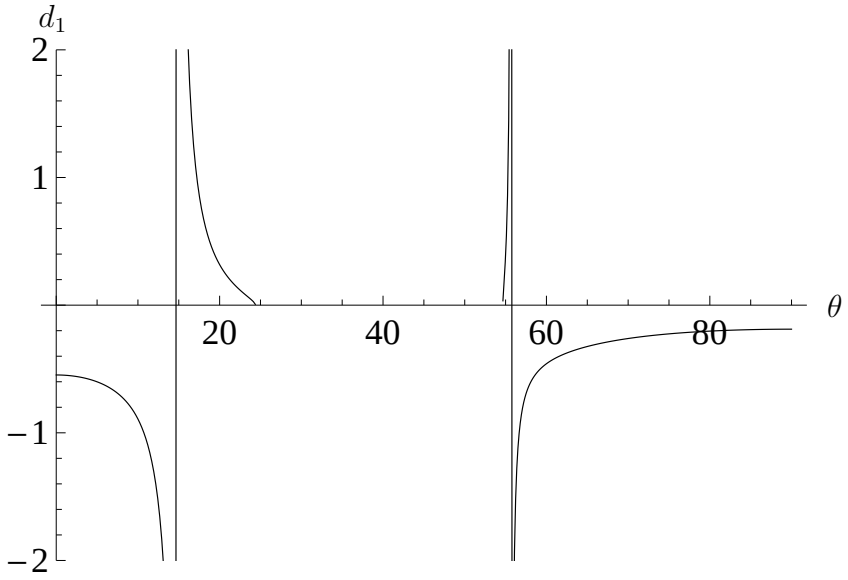

Figure 2.5: Variation of d_1 with respect to θ for the case considered in Fig.2.2

2.5 Isotropic materials

Before solving (2.68) subject to the decay conditions $r(\pm\infty) \to 0$ numerically, we first consider the special case when the material is isotropic. This case has previously been studied by Adams *et al.* (2007), using a procedure that is particularly developed for isotropic materials. We now show that our formulae recover their results in this special case.

First, to facilitate comparison, we write X_0 for X_0/μ throughout this section and introduce κ through $\kappa = \sqrt{(\lambda + 2\mu)/\mu}$. It follows from (1.62)$_1$ that $\kappa > \sqrt{4/3}$. Equation (1.63) can be rewritten as

$$X_0^3 - 8X_0^2 + \frac{8(3\kappa^2 - 2)}{\kappa^2} X_0 - 16\frac{\kappa^2 - 1}{\kappa^2} = 0. \tag{2.78}$$

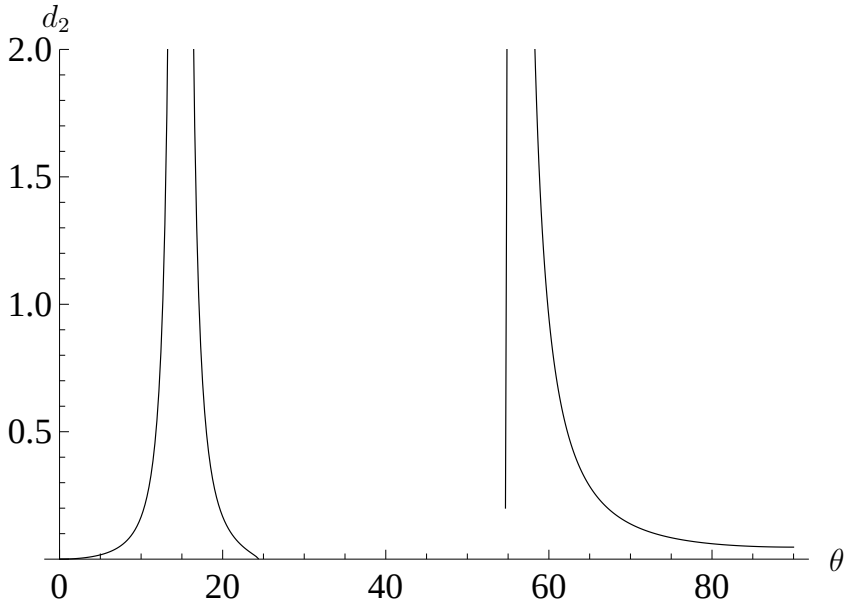

Figure 2.6: Variation of d_2 with respect to θ for the case considered in Fig.2.2

The second order problem now reduces to

$$w_1'' - (1 - X_0)w_1 = -\mathrm{i}\boldsymbol{g}^{(1)} \cdot \boldsymbol{z} - \boldsymbol{g}^{(2)} \cdot \boldsymbol{z}', \tag{2.79}$$

$$w_1' = -\boldsymbol{g}^{(4)} \cdot \boldsymbol{z}, \quad \text{on} \;\; x_2 = 0, \tag{2.80}$$

$$w_2'' - (1 - X_0)w_2 = -\mathrm{i}\boldsymbol{g}^{(1)} \cdot \boldsymbol{z}' - \boldsymbol{g}^{(2)} \cdot \boldsymbol{z}'', \tag{2.81}$$

$$w_2' = -\mathrm{i}\boldsymbol{g}^{(3)} \cdot \boldsymbol{z} - \boldsymbol{g}^{(2)} \cdot \boldsymbol{z}', \quad \text{on} \;\; x_2 = 0, \tag{2.82}$$

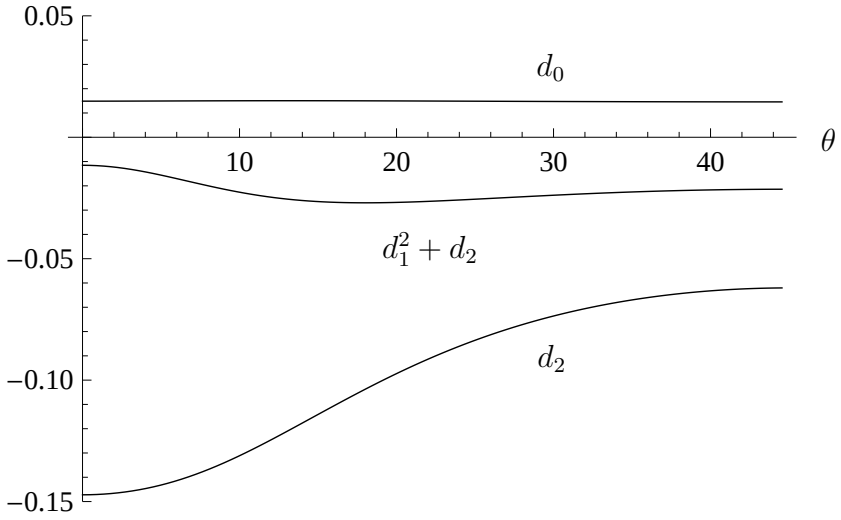

Figure 2.7: Variation of $d_0, d_1^2 + d_2$ and d_2 with respect to θ for the case considered in Fig.2.3

where

$$g_\alpha^{(1)} = (\kappa^2 - 1)\delta_{1\alpha}, \quad g_\alpha^{(2)} = (\kappa^2 - 1)\delta_{2\alpha}, \quad g_\alpha^{(3)} = \lambda\delta_{1\alpha}, \quad g_\alpha^{(4)} = \mu\delta_{2\alpha}.$$

It is then easy to establish that the solutions are given by

$$w_1 = s_1 x_2 \mathrm{e}^{\mathrm{i}p_1 x_2} + s_2 \mathrm{e}^{\mathrm{i}p_2 x_2} + s_3 \mathrm{e}^{\mathrm{i}p_3 x_2},$$

and

$$w_2 = t_1 x_2 \mathrm{e}^{\mathrm{i}p_1 x_2} + t_2 \mathrm{e}^{\mathrm{i}p_2 x_2} + t_3 \mathrm{e}^{\mathrm{i}p_3 x_2},$$

with

$$s_1 = 0, \quad s_2 = \mathrm{i}(2 - X_0), \quad s_3 = -2\mathrm{i}\sqrt{1 - X_0}\sqrt{1 - \frac{X_0}{\kappa^2}},$$

$$t_1 = 0, \quad t_2 = \mathrm{i}(X_0 - 2)\sqrt{1 - \frac{X_0}{\kappa^2}}, \quad t_3 = 2\mathrm{i}\sqrt{1 - \frac{X_0}{\kappa^2}}.$$

As a result, the expressions (2.57)–(2.61) can be evaluated explicitly to give $c_3 = 0$, $c_2 = 0$, and

$$c_0 = \frac{2\hat{c}_0}{2 - X_0}, \quad c_1 = \frac{\hat{c}_1}{\kappa^4}, \quad c_4 = \frac{32(1 - \kappa^2)\hat{c}_4}{(X_0 - 2)^2(\sqrt{1 - X_0} + \sqrt{1 - \frac{X_0}{\kappa^2}})\kappa^6}, \tag{2.83}$$

where

$$\hat{c}_0 = \sqrt{1 - X_0} + 4(1 - \frac{X_0}{\kappa^2})^{3/2} + (1 - X_0)^{3/2}(2 - \frac{X_0}{\kappa^2}) + 7\sqrt{1 - X_0}(-1 + \frac{X_0}{\kappa^2}),$$

$$\hat{c}_1 = X_0^2(14\kappa^2 - 4\kappa^4) + 4X_0(8 - 14\kappa^2 + 3\kappa^4) - 8(4 - 5\kappa^2 + \kappa^4),$$

$$\hat{c}_4 = 52 - 64\kappa^2 + 12\kappa^4 + X_0(-44 + 81\kappa^2 - 17\kappa^4) + X_0^2(-8 - 13\kappa^2 + 4\kappa^4).$$

By cross multiplication, followed by repeated use of (2.78) to eliminate powers of X_0 higher than 3, we have verified using *Mathematica* that our c_4/c_1 and c_4/c_0 are equal to Adams *et al.*'s (2007) $\beta A/B$ and A/C, respectively. The β is the wave number and this reinforce our previous conclusion that the value of X_1 is dependent on the wave number. Additionally, as a check on our derivations, we have used the elastic moduli given by (2.44) to compute the coefficients for

increasingly small γ and have obtained the same values as the above explicit expressions.

We observe that with $d_2 = 0$ the sufficient condition (2.77) is satisfied automatically, and so we may conclude that topography-guided surface waves always exist in an isotropic material. This settles the existence question left open in Adams *et al.* (2007). We may further conclude that when the geometric inhomogeneity is of sufficiently small amplitude, there can only exist a single guided surface wave. Finally, it can easily be verified numerically that c_0/c_4 (=d_0) is positive for all $\kappa > \sqrt{4/3}$. We thus conclude that all topography-guided surface waves on an isotropic elastic half-space travel at a slower speed than the classical Rayleigh wave (see (2.85) below, and also Theorem 1 in Bonnet-Ben Dhia and Joly 1999).

2.6 Numerical results

We still focus on the case $k = 1$. The amplitude equation (2.68) is now solved subject to the decay conditions $r(\pm\infty) \to 0$. We now use shooting method to numerically solve for X_1 and by comparing it with the analytical expression of X_1 (2.76), both results are consistent with each other. We first note that in the limit $x_3 \to \pm\infty$, equation (2.68) can be approximated by

$$r''(x_3) + d_0 X_1 r(x_3) = 0. \tag{2.84}$$

It is clear that $r(x_3)$ will have the required decay behaviour as $x_3 \to \pm\infty$ only if

$$d_0 X_1 < 0, \tag{2.85}$$

and when this is satisfied we have

$$r(x_3) \sim e^{\mp\sqrt{-d_0 X_1}x_3} \quad \text{as} \quad x_3 \to \pm\infty. \tag{2.86}$$

It then follows that if $d_0 < 0$ the topography-guided surface waves travel at a lower speed than their 2D counterpart; whereas if $d_0 > 0$ then the topography-guided surface waves are faster than their 2D counterpart. When $h(x_3)$ is an even function of x_3, $r(-x_3)$ is a solution of (2.68) whenever $r(x_3)$ is a solution. Thus, the eigen solutions of (2.68) are either even or odd. For the even (symmetric) modes, we impose the condition

$$r(0) = 1, \quad r'(0) = 0, \tag{2.87}$$

and the decay behaviour through

$$e(X_1) \equiv r'(L) + \sqrt{-d_0 X_1}\, r(L) = 0, \tag{2.88}$$

where L is a sufficiently large positive constant and the first equation defines the error function $e(X_1)$. In Mathematica, L is a finite number at which the amplitude is infinitesimal to approximate its decay behaviour at infinity. At the interval $[0, L]$, for each fixed shooting parameter X_1, with "NDSolve" $e(X_1)$ can be evaluated after integrating (2.68) subjected to the initial conditions (2.87). We first plot $e(X_1)$ against X_1 to show the approximate locations of any zeros and then use Newton's method to find the exact values of the zeros.

For the odd (anti-symmetric) modes, the initial conditions (2.87) are replaced by

$$r(0) = 0, \quad r'(0) = 1, \tag{2.89}$$

and we integrate (2.56) subject to the initial conditions (2.89) and iterate on X_1 in order to satisfy the decay condition (2.88).

When $h(x_3)$ is not an even function of x_3, the eigen modes do not have any symmetry properties. We may, for instance, integrate (2.68) subject to (2.88) and

$$r'(-L) - \sqrt{-d_0 X_1} r(-L) = 0, \tag{2.90}$$

respectively, and iterate on X_1 so that the two solutions have the same gradient at a matching point, say $x_3 = 0$.

The above numerical scheme is first tested on the eigenvalue problem

$$r''(x_3) + (-\lambda + n(n+1)\text{sech}^2 x_3) r(x_3) = 0, \quad r(\pm\infty) = 0, \quad n \text{ integer}, \tag{2.91}$$

which has n eigenvalues given by $\lambda = i^2, (i = 1, 2, ..., n)$, with odd i corresponding to odd modes and even i to even modes; see, e.g., Lamb (1980, p.37). Our scheme is able to reproduce these exact results correctly. The numerical scheme is then applied to solve (2.68) for a variety of $h(x_3)$ and different values of d_1 and d_2. Our numerical results confirm the validity of the asymptotic formula (2.76) and the existence condition (2.77). In particular, we invariably find that for h sufficiently small, the single eigenvalue tends to zero when $d_2 + d_1^2$ approaches zero from above, and there is no eigenvalue when $d_2 + d_1^2 \leq 0$.

We now present illustrative calculations for the composite material defined by (1.72) and for the case when the topography is described by the 'Gaussian bump' $h(x_3) = e^{-x_3^2}$ (recall that all length variables have been scaled by the wavelength of the surface wave). When $\theta = 2.194°$, we have $d_0 = 0.365$ and the corresponding X_1 must necessarily be negative. It is found that there is only a single solution which is symmetric with $X_1 = -0.146$ (the unit of X_1 is $10^9 N/m^2$) and so the topography has the effect of reducing the 2D surface wave speed. The corresponding profile of $r(x_3)$ is shown in figure 2.8.

When $\theta = 16.821°$, we have $d_0 = -0.750$ and the corresponding X_1 must necessarily be positive. It is found that there exists one odd solution and one even solution, corresponding

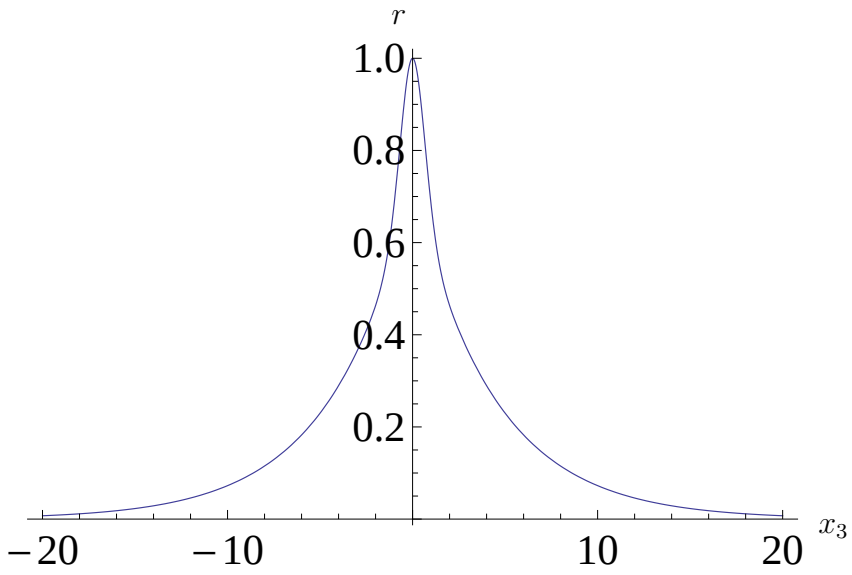

Figure 2.8: Lateral variation of the only topography-guided surface wave possible when $\theta = 2.194°$, whose speed is lower than its 2D counterpart ($X_1 = -0.146$).

to $X_1 = 0.186$ and $X_1 = 0.469$, respectively. The topography has the effect of producing two variations of the original 2D surface wave. Both waves have a higher speed than their 2D counterpart and their lateral variations are shown in figure 2.9.

We have also carried out calculations for the silicon material defined by (1.73) for which $d_2 + d_1^2 < 0$ for all values of θ. We have tried a large number of h profiles, such as $h(x_3) = e^{-x_3^2}$, $h(x_3) = \mathrm{Sech} x_3$ and $h(x_3) = \mathrm{Sech}(x_3 - 2) + \mathrm{Sech}(x_3 + 2)$, but have found no eigenvalues for (2.68).

As the end of this chapter, I would like to highlight some beautiful findings besides the last paragraph in Section 2.5 about isotropic materials, and point to possible future developments.

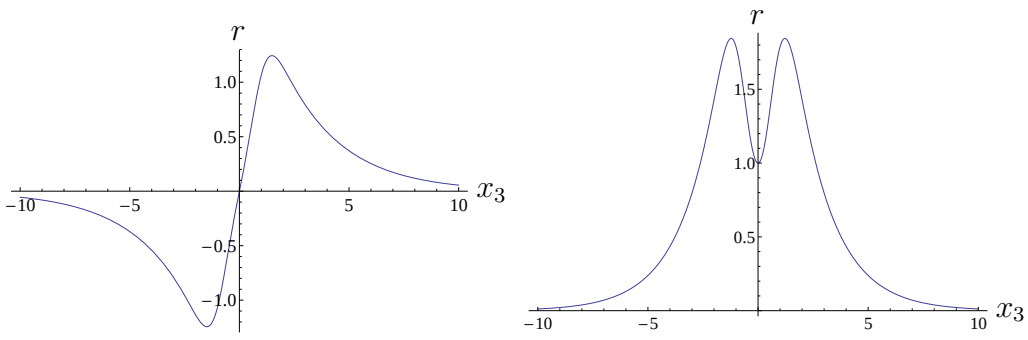

Figure 2.9: Lateral variations of the two topography-guided surface waves possible when $\theta = 16.821°$, whose speeds are higher than their 2D counterpart. The anti-symmetric and symmetric profiles correspond to the eigenvalues $X_1 = 0.186$ and $X_1 = 0.469$, respectively.

when doing numerical experiment on an anisotropic material in Mathematica, we found that the coefficients c_0,...c_4 in the amplitude equation are no longer real but complex. To overcome this difficulty, we tried writing the amplitude function in the polar form, the complex amplitude equation is then transformed into a real one, which is beautiful because of its Schrödinger equation form. Inspired by previous research results on Schrödinger equation, we have (2.76), which has been verified numerically using shooting method analyzing linear isotropic materials, transversely isotropic materials and cubic materials. The existence condition of X_1 given analytically by (2.77) is also obtained.

There are still new questions left open in current anisotropic problem. Firstly, when the $x_3 = 0$ plane is not a plane of material symmetry, the present methodology does not apply. Secondly, there is possibility that the coefficient of the second-order derivative term c_4 in the reduced eigenvalue problem vanishes, in which case a topography-guided surface wave, if it

exists, may be expected to behave very differently.

Chapter 3

Waves propagating in an anisotropic plate with elastically restrained boundary conditions (ERBC)

In this chapter, we focus on wave propagation in an anisotropic plate with elastically restrained boundary conditions. We use the Stroh formalism and we confine the problem to the two dimensional case. Unlike in the previous chapter where the wave number was scaled to be unity, here the wave number becomes a variable in the expression of frequency or wave speed, and the decay condition and traction free boundary condition do not have to be satisfied anymore. The symmetry of material and boundary conditions enables us to decompose the implicit dis-

persion relation into anti-symmetric and symmetric components. For each mode, by taking the long wave limit of the dispersion relation, the solution branches are classified into two families according to different cut-off frequencies: thickness shear and thickness stretch resonance frequencies. In the short wave region, the behavior of wave solutions is also studied. Based on numerical experiments, several asymptotic balances of the dispersion relation are possible. Using a similar perturbation method to that employed for surface waves, our asymptotic expansions of wave speed (or frequency) are established and can accurately predict the behavior of wave solutions for linear isotropic and transversely isotropic materials in both long wave and short wave regions.

3.1 Derivation of dispersion relation

Consider a plane strain problem concerning waves propagation along an arbitrary direction parallel to the face of an infinite plate. A Cartesian coordinate system $Ox_1x_2x_3$ is chosen, with origin O in the mid-plane and Ox_2 normal to the faces of the plate. The plate has uniform thickness $2h$ and is composed of linear homogeneous anisotropic elastic material with density ρ and elastic moduli c_{ijkl}. The transition between traction-free (Neumann) boundary conditions and fixed (Dirichlet) boundary conditions will be investigated by considering so-called elastically restrained boundary conditions (ERBC). This is essentially equivalent to having springs supported on both faces, see Figure 3.1.

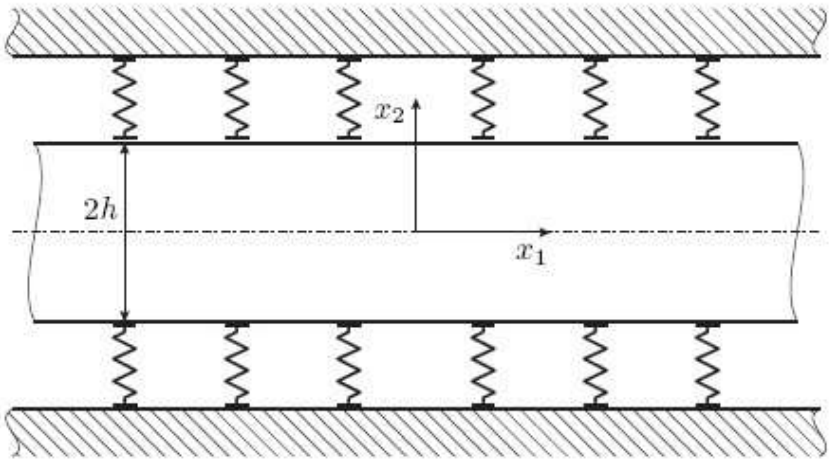

Figure 3.1: The coordinate system of the plate

For the case of elastically restrained boundary conditions, we may assume that the boundary conditions are given by

$$\alpha_1 w_2 t_1 + \frac{\delta_1}{h} u_1 = 0, \tag{3.1}$$

$$\alpha_2 t_2 + \frac{\delta_2}{w_2 h} u_2 = 0, \text{at } \; x_2 = h, \tag{3.2}$$

$$\alpha_3 w_2 t_1 + \frac{\delta_3}{h} u_1 = 0, \tag{3.3}$$

$$\alpha_4 t_2 + \frac{\delta_4}{w_2 h} u_2 = 0, \text{at } \; x_2 = -h, \tag{3.4}$$

where t_i and u_i are components of the traction on the upper or lower face and displacement on x_i direction, respectively; w_2, different from the w_2 in previous chapter, is an element in Stroh matrix and will be defined later in (3.31); α_i and δ_i are constants.

The boundary conditions may be presented in matrix form

$$D\boldsymbol{t} + F\boldsymbol{u} = 0, \text{at } \ x_2 = h, \tag{3.5}$$

$$G\boldsymbol{t} + H\boldsymbol{u} = 0, \text{at } \ x_2 = -h, \tag{3.6}$$

where

$$D = \begin{pmatrix} -\alpha_1 w_2 & 0 \\ 0 & \alpha_2 \end{pmatrix}, F = \begin{pmatrix} \frac{\delta_1}{h} & 0 \\ 0 & -\frac{\delta_2}{w_2 h} \end{pmatrix}, G = \begin{pmatrix} -\alpha_3 w_2 & 0 \\ 0 & \alpha_4 \end{pmatrix}, \tag{3.7}$$

$$H = \begin{pmatrix} \frac{\delta_3}{h} & 0 \\ 0 & -\frac{\delta_4}{w_2 h} \end{pmatrix}, \boldsymbol{t} = \begin{pmatrix} t_1 \\ t_2 \end{pmatrix}, \boldsymbol{u} = \begin{pmatrix} u_1 \\ u_2 \end{pmatrix}. \tag{3.8}$$

To simplify our analysis, and allow decoupling of dispersion relations, symmetry of boundary conditions is required. As a result, we will assume that $D = G,\ F = H$ in later analysis. This implies that $\alpha_1 = \alpha_3,\ \alpha_2 = \alpha_4,\ \delta_1 = \delta_3,\ \delta_2 = \delta_4$.

The displacement $\boldsymbol{u}(x_1, x_2)$ is assumed to have the general form

$$\boldsymbol{u}(x_1, x_2) = \boldsymbol{z}(kx_2)\mathrm{e}^{\mathrm{i}k(x_1 - \upsilon t)}, \tag{3.9}$$

with the traction on the upper face given by

$$\boldsymbol{t} = \boldsymbol{\sigma}\boldsymbol{n}_1 = c_{i2kl}u_{k,l} = (\mathrm{i}kR^T\boldsymbol{z}(kh) + kT\boldsymbol{z}'(kh))\mathrm{e}^{\mathrm{i}k(x_1-\upsilon t)}, \tag{3.10}$$

and the traction on the lower face being obtainable as

$$-\boldsymbol{t} = \boldsymbol{\sigma}\boldsymbol{n}_2 = -c_{i2kl}u_{k,l} = -(\mathrm{i}kR^T\boldsymbol{z}(-kh) + kT\boldsymbol{z}'(-kh))\mathrm{e}^{\mathrm{i}k(x_1-\upsilon t)}, \tag{3.11}$$

where $\boldsymbol{n}_1 = (0,1)$, $\boldsymbol{n}_2 = (0,-1)$, and the matrices *T, R, Q* are defined by

$$T_{ik} = c_{i2k2},\ R_{ik} = c_{i1k2},\ Q_{ik} = c_{i1k1}. \tag{3.12}$$

We shall now define

$$\boldsymbol{t} = -\mathrm{i}k\boldsymbol{l}(kx_2)\mathrm{e}^{\mathrm{i}k(x_1-\upsilon t)}, \tag{3.13}$$

so that

$$-\mathrm{i}\boldsymbol{l}(kx_2) = \mathrm{i}R^T\boldsymbol{z}(kx_2) + T\boldsymbol{z}'(kx_2), \tag{3.14}$$

which implies that

$$-\mathrm{i}\boldsymbol{l}'(kx_2) = \mathrm{i}R^T\boldsymbol{z}'(kx_2) + T\boldsymbol{z}''(kx_2). \tag{3.15}$$

The minus sign on the right-hand side of equation (3.13) follows the notation of Lothe and

Barnett's (1976), which determines the signs of every element in N_2 and $N_3 - \rho v^2 I$, and hence the signs of $H(x)$ and $F(x)$. We remark that the sign of the right-hand side of equation (3.13) has no influence on the sign of $\bar{v}$, and hence the signs of $q_1,\ q_2,\ Q(x)$, which results in the same dispersion relation and the same asymptotic results for the frequency or $\bar{v}$.

The two boundary conditions (3.5) and (3.6) may now be expressed as

$$\mathrm{i}D\boldsymbol{l}(kh) - \frac{1}{k}F\boldsymbol{z}(kh) = 0, \qquad \mathrm{i}D\boldsymbol{l}(-kh) - \frac{1}{k}F\boldsymbol{z}(-kh) = 0. \tag{3.16}$$

Recalling the definitions (3.12), on substituting (3.9) into (1.12), we obtain

$$T\boldsymbol{z}''(kx_2) + \mathrm{i}(R + R^T)\boldsymbol{z}'(kx_2) - (Q - \rho v^2 I)\boldsymbol{z}(kx_2) = \mathbf{0}. \tag{3.17}$$

It is now possible to substitute (3.15) into (3.17) to establish that

$$\mathrm{i}R\boldsymbol{z}'(kx_2) - \mathrm{i}\boldsymbol{l}'(kx_2) - (Q - \rho v^2 I)\boldsymbol{z}(kx_2) = 0. \tag{3.18}$$

Equation (3.14) is now employed to establish that

$$\boldsymbol{z}'(kx_2) = -\mathrm{i}T^{-1}R^T\boldsymbol{z}(kx_2) - \mathrm{i}T^{-1}\boldsymbol{l}(kx_2), \tag{3.19}$$

which on substituting into (3.18), enables us to conclude that

$$\boldsymbol{l}'(kx_2) = -\mathrm{i}(RT^{-1}R^T - Q + \rho v^2 I)\boldsymbol{z}(kx_2) - \mathrm{i}RT^{-1}\boldsymbol{l}(kx_2). \tag{3.20}$$

These two equations, (3.19) and (3.20), may now be incorporated into the form

$$\mathrm{i}N \begin{pmatrix} \boldsymbol{z}(kx_2) \\ \\ \boldsymbol{l}(kx_2) \end{pmatrix} = \begin{pmatrix} \boldsymbol{z}'(kx_2) \\ \\ \boldsymbol{l}'(kx_2) \end{pmatrix}, N = \begin{pmatrix} N_1 & N_2 \\ \\ N_3 - \rho v^2 I & N_1^T \end{pmatrix}, \tag{3.21}$$

where

$$N_1 = -T^{-1}R^T, \qquad N_2 = -T^{-1} = N_2^T, \qquad N_3 = -RT^{-1}R^T + Q. \tag{3.22}$$

Equation (3.21), together with (3.22), is known as the Stroh formalism.

We assume a solution of the general form

$$\begin{pmatrix} \boldsymbol{z}(kx_2) \\ \\ \boldsymbol{l}(kx_2) \end{pmatrix} = \boldsymbol{\zeta}\mathrm{e}^{\mathrm{i}kqx_2}. \tag{3.23}$$

We note that the corresponding form of q in Mukhomodyarov *et al.* (2010) differs, with their use of q instead of our iq on the right-hand side of (3.23). On substituting (3.23) into (3.21), we

obtain

$$N\boldsymbol{\zeta}_\alpha = q_\alpha \boldsymbol{\zeta}_\alpha, \alpha = 1,2,3,4, \boldsymbol{\zeta}_\alpha = \begin{pmatrix} \boldsymbol{a}^{(\alpha)} \\ \\ \boldsymbol{b}^{(\alpha)} \end{pmatrix}. \tag{3.24}$$

The above eigenvalue problem may now be solved to find the values of q and the associated eigenvectors $\boldsymbol{a}$ and $\boldsymbol{b}$. The general solution is therefore given by

$$\begin{pmatrix} \boldsymbol{z}(kx_2) \\ \\ \boldsymbol{l}(kx_2) \end{pmatrix} = \sum_{\alpha=1}^{4} \tilde{d}_\alpha \begin{pmatrix} \boldsymbol{a}^{(\alpha)} \\ \\ \boldsymbol{b}^{(\alpha)} \end{pmatrix} \mathrm{e}^{\mathrm{i}kq_\alpha x_2}, \ \tilde{d}_\alpha \text{ are constants.} \tag{3.25}$$

It follows that (using $\hat{q}_\alpha = \mathrm{i}q_\alpha$)

$$\boldsymbol{z}(\pm kh) = \sum_{\alpha=1}^{4} \tilde{d}_\alpha \boldsymbol{a}^{(\alpha)} (\cosh(\eta\hat{q}_\alpha) \pm \sinh(\eta\hat{q}_\alpha)), \tag{3.26}$$

$$\boldsymbol{l}(kh) = \sum_{\alpha=1}^{4} \tilde{d}_\alpha \boldsymbol{b}^{(\alpha)} (\cosh(\eta\hat{q}_\alpha) + \sinh(\eta\hat{q}_\alpha)), \tag{3.27}$$

$$\boldsymbol{l}(-kh) = -\sum_{\alpha=1}^{4} \tilde{d}_\alpha \boldsymbol{b}^{(\alpha)} (\cosh(\eta\hat{q}_\alpha) - \sinh(\eta\hat{q}_\alpha)), \tag{3.28}$$

where $\eta = kh$.

We will now study orthotropic materials. We use the Voigt notation to present elastic moduli with axes of symmetry along x_1, x_2, x_3; 11 is replaced by 1, 22 by 2, 33 by 3, 23 by 4, 31 by 5

and 12 by 6. For orthotropic materials, $c_{16} = c_{26} = 0$, and thus

$$Q = \begin{pmatrix} c_{11} & 0 \\ 0 & c_{66} \end{pmatrix}, R = \begin{pmatrix} 0 & c_{12} \\ c_{66} & 0 \end{pmatrix}, T = \begin{pmatrix} c_{66} & 0 \\ 0 & c_{22} \end{pmatrix}, \tag{3.29}$$

$$N_1 = \begin{pmatrix} 0 & -1 \\ w_1 & 0 \end{pmatrix}, N_2 = \begin{pmatrix} w_2 & 0 \\ 0 & w_3 \end{pmatrix}, N_3 = \begin{pmatrix} w_4 & 0 \\ 0 & 0 \end{pmatrix}, \tag{3.30}$$

where

$$w_1 = -\frac{c_{12}}{c_{22}},\ w_2 = -\frac{1}{c_{66}},\ w_3 = -\frac{1}{c_{22}},\ w_4 = c_{11} - \frac{c_{12}^2}{c_{22}}. \tag{3.31}$$

Let $\bar{v}^2 = -w_2\rho v^2,\ \kappa = \sqrt{\frac{-w_2}{-w_3}}$. Using Mathematica, we find that q satisfies the equation

$$q^4 + (2w_1 - w_4w_2 - \bar{v}^2 - \frac{\bar{v}^2}{\kappa^2})q^2 + (1 - \bar{v}^2)(w_1^2 - \frac{\bar{v}^2}{\kappa^2} - w_4w_3) = 0, \tag{3.32}$$

and we assume $q_3 = -q_1,\ q_4 = -q_2$. It is also found that

$$\boldsymbol{a}^{(\alpha)} = \begin{pmatrix} H(q_\alpha) \\ F(q_\alpha) \end{pmatrix}, \qquad \boldsymbol{b}^{(\alpha)} = \begin{pmatrix} Q(q_\alpha) \\ 1 \end{pmatrix}, \tag{3.33}$$

where

$$H(x) = \frac{x^2 + w_1 - \bar{v}^2 w_1}{-\frac{\bar{v}^2}{w_2} - w_4 - \frac{\bar{v}^2}{w_2}x^2 + \frac{\bar{v}^4}{w_2} + \bar{v}^2 w_4},$$

$$Q(x) = x\frac{w_4 + \frac{\bar{v}^2}{w_2} - \frac{\bar{v}^2}{w_2}w_1}{-\frac{\bar{v}^2}{w_2} - w_4 - \frac{\bar{v}^2}{w_2}x^2 + \frac{\bar{v}^4}{w_2} + \bar{v}^2 w_4},$$

$$F(x) = \frac{w_2 x}{\bar{v}^2} + \frac{w_2 Q(x)}{\bar{v}^2}. \tag{3.34}$$

On substituting the three equations (3.26)-(3.28), together with (3.33), into (3.16), we obtain

$$\tilde{d}_1(-\mathrm{i}\alpha_1 w_2 Q(q_1) - \tfrac{\delta_1}{\eta}H(q_1))E_1^+ + \tilde{d}_2(-\mathrm{i}\alpha_1 w_2 Q(q_2) - \tfrac{\delta_1}{\eta}H(q_2))E_2^+$$

$$+\tilde{d}_3(\mathrm{i}\alpha_1 w_2 Q(q_1) - \frac{\delta_1}{\eta}H(q_1))E_1^- + \tilde{d}_4(\mathrm{i}\alpha_1 w_2 Q(q_2) - \frac{\delta_1}{\eta}H(q_2))E_2^- = 0, \tag{3.35}$$

$$\tilde{d}_1(\mathrm{i}\alpha_2 + \tfrac{\delta_2}{w_2\eta}F(q_1))E_1^+ + \tilde{d}_2(\mathrm{i}\alpha_2 + \tfrac{\delta_2}{w_2\eta}F(q_2))E_2^+$$

$$+\tilde{d}_3(\mathrm{i}\alpha_2 - \frac{\delta_2}{w_2\eta}F(q_1))E_1^- + \tilde{d}_4(\mathrm{i}\alpha_2 - \frac{\delta_2}{w_2\eta}F(q_2))E_2^- = 0, \tag{3.36}$$

$$\tilde{d}_1(\mathrm{i}\alpha_1 w_2 Q(q_1) - \tfrac{\delta_1}{\eta}H(q_1))E_1^- + \tilde{d}_2(\mathrm{i}\alpha_1 w_2 Q(q_2) - \tfrac{\delta_1}{\eta}H(q_2))E_2^-$$

$$+\tilde{d}_3(-\mathrm{i}\alpha_1 w_2 Q(q_1) - \frac{\delta_1}{\eta}H(q_1))E_1^+ + \tilde{d}_4(-\mathrm{i}\alpha_1 w_2 Q(q_2) - \frac{\delta_1}{\eta}H(q_2))E_2^+ = 0, \tag{3.37}$$

$$\tilde{d}_1(-\mathrm{i}\alpha_2 + \tfrac{\delta_2}{w_2\eta}F(q_1))E_1^- + \tilde{d}_2(-\mathrm{i}\alpha_2 + \tfrac{\delta_2}{w_2\eta}F(q_2))E_2^-$$

$$+\tilde{d}_3(-\mathrm{i}\alpha_2 - \frac{\delta_2}{w_2\eta}F(q_1))E_1^+ + \tilde{d}_4(-\mathrm{i}\alpha_2 - \frac{\delta_2}{w_2\eta}F(q_2))E_2^+ = 0, \tag{3.38}$$

where $E_i^+ = \cosh(\eta\hat{q}_i) + \sinh(\eta\hat{q}_i),\ E_i^- = \cosh(\eta\hat{q}_i) - \sinh(\eta\hat{q}_i)$.

If equations (3.35) and (3.37) are added and subtracted, while equations (3.36) and (3.38) are added and subtracted, we obtain two systems: one system of two equations in $(\tilde{d}_1 + \tilde{d}_3)$ and $(\tilde{d}_2 + \tilde{d}_4)$, the other system of two equations in $(\tilde{d}_1 - \tilde{d}_3)$ and $(\tilde{d}_2 - \tilde{d}_4)$, namely

$$(\tfrac{\delta_1}{\eta}H(q_1)\cosh(\eta\hat{q}_1) + \mathrm{i}\alpha_1 w_2 Q(q_1)\sinh(\eta\hat{q}_1))(\tilde{d}_1 + \tilde{d}_3)$$

$$+(\frac{\delta_1}{\eta}H(q_2)\cosh(\eta\hat{q}_2) + \mathrm{i}\alpha_1 w_2 Q(q_2)\sinh(\eta\hat{q}_2))(\tilde{d}_2 + \tilde{d}_4) = 0, \tag{3.39}$$

$$(\mathrm{i}\alpha_2\cosh(\eta\hat{q}_1) + \tfrac{\delta_2}{w_2\eta}F(q_1)\sinh(\eta\hat{q}_1))(\tilde{d}_1 + \tilde{d}_3)$$

$$+(\mathrm{i}\alpha_2\cosh(\eta\hat{q}_2) + \frac{\delta_2}{w_2\eta}F(q_2)\sinh(\eta\hat{q}_2))(\tilde{d}_2 + \tilde{d}_4) = 0. \tag{3.40}$$

and

$$(\tfrac{\delta_1}{\eta}H(q_1)\sinh(\eta\hat{q}_1) + \mathrm{i}\alpha_1 w_2 Q(q_1)\cosh(\eta\hat{q}_1))(\tilde{d}_1 - \tilde{d}_3)$$

$$+(\frac{\delta_1}{\eta}H(q_2)\sinh(\eta\hat{q}_2) + \mathrm{i}\alpha_1 w_2 Q(q_2)\cosh(\eta\hat{q}_2))(\tilde{d}_2 - \tilde{d}_4) = 0, \tag{3.41}$$

$$(\mathrm{i}\alpha_2\sinh(\eta\hat{q}_1) + \tfrac{\delta_2}{w_2\eta}F(q_1)\cosh(\eta\hat{q}_1))(\tilde{d}_1 - \tilde{d}_3)$$

$$+(\mathrm{i}\alpha_2\sinh(\eta\hat{q}_2) + \frac{\delta_2}{w_2\eta}F(q_2)\cosh(\eta\hat{q}_2))(\tilde{d}_2 - \tilde{d}_4) = 0. \tag{3.42}$$

A non-trivial solution of (3.39) and (3.40) will exist provided

$$\begin{aligned}
&\mathrm{i}\frac{\alpha_2\delta_1}{\eta}(H(q_2)-H(q_1))\coth(\eta\hat{q}_1)\coth(\eta\hat{q}_2)+\mathrm{i}\frac{\alpha_1\delta_2}{\eta}(F(q_1)Q(q_2)-F(q_2)Q(q_1))\\
&+(\alpha_1\alpha_2 w_2 Q(q_1)+\frac{\delta_1\delta_2}{w_2\eta^2}F(q_1)H(q_2))\coth(\eta\hat{q}_2)\\
&-(\alpha_1\alpha_2 w_2 Q(q_2)+\frac{\delta_1\delta_2}{w_2\eta^2}F(q_2)H(q_1))\coth(\eta\hat{q}_1)=0. \qquad (3.43)
\end{aligned}$$

When (3.43) is satisfied, $\tilde{d}_1-\tilde{d}_3=\tilde{d}_2-\tilde{d}_4=0$, and the solution for $\boldsymbol{z}(kx_2)$ is given by

$$\boldsymbol{z}(kx_2)=\tilde{d}_1\begin{pmatrix} H(q_1)\cosh(k\hat{q}_1x_2)\\ F(q_1)\sinh(k\hat{q}_1x_2)\end{pmatrix}+\tilde{d}_2\begin{pmatrix} H(q_2)\cosh(k\hat{q}_2x_2)\\ F(q_2)\sinh(k\hat{q}_2x_2)\end{pmatrix}. \qquad (3.44)$$

Thus, we are able to conclude, from (3.44), that u_2 is an odd function about the mid-plane. It follows that (3.43) is the so-called symmetric dispersion relation. Classical extension shares similar dispersion relation.

Similarly, a non-trivial solution of (3.41) and (3.42) will exist provided

$$\begin{aligned}
&\mathrm{i}\frac{\alpha_2\delta_1}{\eta}(H(q_2)-H(q_1))\tanh(\eta\hat{q}_1)\tanh(\eta\hat{q}_2)+\mathrm{i}\frac{\alpha_1\delta_2}{\eta}(F(q_1)Q(q_2)-F(q_2)Q(q_1))\\
&+(\alpha_1\alpha_2 w_2 Q(q_1)+\frac{\delta_1\delta_2}{w_2\eta^2}F(q_1)H(q_2))\tanh(\eta\hat{q}_2)\\
&-(\alpha_1\alpha_2 w_2 Q(q_2)+\frac{\delta_1\delta_2}{w_2\eta^2}F(q_2)H(q_1))\tanh(\eta\hat{q}_1)=0, \qquad (3.45)
\end{aligned}$$

in which we have $\tilde{d}_1 + \tilde{d}_3 = \tilde{d}_2 + \tilde{d}_4 = 0$, and the general solution for $\boldsymbol{z}(kx_2)$ is given by

$$\boldsymbol{z}(kx_2) = \tilde{d}_1 \begin{pmatrix} H(q_1)\sinh(k\hat{q}_1 x_2) \\ F(q_1)\cosh(k\hat{q}_1 x_2) \end{pmatrix} + \tilde{d}_2 \begin{pmatrix} H(q_2)\sinh(k\hat{q}_2 x_2) \\ F(q_2)\cosh(k\hat{q}_2 x_2) \end{pmatrix}. \tag{3.46}$$

Thus u_2 is even function about the mid-plane. It follows that (3.45) is the so-called anti-symmetric dispersion relation, an analogue of so-called classical flexure or bending.

3.2 Long-wave analysis

For the analogue of classical non-fundamental solution branches, namely harmonics, a numerical experiment (Figure 3.2) shows that $\rho v^2 \to \infty$ as $kh \to 0$. In *Mathematica*, we use "ContourPlot" to draw implicitly the dispersion relations of both anti-symmetric and symmetric motions. Figure 3.2 describes the phase speed against the scaled wave number for a linear isotropic material with $\kappa = \sqrt{3.5}$, where anti-symmetric and symmetric solutions are presented by dashed lines and solid lines, respectively. The two lowest branches give description on the behaviour of fundamental modes and it can be inferred that the long wave limit of phase speed in anti-symmetric mode is zero while that in symmetric mode is a finite value. Equation (3.32) may be used to establish that in the low wave number (long wave) region,

$$q_1^2 = \bar{v}^2 + \bar{q}_1 + \mathcal{O}(\bar{v}^{-2}),\ q_2^2 = \frac{\bar{v}^2}{\kappa^2} + \bar{q}_2 + \mathcal{O}(\bar{v}^{-2}),$$

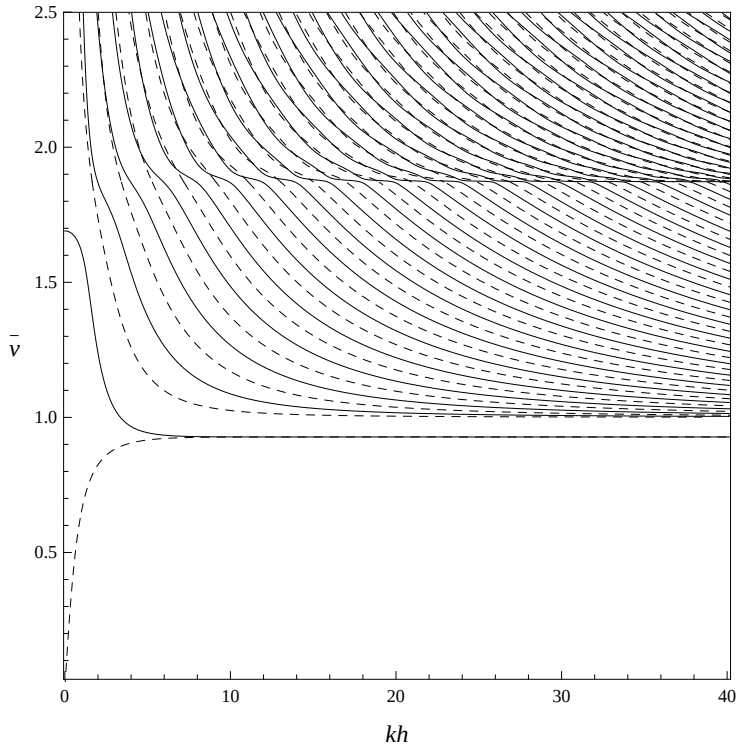

Figure 3.2: A numerical experiment on isotropic material with $\kappa = \sqrt{3.5}$.

$$q_1 = \bar{v} + \frac{\bar{q}_1}{2\bar{v}} + \mathcal{O}(\bar{v}^{-3}), \qquad q_2 = \frac{\bar{v}}{\kappa} + \frac{\kappa\bar{q}_2}{2\bar{v}} + \mathcal{O}(\bar{v}^{-3}), \tag{3.47}$$

where

$$\bar{q}_1 = w_2 w_4 + \frac{w_2(w_1^2 - 2w_1) + w_3}{w_2 - w_3}, \qquad \bar{q}_2 = \frac{2w_1 w_3 - w_1^2 w_2 - w_3}{w_2 - w_3}. \tag{3.48}$$

Let us fix the frequency $\Omega = \bar{v}\eta$ and compute the long-wave limit of the dispersion relations

for two different types of motion. We keep higher order terms like

$$H(q_1) \sim \mathcal{O}(1),\ F(q_2)Q(q_1) \sim \mathcal{O}(1),\ F(q_2)H(q_1) \sim \mathcal{O}(\eta),\ Q(q_1) \sim \mathcal{O}(\eta^{-1}), \tag{3.49}$$

while omitting low order terms like

$$H(q_2) \sim \mathcal{O}(\eta^2),\ F(q_1)Q(q_2) \sim \mathcal{O}(\eta^2),\ F(q_1)H(q_2) \sim \mathcal{O}(\eta^3),\ Q(q_2) \sim \mathcal{O}(\eta). \tag{3.50}$$

Keeping the highest order terms, the anti-symmetric dispersion relation (3.45) is simplified into

$$(\delta_1 \sin(\Omega) + \alpha_1 \Omega \cos(\Omega))(\alpha_2 \kappa \Omega \sin\left(\frac{\Omega}{\kappa}\right) - \delta_2 \cos\left(\frac{\Omega}{\kappa}\right)) = 0, \tag{3.51}$$

while the symmetric dispersion relation is simplified into

$$(\alpha_1 \Omega \sin(\Omega) - \delta_1 \cos(\Omega))(\delta_2 \sin\left(\frac{\Omega}{\kappa}\right) + \alpha_2 \kappa \Omega \cos\left(\frac{\Omega}{\kappa}\right)) = 0. \tag{3.52}$$

Let us study a special case when $\alpha_1 = \alpha_2 = 1,\ \delta_1 = 0,\ \delta_2 = \delta$.

3.2.1 Anti-symmetric waves

Under the condition that $\alpha_1 = \alpha_2 = 1,\ \delta_1 = 0,\ \delta_2 = \delta$, the dispersion relation (3.45) becomes

$$\frac{\delta}{\eta}(F(q_1)Q(q_2) - F(q_2)Q(q_1)) + w_2 Q(q_1)\tan(\eta q_2) - w_2 Q(q_2)\tan(\eta q_1) = 0. \tag{3.53}$$

Solving the equation (3.51), we get

$$\Lambda^a_{sh} = \left(n - \frac{1}{2}\right)\pi, \qquad n = 1, 2, ... \qquad \kappa\Lambda^a_{st}\tan\left(\frac{\Lambda^a_{st}}{\kappa}\right) = \delta. \tag{3.54}$$

The first family $(3.54)_1$ corresponds to the thickness shear resonance frequencies Λ^a_{sh} that are independent of δ. The second family, which is implicitly defined by equation $(3.54)_2$, is associated with thickness stretch resonance frequencies Λ^a_{st}. As $\delta \to 0$, we have $\tan\left(\frac{\Lambda^a_{st}}{\kappa}\right) \to 0$ and $\Lambda^a_{st} \approx \kappa n\pi$; the limiting case is of free faces (see Kaplunov *et al.* (1997)). As $\delta \to \infty$, we have $\tan\left(\frac{\Lambda^a_{st}}{\kappa}\right) \to \infty$ and $\Lambda^a_{st} \approx \kappa(n - 1/2)\pi$; the limiting case is of fixed faces (see Kaplunov (1995)). We focus on low mode number harmonics, which means that n is not too large.

To enable an asymptotic analysis to be carried out, we firstly correlate the magnitudes of η and δ:

$$\delta = \delta_0\eta^{2m},\ \delta_0 = \mathcal{O}(1), \tag{3.55}$$

considering the three cases $m = 1,\ m = -1$ and $m = 0$. These corresponds to the nearly traction-free faces case, the nearly fixed faces case and the transitional faces case.

Case 1 **nearly traction-free faces** ($m = 1$):$\delta \sim \eta^2$

The dispersion relation (3.53) may be rewritten as

$$\delta_0\eta(F(q_1)Q(q_2) - F(q_2)Q(q_1)) + w_2Q(q_1)\tan(\eta q_2) - w_2Q(q_2)\tan(\eta q_1) = 0. \tag{3.56}$$

According to (3.49) and (3.50), there are three asymptotic long wave balances of the dispersion relation. The first one is defined by

$$\tan(\eta q_1) \sim \eta,\ \tan(\eta q_2) \sim \eta,\ \bar{v} \sim 1, \tag{3.57}$$

and associated with a low-frequency fundamental mode. The tangents can be expanded into Maclaurin series for small argument:

$$\tan(\eta q_1) = \eta q_1 + \frac{1}{3}(\eta q_1)^3 + \mathcal{O}((\eta q_1)^5),\ \tan(\eta q_2) = \eta q_2 + \frac{1}{3}(\eta q_2)^3 + \mathcal{O}((\eta q_2)^5). \tag{3.58}$$

By substituting

$$\bar{v}^2 = \bar{v}_0^2 + \bar{v}_2^2\eta^2 + \mathcal{O}(\eta^4), \tag{3.59}$$

and (3.58) into the dispersion relation (3.56) and equating coefficients at every order of η^2 we

may obtain the unknown $\bar{v}_0$,$\bar{v}_2$. The asymptotic approximation for the phase speed is given by

$$\bar{v}^2 = \delta_0 + \frac{1}{3}\left(-\frac{\delta_0^2}{\kappa^2} - w_2 w_4 - \delta_0(1+\bar{q}_1+\bar{q}_2-w_2w_4)\right)\eta^2 + \mathcal{O}(\eta^4), \tag{3.60}$$

with the spurious root $\bar{v}^2 = (\bar{q}_2 - \bar{q}_1)/(1-\frac{1}{\kappa^2})$ ignored.

The second asymptotic regime, dominated by thickness shear resonance frequencies Λ^a_{sh}, is reached when

$$\tan(\eta q_1) \sim \bar{v}^2,\ \tan(\eta q_2) \sim 1,\ \bar{v} \sim \frac{1}{\eta}. \tag{3.61}$$

As $\bar{v}$ is large, we deduce that

$$Q(q_1) \sim \bar{v}\frac{1-w_1}{-1-\bar{q}_1+w_2w_4},\ Q(q_2) \sim \left(\frac{\bar{v}}{\kappa}\right)\cdot\left(\frac{1-w_1}{-1-\bar{q}_2+w_2w_4+\bar{v}^2(1-\frac{1}{\kappa^2})}\right), \tag{3.62}$$

$$F(q_2)Q(q_1) \sim \left(\frac{w_2}{\kappa}\right)\cdot\left(\frac{1-w_1}{-1-\bar{q}_1+w_2w_4}\right), \tag{3.63}$$

we omit $F(q_1)Q(q_2)$ because the order of it is lower than $F(q_2)Q(q_1)$. We may expand ηq_1 into power series for small η, yielding

$$q_1\eta = \Lambda_1^a + \phi_2\eta^2 + \mathcal{O}(\eta^4), \qquad \Lambda_1^a = \left(n-\frac{1}{2}\right)\pi,\ n=1,2,... \tag{3.64}$$

where ϕ_2 is unknown variable. The corresponding expansion for $\tan(\eta q_1)$ is given by

$$\tan(\eta q_1) = \frac{\tan(\Lambda_1^a) + \tan(\phi_2\eta^2)}{1 - \tan(\Lambda_1^a)\tan(\phi_2\eta^2)} = \frac{1 + \frac{\tan(\phi_2\eta^2)}{\tan(\Lambda_1^a)}}{\frac{1}{\tan(\Lambda_1^a)} - \tan(\phi_2\eta^2)} = \frac{-1}{\phi_2\eta^2} + \mathcal{O}(1). \tag{3.65}$$

According to $(3.47)_1$,

$$\bar{v}^2 = q_1^2 - \bar{q}_1 = \left(\frac{\Lambda_1^a}{\eta} + \phi_2\eta\right)^2 - \bar{q}_1 = \frac{(\Lambda_1^a)^2}{\eta^2} + 2\Lambda_1^a\phi_2 - \bar{q}_1 + \mathcal{O}(\eta^2), \tag{3.66}$$

then

$$\bar{v} = \frac{\Lambda_1^a}{\eta} + \phi_2\eta - \frac{\bar{q}_1\eta}{2\Lambda_1^a} + \mathcal{O}(\eta^3), \tag{3.67}$$

$$q_2 = \sqrt{(q_1^2 - \bar{q}_1)/\kappa^2 + \bar{q}_2} = \frac{\Lambda_1^a}{\kappa\eta} + \frac{-\bar{q}_1 + \bar{q}_2\kappa^2 + 2\Lambda_1^a\phi_2}{2\kappa\Lambda_1^a}\eta + \mathcal{O}(\eta^3), \tag{3.68}$$

$$\tan(\eta q_2) = \tan\left(\frac{\Lambda_1^a}{\kappa}\right) + \mathcal{O}(\eta^2). \tag{3.69}$$

Substituting expansions (3.64)-(3.69) into the dispersion relation (3.56), we obtain

$$\phi_2 = \frac{1 + \bar{q}_1 - w_2 w_4}{\kappa(1 - \frac{1}{\kappa^2})\tan(\frac{\Lambda_1^a}{\kappa})(\Lambda_1^a)^2}. \tag{3.70}$$

The approximation for frequency then takes the form

$$\Omega^2 = (\Lambda_1^a)^2 + (2\Lambda_1^a\phi_2 - \bar{q}_1)\eta^2 + \mathcal{O}(\eta^4). \tag{3.71}$$

The third asymptotic regime is associated with thickness stretch resonance frequencies Λ_{st}^a and may be characterized by

$$\tan(\eta q_1) \sim 1,\ \tan(\eta q_2) \sim \bar{v}^{-2},\ \bar{v} \sim \frac{1}{\eta}. \tag{3.72}$$

The derivation procedure is similar to the previous thickness shear regime, except that the cut-off frequencies are given by $\Lambda_2^a = \kappa n \pi$. The corresponding approximation for the frequency has the form

$$\Omega^2 = (\Lambda_2^a)^2 + \left(2\delta_0 - \frac{2\tan(\Lambda_2^a)(1+\bar{q}_1 - w_2 w_4)}{(1-\frac{1}{\kappa^2})\Lambda_2^a} - \kappa^2 \bar{q}_2\right)\eta^2 + \mathcal{O}(\eta^4). \tag{3.73}$$

Case 2 **nearly fixed faces** $(m=-1)$**:**$\delta \sim \eta^{-2}$

The dispersion relation (3.53) may be rewritten as

$$\frac{\delta_0}{\eta^3}(F(q_1)Q(q_2) - F(q_2)Q(q_1)) + w_2 Q(q_1)\tan(\eta q_2) - w_2 Q(q_2)\tan(\eta q_1) = 0, \tag{3.74}$$

which supports two possible asymptotic long wave balances. The first one results in thickness shear resonance modes characterized by

$$\tan(\eta q_1) \sim \bar{v}^4,\ \tan(\eta q_2) \sim 1,\ \bar{v} \sim \frac{1}{\eta}. \tag{3.75}$$

The associated approximation for frequency takes the form

$$\Omega^2 = (\Lambda_1^a)^2 - \bar{q}_1\eta^2 - \frac{8}{\delta_0}\eta^4 + \mathcal{O}(\eta^6). \tag{3.76}$$

The second asymptotic regime is characterized by

$$\tan(\eta q_1) \sim 1,\ \tan(\eta q_2) \sim \bar{v}^2,\ \bar{v} \sim \frac{1}{\eta}. \tag{3.77}$$

The associated asymptotic approximation for frequency is given by

$$\Omega^2 = (\Lambda_4^a)^2 + \left(-\bar{q}_2\kappa^2 - \frac{2\kappa^2(\Lambda_4^a)^2}{\delta_0}\right)\eta^2 + \mathcal{O}(\eta^4), \tag{3.78}$$

where $\Lambda_4^a = \left(n - \frac{1}{2}\right)\kappa\pi$.

Case 3 **transitional case** $(m = 0)$:$\delta = \delta_0 \sim 1$

The dispersion relation (3.53) may be rewritten as

$$\frac{\delta_0}{\eta}(F(q_1)Q(q_2) - F(q_2)Q(q_1)) + w_2Q(q_1)\tan(\eta q_2) - w_2Q(q_2)\tan(\eta q_1) = 0. \tag{3.79}$$

At certain values of $\delta = \delta_*$ a member of Λ_{sh}^a may coincide with a member of Λ_{st}^a, thus it is necessary to develop a uniform asymptotic expansion for such long-wave high frequency

motions.

Thickness shear expansion

The classical asymptotic expansion allows the structure of

$$\tan(\eta q_1) \sim \bar{v}^2,\ \tan(\eta q_2) \sim 1,\ \bar{v} \sim \frac{1}{\eta}. \tag{3.80}$$

We expand every term of (3.79) into power series for small η, and equating the coefficient of the lowest order terms of η to zero, an expression for ϕ_2 may be obtained. The derivation is quite similar to the thickness shear in **Case** 1, with one more term containing δ in the process of obtaining ϕ_2. Thus, when this is done we obtain

$$\phi_2 = \frac{-1 - \bar{q}_1 + w_2 w_4}{(1 - \frac{1}{\kappa^2})\Lambda_3^a(\delta - \delta_*)}, \qquad \delta_* = \kappa\Lambda_3^a \tan\left(\frac{\Lambda_3^a}{\kappa}\right), \qquad \Lambda_3^a = \left(n - \frac{1}{2}\right)\pi. \tag{3.81}$$

If δ is in the close vicinity of δ_*, ϕ_2 becomes very large, and it is no longer suitable for ϕ_2 to appear with the $\mathcal{O}(\eta^2)$ term of the expression in Ω^2. If we then try

$$q_1\eta = \Lambda_3^a + \phi_2\eta + \mathcal{O}(\eta^2), \text{and then} \tan(\eta q_1) \sim \bar{v}, \tag{3.82}$$

so that the highest order we have only two terms: one containing δ and the other containing δ_*, which offset each other. These two experiments inspire us to design a variable ϵ replacing ϕ_2,

and ϵ may vary between $\mathcal{O}(\eta)$ and $\mathcal{O}(1)$. As a result, it is established that

$$\Omega = \Lambda_3^a + \epsilon\eta - \frac{\bar{q}_1}{2\Lambda_3^a}\eta^2 + \mathcal{O}(\epsilon\eta^3),$$

$$q_2 = \frac{\Lambda_3^a}{\kappa\eta} + \frac{\epsilon}{\kappa} + \frac{\kappa^2\bar{q}_2 - \bar{q}_1}{2\kappa\Lambda_3^a}\eta + \mathcal{O}(\epsilon\eta^2), \tag{3.83}$$

$$\tan(\eta q_2) = \tan\left(\frac{\Lambda_3^a}{\kappa}\right) + \frac{\epsilon\eta}{\kappa\cos^2(\frac{\Lambda_3^a}{\kappa})} + \mathcal{O}(\eta^2).$$

Substituting these expansions into the dispersion relation (3.79), we obtain the equation for ϵ

$$\left(-\kappa\Lambda_3^a\tan(\frac{\Lambda_3^a}{\kappa}) - \frac{(\Lambda_3^a)^2}{\cos^2(\frac{\Lambda_3^a}{\kappa})}\right)\epsilon^2 + \Lambda_3^a\left(\delta - \kappa\Lambda_3^a\tan(\frac{\Lambda_3^a}{\kappa})\right)\frac{\epsilon}{\eta} + \frac{1+\bar{q}_1 - w_2w_4}{1-\frac{1}{\kappa^2}} = 0. \tag{3.84}$$

If we denote the smaller root of above equation as ϵ_1 and the larger root as ϵ_2, the following simple condition enables selection of the correct root:

$$\epsilon = \begin{cases} \epsilon_2, \ \delta \leq \delta_*; \\ \epsilon_1, \ \delta > \delta_*. \end{cases} \tag{3.85}$$

Thickness stretch expansion

Unlike **Case** 1 and **Case** 2, the cut-off frequencies Λ_4^a are δ-dependent; they are, according

to $(3.54)_2$, defined through

$$\kappa\Lambda_4^a \tan\left(\frac{\Lambda_4^a}{\kappa}\right) = \delta. \tag{3.86}$$

This is because for the transitional case, δ is neither zero nor ∞ in $(3.54)_2$, which makes the associated family of cut-off frequencies Λ_{st}^a δ-dependent. The classical asymptotic structure

$$\tan(\eta q_1) \sim 1,\ \tan(\eta q_2) \sim \bar{v}^{-2},\ \bar{v} \sim \frac{1}{\eta}, \tag{3.87}$$

again fails to solve this problem. Similarly, to the thickness shear case, we introduce

$$\eta q_2 = \frac{\Lambda_4^a}{\kappa} + \epsilon\eta, \text{ and then } \tan(\eta q_2) = \frac{\delta}{\kappa\Lambda_4^a} + \left(1 + (\frac{\delta}{\kappa\Lambda_4^a})^2\right)\epsilon\eta, \tag{3.88}$$

from which it follows that

$$\bar{v} = \frac{\Lambda_4^a}{\eta} + \kappa\epsilon - \frac{\kappa^2\bar{q}_2}{2\Lambda_4^a}\eta, \qquad \Omega = \Lambda_4^a + \kappa\epsilon\eta - \frac{\kappa^2\bar{q}_2}{2\Lambda_4^a}\eta^2,$$

$$q_1 = \frac{\Lambda_4^a}{\eta} + \kappa\epsilon + \frac{\bar{q}_1 - \kappa^2\bar{q}_2}{2\Lambda_4^a}\eta, \qquad \tan(\eta q_1) = \tan(\Lambda_4^a) + \kappa\epsilon\eta(1 + \tan^2(\Lambda_4^a)). \tag{3.89}$$

If these expansions are inserted into the dispersion relation (3.79), we obtain a quadratic equation for ϵ, given by

$$\left(-A\tan(\Lambda_4^a) + \frac{B\cdot A - \kappa^2\delta}{\Lambda_4^a}\right)\epsilon^2 + \frac{A\epsilon}{\kappa\eta} + B\tan(\Lambda_4^a) - \frac{\delta}{\Lambda_4^a}(B + \bar{q}_2\kappa^2) = 0, \tag{3.90}$$

where

$$A = \delta^2 + \kappa^2\delta + \kappa^2(\Lambda_4^a)^2,\ B = (1 + \bar{q}_1 - w_2w_4)/(1 - \frac{1}{\kappa^2}).$$

If we denote the smaller root of the above equation as ϵ_1 and the larger root as ϵ_2, the following simple condition enables selection of the correct root:

$$\epsilon = \begin{cases} \epsilon_1,\ \delta \leq \delta_*; \\ \\ \epsilon_2,\ \delta > \delta_*. \end{cases} \tag{3.91}$$

3.2.2 Symmetric waves

The dispersion relation for the symmetric case is given by

$$\frac{\delta}{\eta}(F(q_1)Q(q_2) - F(q_2)Q(q_1)) + w_2Q(q_1)\cot(\eta q_2) - w_2Q(q_2)\cot(\eta q_1) = 0. \tag{3.92}$$

Solving equation (3.52), we deduce that the relevant cut-off frequencies are given by

$$\Lambda_{sh}^s = n\pi, \qquad n = 0, 1, 2, ... \qquad -\kappa\Lambda_{st}^s \cot\left(\frac{\Lambda_{st}^s}{\kappa}\right) = \delta. \tag{3.93}$$

The symmetric fundamental mode is obtained from $(3.93)_1$ when $n = 0$. The first family $(3.93)_1$ corresponds to the thickness shear resonance frequencies Λ_{sh}^s that are independent of δ. The second family, which is implicitly defined by equation $(3.93)_2$, is associated with thickness stretch

resonance frequencies Λ^s_{st}. The symmetric fundamental mode does not change its asymptotic structure due to the effect of the normal restraint on the layer faces. Thus, the following long-wave low-frequency expansion for the phase speed of fundamental mode is appropriate

$$\bar{v}^2 = \frac{-\Delta_1 - \sqrt{\Delta_1^2 - 4(\delta - \kappa^2)\Delta_2}}{2(\delta - \kappa^2)} + \mathcal{O}(\eta^2), \tag{3.94}$$

where

$$\Delta_1 = \kappa^2 - \kappa^2 w_2 w_4 + \bar{q}_2 \kappa^2 \delta + \bar{q}_1 \delta,\ \Delta_2 = \kappa^2 w_2 w_4 + \bar{q}_1 \bar{q}_2 \kappa^2 \delta,$$

is valid for all values of δ.

To proceed with an asymptotic analysis we again have to consider separately various possible asymptotic balances of δ with respect to the scaled wave number η, as described by (3.55).

Case 1 **nearly traction-free faces** $(m = 1)$:$\delta \sim \eta^2$

In this case, the expansion of frequency related to thickness shear has the form

$$\Omega^2 = (\Lambda^s_1)^2 - \left(\frac{2(1 + \bar{q}_1 - w_2 w_4)}{\kappa(1 - \frac{1}{\kappa^2}) \cot(\frac{\Lambda^s_1}{\kappa})(\Lambda^s_1)} + \bar{q}_1 \right) \eta^2 + \mathcal{O}(\eta^4). \tag{3.95}$$

where $\Lambda^s_1 = n\pi$. This expression is quite similar to the corresponding one in the anti-symmetric case, except replacing Λ^a_1 with Λ^s_1 and $\tan$ with $-\cot$. The modes associated with thickness

stretch have the following expansion

$$\Omega^2 = (\Lambda_2^s)^2 + \left(2\delta_0 - \frac{2\cot(\Lambda_2^s)(-1-\bar{q}_1+w_2w_4)}{(1-\frac{1}{\kappa^2})\Lambda_2^s} - \kappa^2\bar{q}_2\right)\eta^2 + \mathcal{O}(\eta^4), \tag{3.96}$$

where $\Lambda_2^s = \kappa\left(n-\frac{1}{2}\right)\pi$.

Case 2 **nearly fixed faces** $(m=-1)$:$\delta \sim \eta^{-2}$

The thickness shear and thickness stretch mode expansions are very similar to the anti-symmetric case, except that Λ_1^a must be replaced by $\Lambda_1^s = n\pi$, and Λ_4^a by $\Lambda_4^s = \kappa n\pi$.

Case 3 **transitional case** $(m=0)$:$\delta = \delta_0 \sim 1$

The expansions for frequency within the vicinity of thickness shear and thickness stretch modes are identical in form to those of the anti-symmetric case, which should be used with slightly modified equations for ϵ. For the thickness shear modes ϵ is found from

$$\left(\kappa\Lambda_3^s\cot(\frac{\Lambda_3^s}{\kappa}) - \frac{(\Lambda_3^s)^2}{\sin^2(\frac{\Lambda_3^s}{\kappa})}\right)\epsilon^2 + \Lambda_3^s\left(\delta + \kappa\Lambda_3^s\cot(\frac{\Lambda_3^s}{\kappa})\right)\frac{\epsilon}{\eta} + \frac{1+\bar{q}_1-w_2w_4}{1-\frac{1}{\kappa^2}} = 0, \tag{3.97}$$

whereas for thickness stretch, (3.97) is replaced by

$$\left(A\cot(\Lambda_4^a) + \frac{B\cdot A - \kappa^2\delta}{\Lambda_4^a}\right)\epsilon^2 + \frac{A\epsilon}{\kappa\eta} - B\cot(\Lambda_4^a) - \frac{\delta}{\Lambda_4^a}(B+\bar{q}_2\kappa^2) = 0, \tag{3.98}$$

in which $\Lambda_3^s = n\pi$, Λ_4^s satisfies the relation $(3.93)_2$.

3.3 Short-wave analysis

Through numerical experiment, we find that as $\eta \to \infty$, for harmonics the velocity of both anti-symmetric and symmetric motions, for all modes, approaches that of the associated shear wave speed. While the velocity in fundamental modes approaches that of the associated surface wave speed $\bar{v}_r$. Initially we focus on the behavior of fundamental modes. By intuition, it is helpful to set $\bar{v}^2 = \bar{v}_r^2 + \frac{\varphi}{\eta}$ to approximate the real behavior of short waves.

With the help of Mathematica, we are able to verify numerically that

$$2w_1 - w_4 w_2 - 1 - \frac{1}{\kappa^2} > 0, \qquad w_1^2 - \frac{1}{\kappa^2} - w_4 w_3 > 0, \tag{3.99}$$

for isotropic and transversely isotropic materials, such as Glass-Epoxy composite with any angle θ. It then follows that in the subsonic region $\bar{v} < 1$, according to (3.32),

$$q_1^2 + q_2^2 = -(2w_1 - w_4 w_2 - \bar{v}^2 - \frac{\bar{v}^2}{\kappa^2}) < 0,$$

$$q_1^2 q_2^2 = (1 - \bar{v}^2)(w_1^2 - \frac{\bar{v}^2}{\kappa^2} - w_4 w_3) > 0, \tag{3.100}$$

and we can infer that both q_1 and q_2 are pure imaginary. This also means that

$$\lim_{\eta\to\infty} \tanh(\eta\hat{q}_1) = \lim_{\eta\to\infty} \coth(\eta\hat{q}_1) = \lim_{\eta\to\infty} \tanh(\eta\hat{q}_2) = \lim_{\eta\to\infty} \coth(\eta\hat{q}_2) = -1. \tag{3.101}$$

Therefore, for sufficiently short waves both the anti-symmetric and symmetric dispersion relations tend to the same limit, given by

$$\mathrm{i}\alpha_1\alpha_2 w_2(Q(q_1)-Q(q_2))+\mathrm{i}\frac{\delta_1\delta_2}{w_2\eta^2}(F(q_1)H(q_2)-F(q_2)H(q_1))$$

$$+\frac{\alpha_2\delta_1}{\eta}(H(q_2)-H(q_1))+\frac{\alpha_1\delta_2}{\eta}(F(q_1)Q(q_2)-F(q_2)Q(q_1))=0. \tag{3.102}$$

Equation (3.102) is the secular equation for surface waves propagating in an elastic anisotropic half-space with elastically restrained boundary conditions. Numerically we find that as $\delta \to \infty$, there is no subsonic solution, so surface waves can not propagate along a fixed boundary. So we remark that for short-waves with finite δ, as $\eta \to \infty$, the influence of the elastically restrained boundaries within dispersion relations (3.43) and (3.45) is relatively minor. In fact, what we study here is the nearly traction-free case (for example, in the following numerical experiment $\delta = 100$, which is relatively small compared to $\eta = 1000$), so that we keep only the first term in (3.102) as leading order term, which can be recognized as the classical Rayleigh secular equation (free faces) when it is simplified within the isotropic case. From the expression of φ, we deduce that in the short wave region the influence of the elastically restrained boundaries δ only determines how fast the wave speed is approaching the classical surface wave speed (free faces). Similar to Rayleigh wave speed v_R for isotropic case, the short-wave limit of velocity $\bar{v}_r$

is the solution at the leading order of

$$\mathrm{i}(Q(q_1) - Q(q_2)) = 0. \tag{3.103}$$

Substituting $\bar{v}^2 = \bar{v}_r^2 + \frac{\varphi}{\eta}$ into (3.102), we obtain φ which is rather complicated and we will not show it here. We have verified numerically that for all $\nu \in (-1, \frac{1}{2})$, namely $\kappa^2 > \frac{4}{3}$, φ is positive, which means the velocity of surface wave grows as the wave number decreases. At some point η_*, the velocity reaches 1 and the surface wave degenerates into a shear wave. When $\bar{v} = 1$, $q_2 = \mathrm{i}\sqrt{-1 + 2w_1 - \frac{w_3}{w_2} - w_2 w_4}$, q_1 vanishes, which makes (3.102) invalid. Thus, we have to return back to original dispersion relations to determine η_*. The expansion for anti-symmetric dispersion relation reads

$$\left(1 - \frac{\delta_1\delta_2}{\alpha_1\alpha_2}\frac{1}{\eta_*^2}\right)\tan(\eta_* q_2) = \frac{\delta_2}{\alpha_2}\frac{q_2}{\eta_*}; \tag{3.104}$$

while the expansion for symmetric dispersion relation reads

$$\frac{\delta_1\delta_2}{\alpha_1\alpha_2}(-1 + q_2^2 + w_1 - w_2 w_4) - (-1 + w_1 - w_2 w_4)(1 + \frac{\delta_2}{\alpha_2}q_2^2)\eta_*^2$$

$$+q_2(-1 + w_1 - w_2 w_4)\eta_*(\eta_*^2 - \frac{\delta_1\delta_2}{\alpha_1\alpha_2})\cot(\eta_* q_2) = 0. \tag{3.105}$$

We still focus on the case when $\alpha_1 = \alpha_2 = 1,\ \delta_1 = 0,\ \delta_2 = \delta$. As δ grows larger,

$$\eta_* \sim \delta\sqrt{-1 + 2w_1 - \frac{w_3}{w_2} - w_2 w_4}. \tag{3.106}$$

3.4 Linear isotropic materials

The general results presented in Sections 3.2 and 3.3 will now be specialized to a linear isotropic elastic material. This case has previously been studied by Mukhomodyarov *et al.* (2010) using a procedure that is particularly developed for isotropic materials. We now show that our formulae recover their results in this special case. For linear isotropic material, $c_{16} = c_{26} = 0$, by referring back to (1.61), (3.31) and (3.48), we have

$$w_1 = -\frac{\lambda}{\lambda + 2\mu},\ w_2 = -\frac{1}{\mu},\ w_3 = -\frac{1}{\lambda + 2\mu},\ w_4 = 4\mu\left(1 - \frac{\mu}{\lambda + 2\mu}\right), \tag{3.107}$$

and

$$\bar{q}_1 = -1,\ \bar{q}_2 = -1,\ \frac{1 + \bar{q}_1 - w_2 w_4}{1 - \frac{1}{\kappa^2}} = 4,\ \kappa^2 = \frac{\lambda + 2\mu}{\mu}. \tag{3.108}$$

In the long-wave analysis, regarding the dispersion relation for anti-symmetric modes given by (3.53) in general, the specific isotropic form is given by

$$-\frac{\delta}{\eta} q_2 \bar{v}^2 + (\bar{v}^2 - 2)^2 \tan(\eta q_2) + 4 q_1 q_2 \tan(\eta q_1) = 0. \tag{3.109}$$

Case 1 **nearly traction-free faces** $(m = 1)$:$\delta \sim \eta^2$

By substituting (3.107) and (3.108) into the corresponding general results (3.60), (3.71) and (3.73) for nearly traction-free faces, we obtain

$$\text{fundamental waves } \bar{v}^2 = \delta_0 + \left(\frac{4}{3} - \delta_0 - \frac{(\delta_0 - 2)^2}{3\kappa^2}\right)\eta^2 + \mathcal{O}(\eta^4). \tag{3.110}$$

$$\text{thickness shear } \Omega^2 = (\Lambda_1^a)^2 + \left(\frac{8}{\kappa \tan(\frac{\Lambda_1^a}{\kappa})\Lambda_1^a} + 1\right)\eta^2 + \mathcal{O}(\eta^4). \tag{3.111}$$

$$\text{thickness stretch } \Omega^2 = (\Lambda_2^a)^2 + \left(2\delta_0 - \frac{8\tan(\Lambda_2^a)}{\Lambda_2^a} + \kappa^2\right)\eta^2 + \mathcal{O}(\eta^4). \tag{3.112}$$

Case 2 **nearly fixed faces** $(m = -1)$:$\delta \sim \eta^{-2}$

By substituting (3.107) and (3.108) into the corresponding general results (3.76) and (3.78) for nearly fixed faces, we obtain

$$\text{thickness shear } \Omega^2 = (\Lambda_1^a)^2 + \eta^2 - \frac{8}{\delta_0}\eta^4 + \mathcal{O}(\eta^6). \tag{3.113}$$

$$\text{thickness stretch } \Omega^2 = (\Lambda_4^a)^2 + \left(\kappa^2 - \frac{2\kappa^2(\Lambda_4^a)^2}{\delta_0}\right)\eta^2 + \mathcal{O}(\eta^4). \tag{3.114}$$

Figure 3.3 demonstrates anti-symmetric modes for a linear isotropic material with nearly traction-free faces and nearly fixed faces. Both numerical and asymptotic solutions, either fundamental mode, or thickness shear or thickness stretch, show very good agreement over a large wave number region.

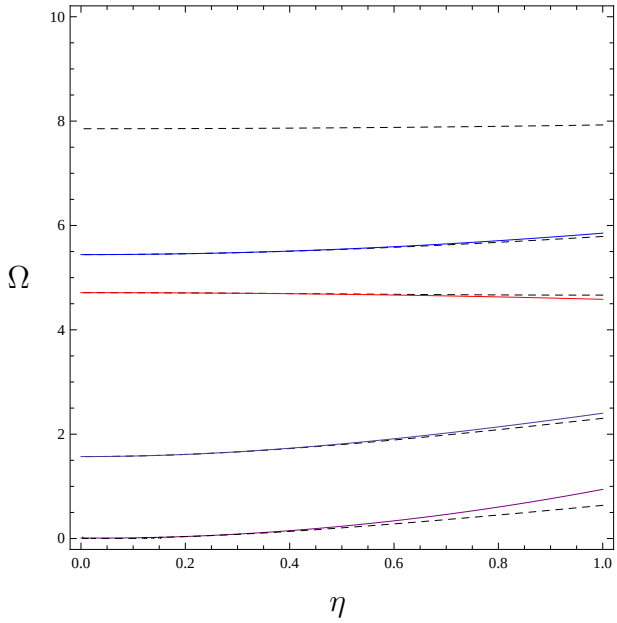

(a)

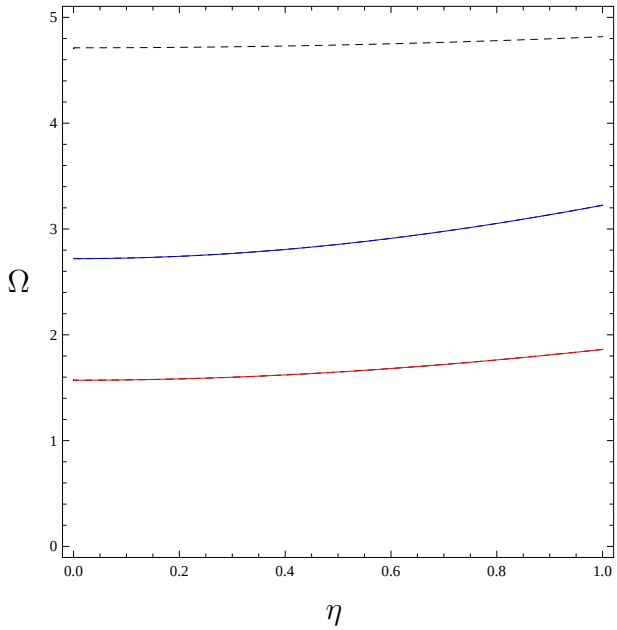

(b)

Figure 3.3: Comparison of the asymptotic solutions with the numerical solutions (dashed lines) for $\kappa = \sqrt{3}$ and (a) $\delta = 10^{-4}$, (b) $\delta = 10^{4}$.

Case 3 **transitional case** $(m = 0)$:$\delta = \delta_0 \sim 1$

Figure 3.4 displays anti-symmetric modes for a linear isotropic material in the transitional case. We refer the reader to Figure 3.4 for the accurate prediction from the uniform asymptotic expansion derived in equations (3.83) and (3.89).

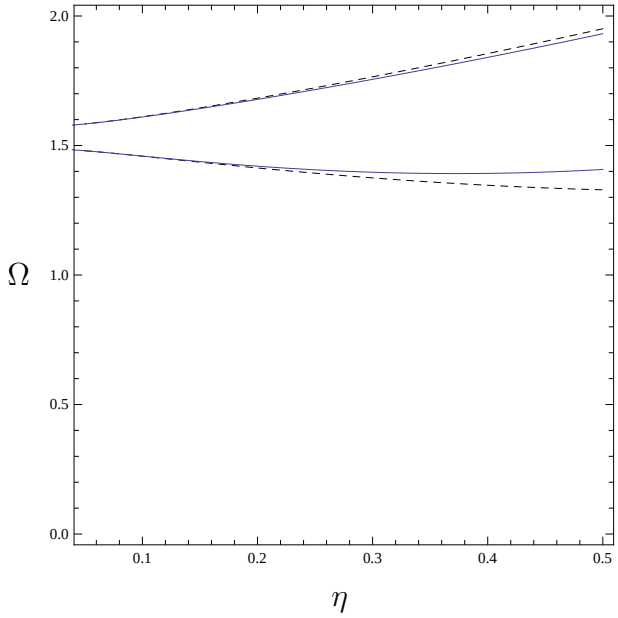

Figure 3.4: Comparison of uniform asymptotic solution and numerical solution (dashed lines) when $\delta = 3$ and $\kappa = \sqrt{3}$.

In the long-wave analysis, the dispersion relation for symmetric modes given by (3.92) in general is specialized into isotropic form

$$-\frac{\delta}{\eta} q_2 \bar{v}^2 + (\bar{v}^2 - 2)^2 \cot(\eta q_2) + 4 q_1 q_2 \cot(\eta q_1) = 0. \tag{3.115}$$

By substituting (3.107) and (3.108) into the corresponding general result (3.94) for fundamental

mode, we obtain

$$\text{fundamental mode } \bar{v}^2 = \frac{\kappa^2(\delta-4)+4}{\delta-\kappa^2} + \frac{(\kappa^2-2)^2(\delta\kappa^2-4\kappa^2+4)}{3(\kappa^2-\delta)^3}\eta^2. \tag{3.116}$$

Case 1 **nearly traction-free faces** $(m=1)$:$\delta \sim \eta^2$

By substituting (3.107) and (3.108) into the corresponding general results (3.95) and (3.96) for nearly traction-free faces, we obtain

$$\text{thickness shear } \Omega^2 = (\Lambda_1^s)^2 - \left(1 - \frac{8}{\kappa\Lambda_1^s \cot(\frac{\Lambda_1^s}{\kappa})}\right)\eta^2 + \mathcal{O}(\eta^4). \tag{3.117}$$

$$\text{thickness stretch } \Omega^2 = (\Lambda_2^s)^2 + \left(2\delta_0 - \frac{8\cot(\Lambda_2^s)}{\Lambda_2^s} + \kappa^2\right)\eta^2 + \mathcal{O}(\eta^4), \tag{3.118}$$

Case 2 **nearly fixed faces** $(m=-1)$:$\delta \sim \eta^{-2}$

The symmetric thickness shear and thickness stretch modes have the similar expansions as in the anti-symmetric case, except that Λ_1^a must be replaced by $\Lambda_1^s = n\pi$, and Λ_4^a by $\Lambda_4^s = \kappa n\pi$.

In the short-wave analysis, we are able to readily deduce that

$$\bar{v}^2 = \bar{v}_R^2 + \frac{\kappa^2\bar{v}_R^2(\bar{v}_R^2-2)^2}{2(4-4\kappa^2-6\kappa^2\bar{v}_R^4+\kappa^2\bar{v}_R^6+4\bar{v}_R^2(3\kappa^2-2))}$$

$$\left(\frac{\delta_1}{\alpha_1}\sqrt{1-\bar{v}_R^2} + \frac{\delta_2}{\alpha_2}\sqrt{1-\frac{\bar{v}_R^2}{\kappa^2}}\right)\frac{1}{\eta} + \mathcal{O}(\eta^{-2}), \tag{3.119}$$

and this result is equivalent to (6.4) in Moukhomodiarov *et al.* (2010); with (3.106) now given by

$$\eta_* \sim \delta \frac{\sqrt{\kappa^2 - 1}}{\kappa}. \tag{3.120}$$

The short wave behavior for an isotropic material with $\kappa = \sqrt{3}$, in respect of anti-symmetric and symmetric fundamental modes is presented in Figure 3.5. In addition, the asymptotic expansion (3.119) form a dashed line in the figure.

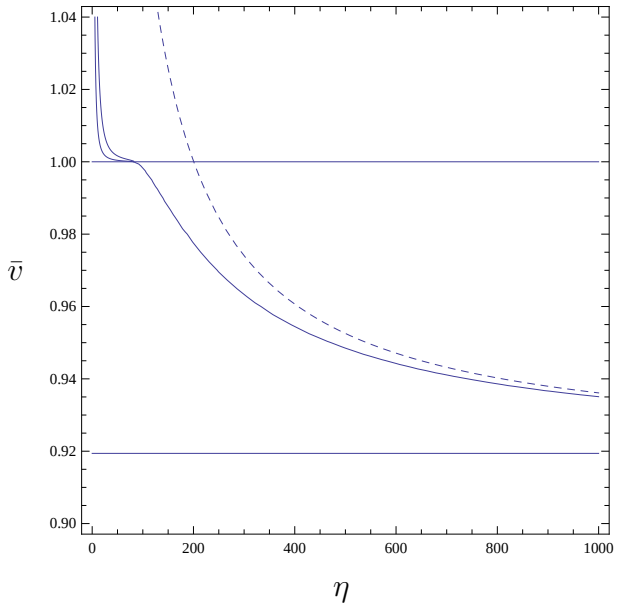

Figure 3.5: Anti-symmetric and symmetric fundamental modes shown together with surface and shear wave speeds, as well as asymptotic expansion (3.119) (dashed line) for $\delta = 100$ and $\kappa = \sqrt{3}$.

3.5 Transversely isotropic materials

In the previous chapter, $x_3 = 0$ is symmetry plane and the fibre is in the (x_1, x_2) plane, while for the plate, $x_2 = 0$ is symmetry plane, with the fibre direction in the (x_1, x_3) plane. This geometrical set-up ensures material symmetry and the decoupling of dispersion relations. The angle between the fibre and x_1 axis is θ, so $\mathbf{m} = (\cos\theta, 0, \sin\theta)$. When the angle θ is $90°$, the problem is essentially reduced to that of an isotropic material. We use previous materials as examples for numerical illustration of the variation of θ on phase speed or frequency, and compare asymptotic expansions of frequency with the numerical solution. For a linear transversely isotropic material, $c_{16} = c_{26} = 0$. By referring back to (1.71), (3.31) and (3.48), we have

$$w_1 = \frac{-\lambda - \alpha\cos^2\theta}{\lambda + 2\mu_T},\ w_2 = -\frac{1}{\mu_T + (\mu_L - \mu_T)\cos^2\theta},\ w_3 = -\frac{1}{\lambda + 2\mu_T},$$

$$w_4 = \lambda + 2\mu_T + 2\alpha\cos^2\theta + 4(\mu_L - \mu_T)\cos^2\theta + \beta\cos^4\theta - \frac{(\lambda + \alpha\cos^2\theta)^2}{\lambda + 2\mu_T}, \tag{3.121}$$

and

$$\kappa^2 = \frac{\lambda + 2\mu_T}{\mu_T + (\mu_L - \mu_T)\cos^2\theta},$$

$$\frac{1 + \bar{q}_1 - w_2 w_4}{1 - \frac{1}{\kappa^2}} = \frac{(\alpha + 4(\lambda + \mu_T) + \alpha\cos(2\theta))^2}{(2\lambda - \mu_L + 3\mu_T - (\mu_L - \mu_T)\cos(2\theta))^2}. \tag{3.122}$$

We study Glass-Epoxy composite. From $(3.122)_1$ we know that κ changes with θ.

3.5.1 Long wave analysis for anti-symmetric modes

To avoid redundant and similar derivation to that presented in previous sections, we only presents two cases for anti-symmetric modes in the long wave analysis, while the analysis for symmetric modes are omitted.

Case 1 **nearly traction-free faces** ($m = 1$):$\delta \sim \eta^2$

Figure 3.6 illustrates $\tan\left(\frac{\Lambda_1^a}{\kappa}\right)$ in (3.70) against θ for a transversely isotropic material with nearly traction-free faces. In the long wave region, for anti-symmetric waves, $\tan\left(\frac{\Lambda_1^a}{\kappa}\right)$ in (3.70) vanishes to zero at certain value θ_0 (see Figure 3.6) ($\kappa \approx \frac{3}{2}$), which means that the cut-off frequency of the thickness shear branch ($\frac{3}{2}\pi$) coincides with that of thickness stretch branch ($\kappa\pi$). Within a certain interval near θ_0, the classical asymptotic expansion fails to provide accurate approximation to the numerical solution because ϕ_2 in (3.70) is too large or does not exist. We focus on the low frequency region $0 \leq \Omega \leq 10$, where only the first three harmonics exist. In this region, it is only when $\Lambda_1^a = \frac{3}{2}\pi$ that $\tan\left(\frac{\Lambda_1^a}{\kappa}\right)$ vanishes. Figure 3.7 describes the anti-symmetric wave solutions for a transversely isotropic material with nearly traction-free faces and $\theta = 15^\circ$. Through our numerical calculation, it is found that for $\theta \in [0, 20^\circ]$ or $\theta \in [70^\circ, 90^\circ]$, the classical asymptotic expansion gives a very good approximation to the numerical solution, see Figure 3.7. In the interval $\theta \in [20^\circ, 70^\circ]$, a new asymptotic expansion based on the method used to establish

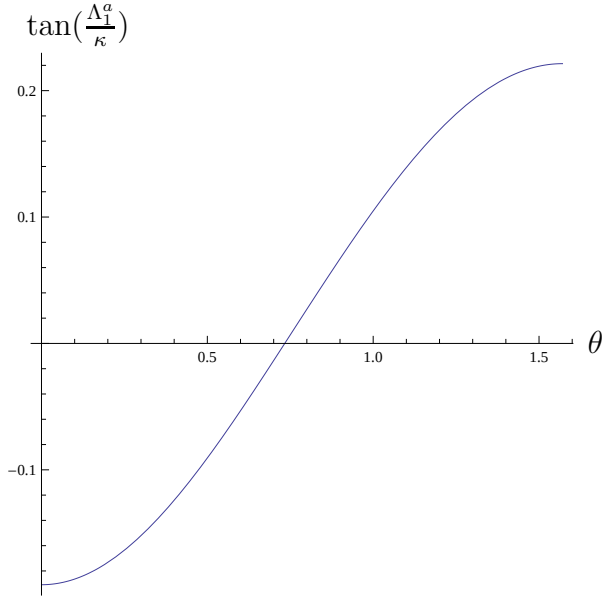

Figure 3.6: $\tan(\frac{\Lambda_1^a}{\kappa})$ vanishes at $\theta_0 = 42.019°$ and $\Lambda_1^a = \frac{3}{2}\pi$.

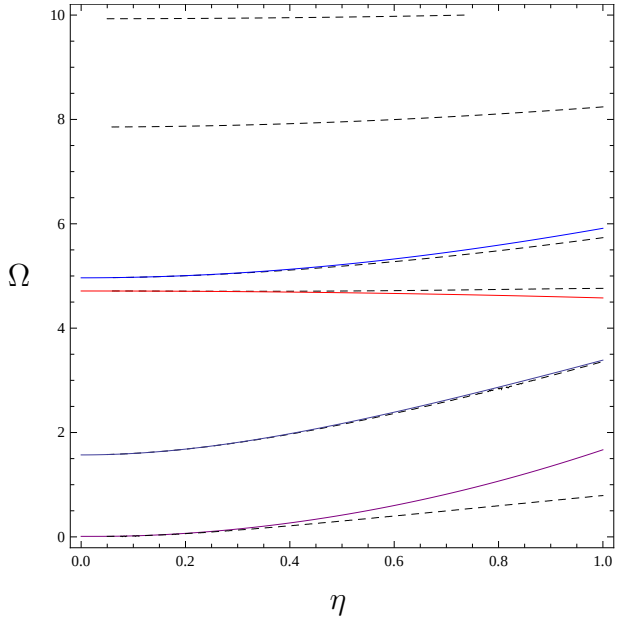

Figure 3.7: Comparison of the asymptotic solutions with the numerical solutions (dashed lines) for $\delta = 10^{-4}$ and $\theta = 15°$.

(3.82) is needed. For thickness shear, we note that

$$\eta q_1 = \frac{3}{2}\pi + \epsilon, \text{ and then } \tan(\eta q_1) = -\cot(\epsilon),$$

$$\Omega = \bar{v}\eta = \sqrt{q_1^2 - \bar{q}_1}\eta = \frac{3}{2}\pi + \epsilon - \frac{\bar{q}_1}{3\pi + 2\epsilon}\eta^2,$$

$$q_2 = \sqrt{(q_1^2 - \bar{q}_1)/\kappa^2 + \bar{q}_2} = \frac{3\pi + 2\epsilon}{2\kappa\eta} + \frac{\kappa^2\bar{q}_2 - \bar{q}_1}{\kappa(3\pi + 2\epsilon)}\eta, \tag{3.123}$$

and then

$$\tan(\eta q_2) = \tan(\frac{3\pi + 2\epsilon}{2\kappa}).$$

Similarly, for the thickness stretch expansion, we deduce that

$$\eta q_2 = \pi + \epsilon, \ \tan(\eta q_2) = \tan(\epsilon), \ \Omega = \pi + \epsilon - \frac{\bar{q}_2\kappa}{2(\pi + \epsilon)}\eta^2,$$

$$q_1 = \frac{\kappa(\pi + \epsilon)}{\eta} + \frac{\bar{q}_1 - \kappa^2\bar{q}_2}{2\kappa(\pi + \epsilon)}\eta, \qquad \tan(\eta q_1) = \tan(\kappa(\pi + \epsilon)). \tag{3.124}$$

The quadratic equations, analogous to (3.84), are too large and for brevity we will not show them here. Figure 3.8 demonstrates the anti-symmetric wave solutions for a transversely isotropic material with nearly traction-free faces and $\theta = 45°$, and it can be seen that the new asymptotic expansions (3.123) and (3.124) give much better approximation to numerical solution (dashed lines) than classical ones.

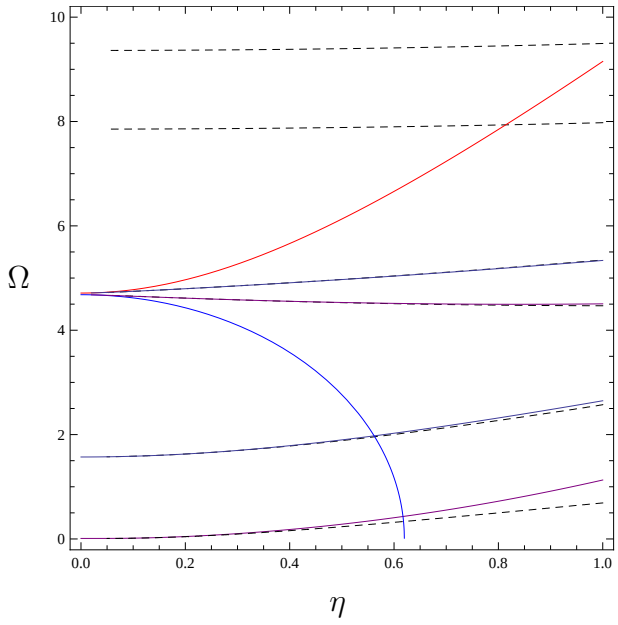

Figure 3.8: Comparison of both classical and new asymptotic solutions with the numerical solutions (dashed lines) for $\delta = 10^{-4}$ and $\theta = 45°$.

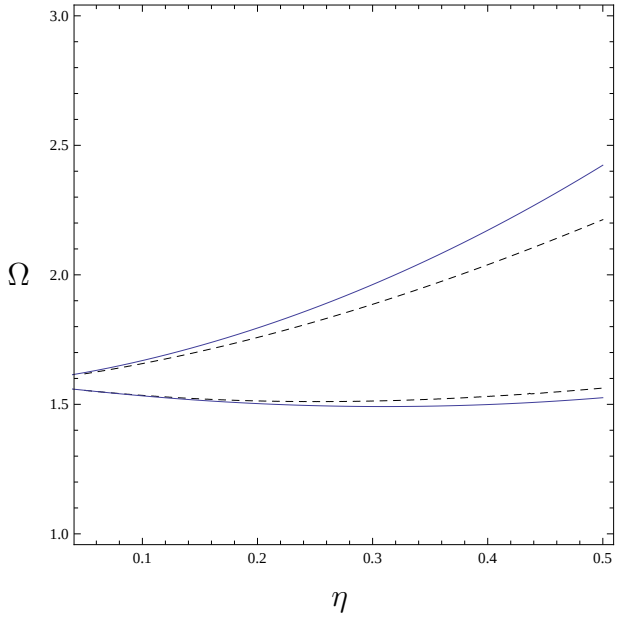

Figure 3.9: Comparison of the asymptotic solutions with the numerical solutions (dashed lines) for $\delta = 4$ and $\theta = 15°$.

Case 2 **transitional case** $(m = 0)$:$\delta \sim 1$

When $\theta = 15^\circ$, $\delta_* = 3.81$, we set $\delta = 4$. A transversely isotropic material in transitional case and $\theta = 15^\circ$ is studied in Figure 3.9 and it can be inferred that the uniform asymptotic expansion for anti-symmetric modes again works well to deal with such material.

3.5.2 Short wave

In the short wave region, the reader is referred to Figure 3.10 for the variation of η_* against θ, and it can be inferred that η_* decreases as θ increases. The reader is also referred to Figure 3.11 for the variation of $\bar{v}_r$ against θ, and it can be deduced that $\bar{v}_r$ decreases slowly as θ increases. For a Glass-Epoxy composite with $\theta = 45^\circ$ in transitional case, the short wave behavior of both anti-symmetric and symmetric fundamental modes is demonstrated in Figure 3.12. The dashed line represents the asymptotic expansion, which shows excellent approximation to numerical solution in the short wave region.

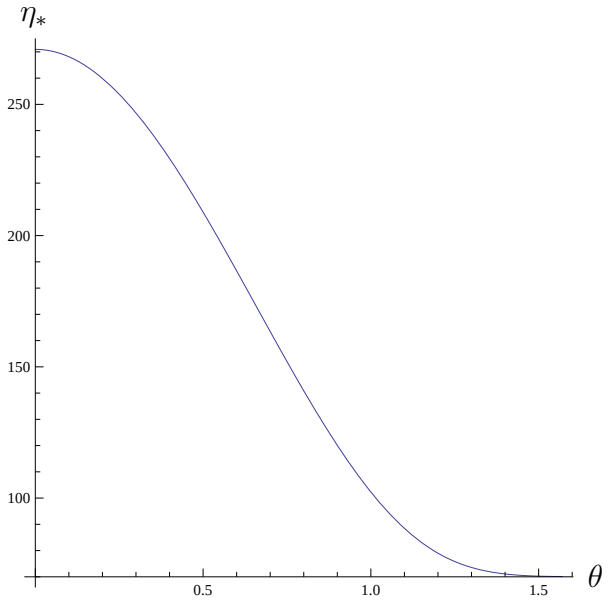

Figure 3.10: η_* against θ when $\delta = 100$.

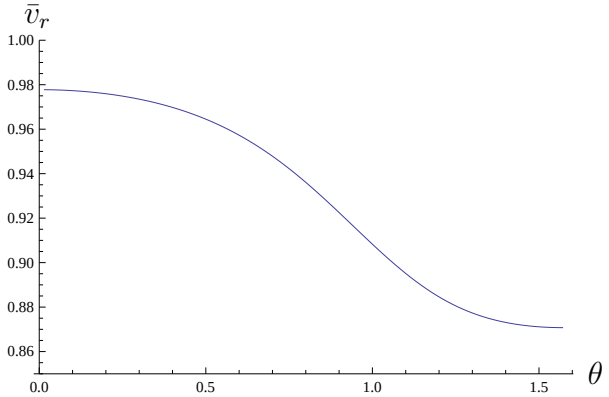

Figure 3.11: $\bar{v}_r$ against θ for a transversely isotropic elastic solids.

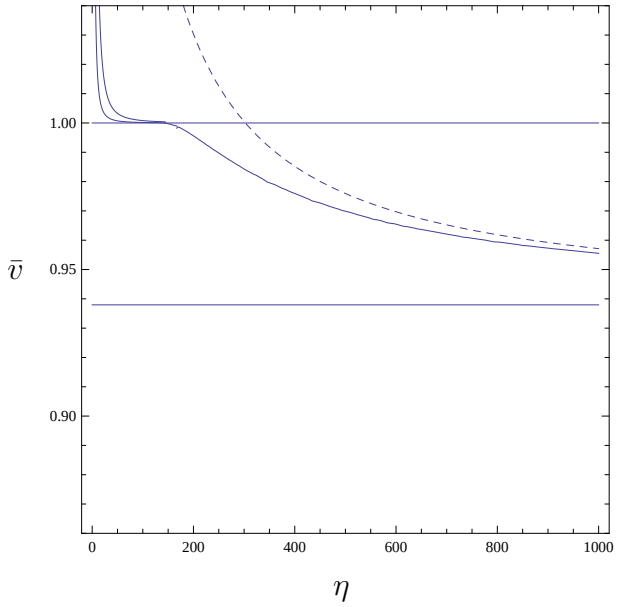

Figure 3.12: Anti-symmetric and symmetric fundamental modes shown together with surface and shear wave speeds, as well as asymptotic expansion (dashed line) for $\delta = 100$ and $\theta = 45°$.

Chapter 4

Waves propagating in a pre-stressed incompressible plate with ERBC

In this chapter, we focus on wave propagation in a pre-stressed incompressible plate with elastically restrained boundary conditions. The Stroh formalism is a very effective tool to deal with a pre-stressed material, with the effect of pre-stress incorporated in the Stroh matrix. By substituting the equations of motion with pre-stressed elements into the elastically restrained boundary conditions discussed in Chapter 3, the dispersion relations are derived. Similarly to Chapter 3, asymptotic expansions of wave frequency or speed are established for a neo-Hookean material to predict its behavior in both the long wave and short wave regions. Numerical analysis shows that our asymptotic schemes are very successful in providing accurate approximations of wave speed or frequency over a wider range of wave number than might be expected.

4.1 Derivation of dispersion relation

We again use the Stroh formalism to solve the problem of wave propagation in incompressible pre-stressed plates with ERBC. The basic equations for wave propagation in a pre-stressed incompressible elastic plate can be found in Rogerson and Fu (1995) or Rogerson (1997). However, within our analysis, use is made of a different method–the Stroh formalism. Stroh formalism has been used for pre-stressed media before, see Chadwick (1997). Similar to the previous chapter, let the incremental traction on the upper surface be given by

$$\boldsymbol{t} = -\mathrm{i}k\boldsymbol{l}(kx_2)\mathrm{e}^{\mathrm{i}k(x_1-\upsilon t)}, \tag{4.1}$$

and according to (1.36), its components can be simplified into the linearized form

$$t_i = \mathcal{A}_{2ilk}u_{k,l} + \bar{p}u_{2,i} - p^*\delta_{2i}, \ \text{ on } x_2 = \pm h. \tag{4.2}$$

The incremental displacement $\boldsymbol{u}(x_1, x_2)$ is assumed to have the general form

$$\boldsymbol{u}(x_1, x_2) = \boldsymbol{z}(kx_2)\mathrm{e}^{\mathrm{i}k(x_1-\upsilon t)}. \tag{4.3}$$

The incremental pressure $p^*(x_1, x_2)$ is assumed to have the form

$$p^*(x_1, x_2) = kP(kx_2)\mathrm{e}^{\mathrm{i}k(x_1 - \upsilon t)}. \tag{4.4}$$

Let $\boldsymbol{m} = (1, 0)$, $\boldsymbol{n} = (0, 1)$, and

$$T_{ik} = \mathcal{A}_{2i2k} + \bar{p}(\boldsymbol{n} \otimes \boldsymbol{n}),\ R_{ik} = \mathcal{A}_{1i2k} + \bar{p}(\boldsymbol{n} \otimes \boldsymbol{m}),\ Q_{ik} = \mathcal{A}_{1i1k} + \bar{p}(\boldsymbol{m} \otimes \boldsymbol{m}). \tag{4.5}$$

Because of the pairwise symmetry property of $\mathcal{A}_{jilk}$ in (1.33), we note that $T_{12} = T_{21},\ Q_{12} = Q_{21}$. Making use of (4.5), we can derive from (4.2) and (4.1) that

$$-\mathrm{i}\boldsymbol{l}(kx_2) = \mathcal{A}_{2i2k}\boldsymbol{z}'(kx_2) + \mathrm{i}\mathcal{A}_{2i1k}\boldsymbol{z}(kx_2) + \bar{p}(\mathrm{i}(\boldsymbol{z}(kx_2) \cdot \boldsymbol{n})\boldsymbol{m} + (\boldsymbol{z}'(kx_2) \cdot \boldsymbol{n})\boldsymbol{n}) - P(kx_2)\boldsymbol{n}$$

$$= T\boldsymbol{z}'(kx_2) + \mathrm{i}R^T\boldsymbol{z}(kx_2) - P(kx_2)\boldsymbol{n}, \tag{4.6}$$

which implies that

$$-\mathrm{i}\boldsymbol{l}'(kx_2) = T\boldsymbol{z}''(kx_2) + \mathrm{i}R^T\boldsymbol{z}'(kx_2) - P'(kx_2)\boldsymbol{n}. \tag{4.7}$$

We can now establish from (1.42) that

$$\mathrm{i}z_1(kx_2) + z_2'(kx_2) = 0,\ \mathrm{i}z_1'(kx_2) + z_2''(kx_2) = 0. \tag{4.8}$$

With the help of (4.8), the linearized equations of motion can be written as

$$T\boldsymbol{z}''(kx_2) + \mathrm{i}(R + R^T)\boldsymbol{z}'(kx_2) - (Q - \rho_0 v^2 I)\boldsymbol{z}(kx_2) - \mathrm{i}P(kx_2)\boldsymbol{m} - P'(kx_2)\boldsymbol{n} = \boldsymbol{0}. \quad (4.9)$$

It is now possible to substitute (4.7) into (4.9), to deduce that

$$\boldsymbol{l}'(kx_2) = R\boldsymbol{z}'(kx_2) + \mathrm{i}(Q - \rho_0 v^2 I)\boldsymbol{z}(kx_2) - P(kx_2)\boldsymbol{m}. \quad (4.10)$$

Equation (4.6) may now be employed to establish that

$$\boldsymbol{z}'(kx_2) = -\mathrm{i}T^{-1}R^T\boldsymbol{z}(kx_2) - \mathrm{i}T^{-1}\boldsymbol{l}(kx_2) + P(kx_2)T^{-1}\boldsymbol{n}, \quad (4.11)$$

which on substituting into (4.10), enables us to conclude that

$$\boldsymbol{l}'(kx_2) = -\mathrm{i}(RT^{-1}R^T - Q + \rho_0 v^2 I)\boldsymbol{z}(kx_2) - \mathrm{i}RT^{-1}\boldsymbol{l}(kx_2) + P(kx_2)(RT^{-1}\boldsymbol{n} - \boldsymbol{m}). \quad (4.12)$$

Equation $(4.8)_1$ can be rewritten as

$$\mathrm{i}\boldsymbol{m}\cdot\boldsymbol{z}(kx_2) + \boldsymbol{n}\cdot\boldsymbol{z}'(kx_2) = 0. \quad (4.13)$$

Multiplying both sides of equation (4.11) with the vector $\boldsymbol{n}$ on the left hand side, and making

use of (4.13), we obtain

$$P(kx_2) = \mathrm{i}\tau((-\boldsymbol{m} + \boldsymbol{n}T^{-1}R^T) \cdot \boldsymbol{z}(kx_2) + \boldsymbol{n}T^{-1} \cdot \boldsymbol{l}(kx_2)), \tag{4.14}$$

where $\tau = \frac{1}{\boldsymbol{n} \cdot T^{-1}\boldsymbol{n}}$. On substituting (4.14) into (4.11) and (4.12), and using the definition of the tensor product, we obtain

$$\boldsymbol{z}'(kx_2) = \mathrm{i}(-T^{-1}R^T + \tau(T^{-1}\boldsymbol{n}) \otimes (-\boldsymbol{m} + \boldsymbol{n}T^{-1}R^T))\boldsymbol{z}(kx_2)$$

$$+\mathrm{i}(-T^{-1} + \tau(T^{-1}\boldsymbol{n}) \otimes (\boldsymbol{n}T^{-1}))\boldsymbol{l}(kx_2), \tag{4.15}$$

and

$$\boldsymbol{l}'(kx_2) = \mathrm{i}(-RT^{-1}R^T + Q - \rho_0 v^2 I + \tau(RT^{-1}\boldsymbol{n} - \boldsymbol{m}) \otimes (-\boldsymbol{m} + \boldsymbol{n}T^{-1}R^T))\boldsymbol{z}(kx_2)$$

$$+\mathrm{i}(-RT^{-1} + \tau(RT^{-1}\boldsymbol{n} - \boldsymbol{m}) \otimes (\boldsymbol{n}T^{-1}))\boldsymbol{l}(kx_2). \tag{4.16}$$

The two equations (4.15) and (4.16) may now be incorporated into the form

$$\mathrm{i}N \begin{pmatrix} \boldsymbol{z}(kx_2) \\ \\ \boldsymbol{l}(kx_2) \end{pmatrix} = \begin{pmatrix} \boldsymbol{z}'(kx_2) \\ \\ \boldsymbol{l}'(kx_2) \end{pmatrix}, N = \begin{pmatrix} N_1 & N_2 \\ \\ N_3 - \rho_0 v^2 I & N_1^T \end{pmatrix}, \tag{4.17}$$

where

$$N_1 = -T^{-1}R^T + \tau(T^{-1}\boldsymbol{n}) \otimes (-\boldsymbol{m} + \boldsymbol{n}T^{-1}R^T), \tag{4.18}$$

$$N_2 = -T^{-1} + \tau(T^{-1}\boldsymbol{n}) \otimes (\boldsymbol{n}T^{-1}) = N_2^T, \tag{4.19}$$

$$N_3 = -RT^{-1}R^T + Q + \tau(RT^{-1}\boldsymbol{n} - \boldsymbol{m}) \otimes (-\boldsymbol{m} + \boldsymbol{n}T^{-1}R^T). \tag{4.20}$$

Making use of Mathematica, we obtain

$$N_1 = \begin{pmatrix} \frac{T_{12}-R_{11}}{T_{11}} & -\frac{R_{21}}{T_{11}} \\ -1 & 0 \end{pmatrix}, N_2 = \begin{pmatrix} -\frac{1}{T_{11}} & 0 \\ 0 & 0 \end{pmatrix},$$

$$N_3 = \begin{pmatrix} -\frac{(T_{12}-R_{11})^2}{T_{11}} - Q_{11} + 2R_{12} - T_{22} & \frac{(T_{12}-R_{11})R_{21}}{T_{11}} + Q_{12} - R_{22} \\ \frac{(T_{12}-R_{11})R_{21}}{T_{11}} + Q_{12} - R_{22} & Q_{22} - \frac{R_{21}^2}{T_{11}} \end{pmatrix}. \tag{4.21}$$

With (1.55), the matrices T, R, Q given by (4.5), are represented in the form

$$T = \begin{pmatrix} \bar{\lambda}^{-2} & 0 \\ 0 & 2\bar{\lambda}^{-2} - \bar{\sigma}_2 \end{pmatrix}, R = \begin{pmatrix} 0 & 0 \\ \bar{\lambda}^{-2} - \bar{\sigma}_2 & 0 \end{pmatrix}, Q = \begin{pmatrix} \bar{\lambda}^2 + \bar{\lambda}^{-2} - \bar{\sigma}_2 & 0 \\ 0 & \bar{\lambda}^2 \end{pmatrix}, \tag{4.22}$$

with N_1, N_2 and N_3 now becoming

$$N_1 = \begin{pmatrix} 0 & -\bar{\lambda}^2(\bar{\lambda}^{-2} - \bar{\sigma}_2) \\ -1 & 0 \end{pmatrix}, N_2 = \begin{pmatrix} -\bar{\lambda}^2 & 0 \\ 0 & 0 \end{pmatrix},$$

$$N_3 = \begin{pmatrix} \bar{\lambda}^2 + \frac{3}{\bar{\lambda}^2} - 2\bar{\sigma}_2 & 0 \\ 0 & \bar{\lambda}^2 - \bar{\lambda}^2(\bar{\lambda}^{-2} - \bar{\sigma}_2)^2 \end{pmatrix}. \tag{4.23}$$

If we now let $\bar{v}^2 = \rho_0 v^2$, Mathematica may again be used to obtain the eigenvalue q_i and the corresponding eigenvector $\boldsymbol{a}^{(i)}$ and $\boldsymbol{b}^{(i)}$ of Stroh matrix N, thus

$$q_1 = \mathrm{i},\ q_2 = \bar{\lambda}\sqrt{\bar{v}^2 - \bar{\lambda}^2},\ q_3 = -q_1,\ q_4 = -q_2, \tag{4.24}$$

$$\boldsymbol{a}^{(1)} = -\frac{\bar{\lambda}^2}{U_1}\begin{pmatrix} 1 \\ q_1 \end{pmatrix}, \qquad \boldsymbol{b}^{(1)} = \begin{pmatrix} \frac{q_1 U_2}{U_1} \\ 1 \end{pmatrix},$$

$$\boldsymbol{a}^{(2)} = \frac{\bar{\lambda}^2}{U_2}\begin{pmatrix} 1 \\ -\frac{1}{q_2} \end{pmatrix}, \qquad \boldsymbol{b}^{(2)} = \begin{pmatrix} -\frac{U_1}{q_2 U_2} \\ 1 \end{pmatrix},$$

$$\boldsymbol{a}^{(3)} = -\frac{\bar{\lambda}^2}{U_1}\begin{pmatrix} 1 \\ -q_1 \end{pmatrix}, \qquad \boldsymbol{b}^{(3)} = \begin{pmatrix} -\frac{q_1 U_2}{U_1} \\ 1 \end{pmatrix},$$

$$\boldsymbol{a}^{(4)} = \frac{\bar{\lambda}^2}{U_2}\begin{pmatrix} 1 \\ \frac{1}{q_2} \end{pmatrix}, \qquad \boldsymbol{b}^{(4)} = \begin{pmatrix} \frac{U_1}{q_2 U_2} \\ 1 \end{pmatrix}, \tag{4.25}$$

where

$$U_1 = \bar{\lambda}^2(\bar{v}^2 - \bar{\lambda}^2) - 1 + \bar{\lambda}^2\bar{\sigma}_2, \qquad U_2 = 2 - \bar{\lambda}^2\bar{\sigma}_2. \tag{4.26}$$

It should be noted that (4.24)$_2$ describes the value of q_2 when $\bar{v} > \bar{\lambda}$. When $\bar{v} < \bar{\lambda}$,

$$q_2 = \mathrm{i}\bar{\lambda}\sqrt{\bar{\lambda}^2 - \bar{v}^2}, \qquad \hat{q}_2 = \mathrm{i}q_2 = -\bar{\lambda}\sqrt{\bar{\lambda}^2 - \bar{v}^2}. \tag{4.27}$$

In a similar manner to that employed in the previous chapter, after substituting three equations (3.26)-(3.28), together with (4.25), into the elastically restrained boundary condition (3.16), we finally arrive at the dispersion relation. The dispersion relation for anti-symmetric motion is

$$\begin{aligned}&(-\alpha_1\alpha_2\frac{U_1}{q_2U_2} + \frac{\delta_1\delta_2\bar{\lambda}^4}{\eta^2U_1U_2q_2})\tanh(\eta\hat{q}_1) + q_1(\frac{\delta_1\delta_2\bar{\lambda}^4}{\eta^2U_1U_2} - \alpha_1\alpha_2\frac{U_2}{U_1})\tanh(\eta\hat{q}_2)\\ &-\mathrm{i}\frac{\alpha_2\delta_1\bar{\lambda}^2}{\eta}(\frac{1}{U_1}+\frac{1}{U_2})\tanh(\eta\hat{q}_1)\tanh(\eta\hat{q}_2) - \mathrm{i}\frac{\alpha_1\delta_2q_1\bar{\lambda}^2}{\eta q_2}(\frac{1}{U_1}+\frac{1}{U_2}) = 0,\end{aligned} \tag{4.28}$$

with $\tilde{d}_1 + \tilde{d}_3 = \tilde{d}_2 + \tilde{d}_4 = 0$ (an analogue of our result at the end of Section 3.1) and

$$\boldsymbol{z}(kx_2) = \tilde{d}_1\frac{-\bar{\lambda}^2}{U_1}\begin{pmatrix}\sinh(k\hat{q}_1x_2)\\ q_1\cosh(k\hat{q}_1x_2)\end{pmatrix} + \tilde{d}_2\frac{\bar{\lambda}^2}{U_2}\begin{pmatrix}\sinh(k\hat{q}_2x_2)\\ -\frac{1}{q_2}\cosh(k\hat{q}_2x_2)\end{pmatrix}; \tag{4.29}$$

while the dispersion relation in symmetric mode is

$$\begin{aligned}&(-\alpha_1\alpha_2\frac{U_1}{q_2U_2} + \frac{\delta_1\delta_2\bar{\lambda}^4}{\eta^2U_1U_2q_2})\coth(\eta\hat{q}_1) + q_1(\frac{\delta_1\delta_2\bar{\lambda}^4}{\eta^2U_1U_2} - \alpha_1\alpha_2\frac{U_2}{U_1})\coth(\eta\hat{q}_2)\\ &-\mathrm{i}\frac{\alpha_2\delta_1\bar{\lambda}^2}{\eta}(\frac{1}{U_1}+\frac{1}{U_2})\coth(\eta\hat{q}_1)\coth(\eta\hat{q}_2) - \mathrm{i}\frac{\alpha_1\delta_2q_1\bar{\lambda}^2}{\eta q_2}(\frac{1}{U_1}+\frac{1}{U_2}) = 0,\end{aligned} \tag{4.30}$$

with $\tilde{d}_1 - \tilde{d}_3 = \tilde{d}_2 - \tilde{d}_4 = 0$ (an analogue of our result at the end of Section 3.1) and

$$\boldsymbol{z}(kx_2) = \tilde{d}_1 \frac{-\bar{\lambda}^2}{U_1} \begin{pmatrix} \cosh(k\hat{q}_1 x_2) \\ q_1 \sinh(k\hat{q}_1 x_2) \end{pmatrix} + \tilde{d}_2 \frac{\bar{\lambda}^2}{U_2} \begin{pmatrix} \cosh(k\hat{q}_2 x_2) \\ -\frac{1}{q_2} \sinh(k\hat{q}_2 x_2) \end{pmatrix}. \tag{4.31}$$

We still focus on the special case when $\alpha_1 = \alpha_2 = 1,\ \delta_1 = 0,\ \delta_2 = \delta$. For anti-symmetric waves, when $\bar{v} < \bar{\lambda}$, the dispersion relation becomes

$$-U_1^2 \tanh(\eta) + \mathrm{i}q_2 U_2^2 \tanh(\eta\hat{q}_2) - \frac{\delta}{\eta}\bar{\lambda}^2(U_1 + U_2) = 0; \tag{4.32}$$

when $\bar{v} > \bar{\lambda}$, the dispersion relation becomes

$$U_1^2 \tanh(\eta) + q_2 U_2^2 \tan(\eta q_2) + \frac{\delta}{\eta}\bar{\lambda}^2(U_1 + U_2) = 0. \tag{4.33}$$

For symmetric waves, when $\bar{v} < \bar{\lambda}$, the dispersion relation becomes

$$-U_1^2 \coth(\eta) + \mathrm{i}q_2 U_2^2 \coth(\eta\hat{q}_2) - \frac{\delta}{\eta}\bar{\lambda}^2(U_1 + U_2) = 0; \tag{4.34}$$

when $\bar{v} > \bar{\lambda}$, the dispersion relation becomes

$$U_1^2 \coth(\eta) + q_2 U_2^2 \cot(\eta q_2) + \frac{\delta}{\eta}\bar{\lambda}^2(U_1 + U_2) = 0. \tag{4.35}$$

To derive an asymptotic expansion, we firstly correlate the magnitudes of η and δ:

$$\delta = \delta_0 \eta^{2m},\ \delta_0 = \mathcal{O}(1). \tag{4.36}$$

4.2 Long-wave analysis

Let us fix the frequency $\Omega = \bar{v}\eta$. The cut-off frequency for anti-symmetric motion is given by $\frac{\Lambda_1^a}{\lambda}$, with the cut-off frequency for symmetric motion $\frac{\Lambda_1^s}{\lambda}$. Let $\bar{\lambda} = 0.8$ and $\bar{\sigma}_2 = 1$ in the subsequent numerical analysis. Numerically we find that $\delta \sim \eta^2$ and $\delta \sim 1$ have almost the same effect on the asymptotic long wave behavior, so we only focus on the former case. Also, according to our numerical results, the fundamental modes are more sensitive to variation in $\bar{\sigma}_2$ than are harmonics. Firstly, the fundamental modes for both anti-symmetric and symmetric waves only exist when $\bar{\sigma}_2 \in [-\infty, 2.6]$; secondly, when $\bar{\sigma}_2 \in [-\infty, 0.6]$, the fundamental mode for anti-symmetric wave starts to exist from a certain positive value η_0 instead of 0, and η_0 becomes larger as $\bar{\sigma}_2$ decreases; thirdly, the intersection point of the fundamental mode for symmetric waves and the $\bar{v}$ axis moves upward as $\bar{\sigma}_2$ decreases.

4.2.1 Anti-symmetric waves

Case 1 **nearly traction-free faces** $(m = 1)$:$\delta \sim \eta^2$

There are two asymptotic regimes to balance the dispersion relation in this case. The first

one is defined by

$$\tanh(\eta) \sim \eta,\ \tanh(\eta\hat{q}_2) \sim -\eta,\ \bar{v} \sim 1, \tag{4.37}$$

and associated with low-frequency fundamental mode. Using both the value of q_2 and dispersion relation when $\bar{v} < \bar{\lambda}$, the asymptotic approximation for the phase speed is given by

$$\bar{v}^2 = \bar{\lambda}^2 - \delta_0 - \frac{(\bar{\lambda}^2\bar{\sigma}_2 - 1)^2}{\bar{\lambda}^2} + \frac{(\bar{\lambda}^2\bar{\sigma}_2 - 1)((\bar{\lambda}^2\bar{\sigma}_2 - 1)(\bar{\lambda}^2\bar{\sigma}_2 - 2)^2 + \delta_0\bar{\lambda}^2(\bar{\lambda}^2\bar{\sigma}_2 - 3))}{3\bar{\lambda}^2}\eta^2,$$

while a spurious root $\bar{v}^2 = \bar{\lambda}^2 - \frac{1}{\bar{\lambda}^2}$ has been ignored. This asymptotic expansion shows excellent agreement with the numerical solution only for $\bar{\sigma}_2 \in [0.6, 2.6]$.

The second asymptotic regime is related to the harmonics under the condition that $\bar{v} > \bar{\lambda}$, and following traditional method, is defined by

$$\tanh(\eta) \sim \eta,\ \tan(\eta q_2) \sim \bar{v}^2,\ \bar{v} \sim \frac{1}{\eta}. \tag{4.38}$$

The asymptotic approximation for the phase speed is given by

$$\Omega = \frac{\Lambda_1^a}{\bar{\lambda}} + \frac{\bar{\lambda}^3}{2\Lambda_1^a}\eta^2 + \frac{(\bar{\lambda}^2\bar{\sigma}_2 - 2)^2}{(\Lambda_1^a)^3\bar{\lambda}}\eta^2. \tag{4.39}$$

If we try a similar method used for the corresponding part in transversely isotropic material

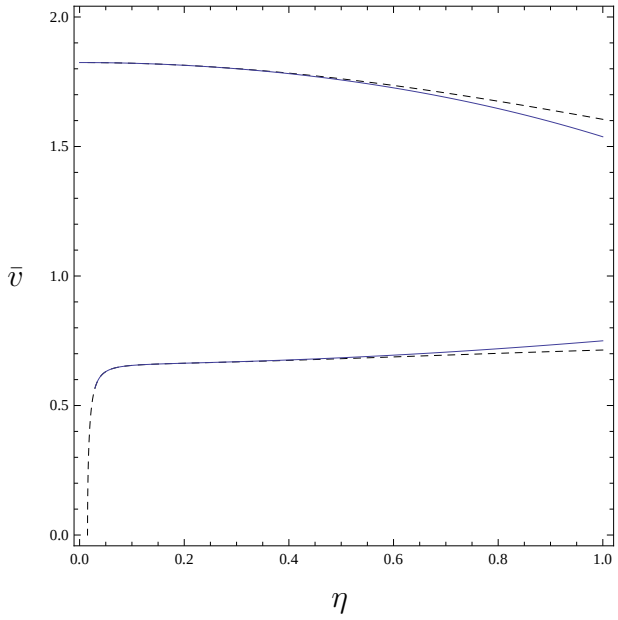

Figure 4.1: Comparison of asymptotic solutions with the numerical solutions (dashed lines) for fundamental modes of anti-symmetric (lower lines) and symmetric (upper lines) waves when $\delta = 10^{-4}$, $\bar{\lambda} = 0.8$ and $\bar{\sigma}_2 = 1$.

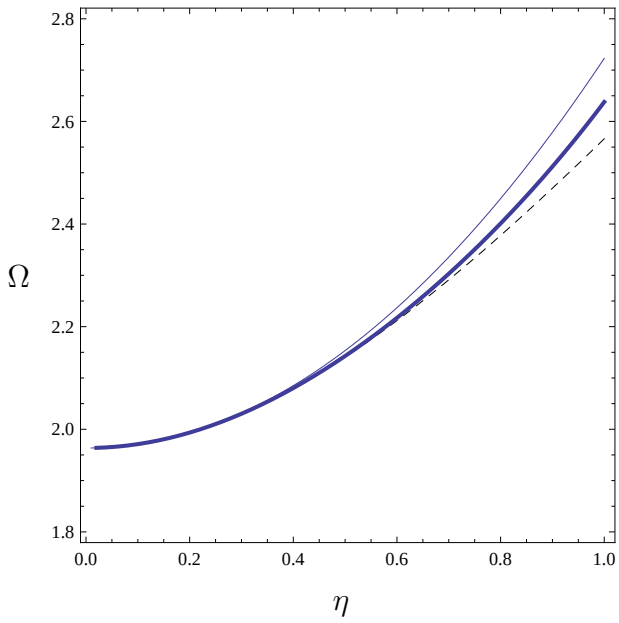

Figure 4.2: Comparison of both traditional and new (thick line) asymptotic solutions with the numerical solutions (dashed line) for first harmonic when $\delta = 10^{-4}$, $\bar{\lambda} = 0.8$ and $\bar{\sigma}_2 = 1$.

analysis, we will define

$$q_2 = \frac{\Lambda_1^a + \epsilon}{\eta}, \qquad \tan(\eta q_2) = -\cot(\epsilon), \qquad \Omega = \frac{\Lambda_1^a + \epsilon}{\bar{\lambda}} + \frac{\bar{\lambda}^3 \eta^2}{2(\Lambda_1^a + \epsilon)}. \tag{4.40}$$

After solving a quadratic equation and choosing the correct ϵ, we get a better approach to numerical solution than traditional asymptotic result, see Figure 4.2.

Case 2 **nearly fixed faces** ($m = -1$):$\delta \sim \eta^{-2}$

The asymptotic regime is related to harmonics under the condition that $\bar{v} > \bar{\lambda}$, and is defined by

$$\tanh(\eta) \sim \eta, \ \tan(\eta q_2) \sim \bar{v}^4, \ \bar{v} \sim \frac{1}{\eta}. \tag{4.41}$$

The asymptotic approximation for the phase speed in this case is given by

$$\Omega = \frac{\Lambda_1^a}{\bar{\lambda}} + \frac{\bar{\lambda}^3}{2\Lambda_1^a}\eta^2. \tag{4.42}$$

4.2.2 Symmetric waves

Case 1 **nearly traction-free faces** ($m = 1$):$\delta \sim \eta^2$

In this case there are two asymptotic regimes to balance the dispersion relation. The first is associated with low-frequency fundamental mode with $\bar{v} < \bar{\lambda}$. The appropriate leading order

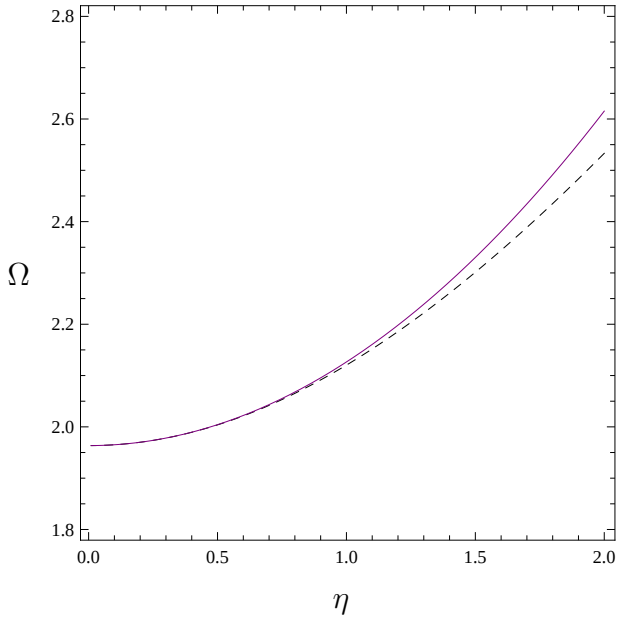

Figure 4.3: Comparison of asymptotic solution with the numerical solutions (dashed line) for first harmonic when $\delta = 10^4$, $\bar{\lambda} = 0.8$ and $\bar{\sigma}_2 = 1$.

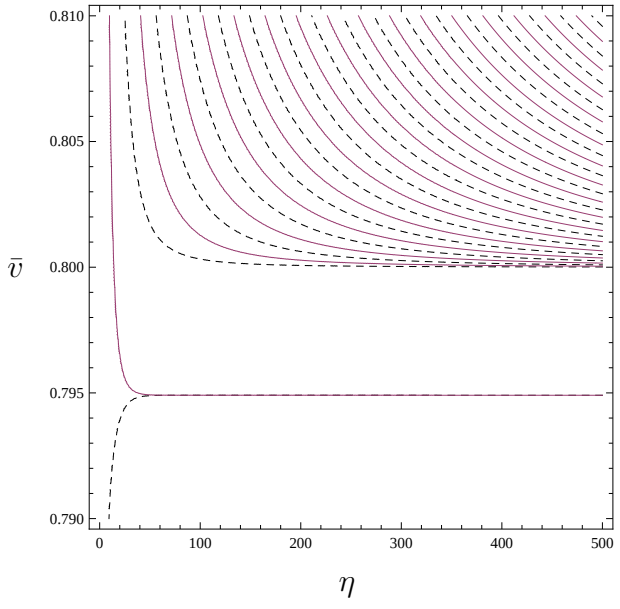

Figure 4.4: Anti-symmetric (dashed lines) and symmetric (solid lines) solutions for $\delta = 10^{-4}$, $\bar{\lambda} = 0.8$ and $\bar{\sigma}_2 = 1$.

asymptotic approximation for the phase speed is given by

$$\bar{v}^2 = \bar{\lambda}^2 + \frac{3}{\bar{\lambda}^2} - 2\bar{\sigma}_2 - \delta - \frac{(\bar{\lambda}^2\bar{\sigma}_2 - 2)^2}{3\bar{\lambda}^2}\eta^2,$$

while the spurious root $\bar{v}^2 = \bar{\lambda}^2 - \frac{1}{\bar{\lambda}^2}$ has again been ignored. With Mathematica, it can be verified that the asymptotic approximation for the phase speed in fundamental mode is the same when $\bar{v} > \bar{\lambda}$. This asymptotic expansion shows excellent prediction for all values of $\bar{\sigma}_2$ that we have tried in the numerical experiment. The second asymptotic regime is related to harmonics under the condition that $\bar{v} > \bar{\lambda}$. The asymptotic approximation for the phase speed is given by

$$\Omega = \frac{\Lambda_1^s}{\bar{\lambda}} + \frac{\bar{\lambda}^3}{2\Lambda_1^s}\eta^2. \tag{4.43}$$

4.3 Short-wave analysis

From Figure 4.4, as η is increasing, all harmonics of both anti-symmetric and symmetric waves approach $\bar{\lambda}$, while the fundamental modes meet at η_* from both sides and stabilize themselves at $\bar{v} = \bar{v}_r$, which is quite different from the short wave behavior in the previous chapter.

4.3.1 Fundamental modes

It is simple to show that

$$\lim_{\eta\to\infty}\tanh(\eta)=\lim_{\eta\to\infty}\coth(\eta)=1,\qquad \lim_{\eta\to\infty}\tanh(\eta\hat{q}_2)=\lim_{\eta\to\infty}\coth(\eta\hat{q}_2)=-1, \tag{4.44}$$

so both anti-symmetric and symmetric dispersion relations tend to the same limit at $\bar{v}=\bar{v}_r$, thus from (4.32)-(4.35) we deduce that in the limit $\eta\to\infty$

$$U_1^2+\mathrm{i}q_2U_2^2=0, \tag{4.45}$$

which by solving we obtain $\bar{v}_r$.

When $\bar{\lambda}=0.8$, $\tanh(-\eta\hat{q}_2)<\tanh(\eta)$, as η increases, $\tanh(\eta)$ firstly approaches the limit 1; as η is even larger at η_*, $\tanh(-\eta\hat{q}_2)$ also approaches the limit 1, then (4.45) is satisfied. Numerically we find that δ has little influence on η_* and $\eta_*\sim\frac{3}{\bar{\lambda}\sqrt{\bar{\lambda}^2-\bar{v}_r^2}}$. When $\bar{\sigma}_2$ is around 1.56, $\bar{v}_r=\bar{\lambda}$ (see Figure 4.5) and $q_2=0$, fundamental modes approach $\bar{v}=\bar{\lambda}$ as harmonics do, which means they meet at $\eta_*=\infty$, as shown in Figure 4.6. It is remarked that the plateau in Figure 4.5 is not flat and $\bar{\sigma}_2\approx 1.56$ is its peak point, which is the reason why the blow up behaviour only occurs at $\bar{\sigma}_2\approx 1.56$ in Figure 4.6.

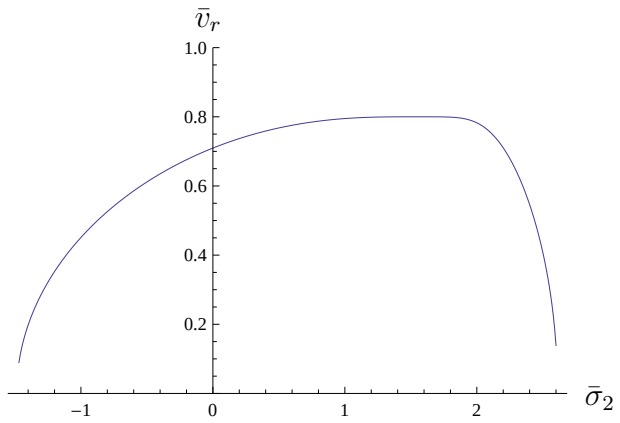

Figure 4.5: $\bar{v}_r$ against $\bar{\sigma}_2$ when $\bar{\lambda} = 0.8$.

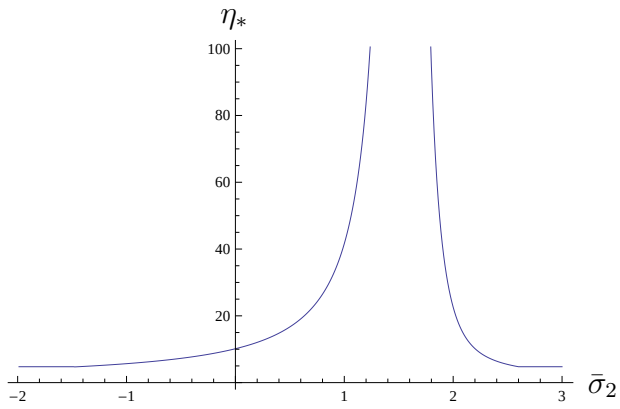

Figure 4.6: η_* against $\bar{\sigma}_2$ when $\bar{\lambda} = 0.8$.

4.3.2 Harmonics

From the numerical results, it would seem that as $\eta \to \infty$ for all modes of both anti-symmetric and symmetric motion $\bar{v} \to \bar{\lambda}$. Thus, q_2 is infinitesimal and could be regarded as $q_2 \sim \mathcal{O}(\eta^{-1})$. We find that provided δ is not too large, the influence of elastically restrained boundaries is small for short waves, which means $\delta \sim \eta^{-2}$ and $\delta \sim 1$ share the same asymptotic expansion of phase speed with free faces (Rogerson and Fu 1995).

Anti-symmetric waves

To balance the dispersion relation, we set $\tan(\eta q_2) \sim \eta$, and it is assumed that

$$\eta q_2 = \Lambda_1^a + \phi\varepsilon, \qquad \tan(\eta q_2) = -\frac{1}{\phi\varepsilon}. \tag{4.46}$$

After substituting these into the dispersion relation, we obtain

$$\phi = \frac{\Lambda_1^a(\bar{\lambda}^2\bar{\sigma}_2 - 2)^2}{(\bar{\lambda}^2\bar{\sigma}_2 - 1)^2}, \tag{4.47}$$

and the asymptotic expansion of phase speed

$$\bar{v}^2 = \bar{\lambda}^2 + \frac{(\Lambda_1^a)^2}{\bar{\lambda}^2}\varepsilon^2 + \frac{2(\Lambda_1^a)^2(\bar{\lambda}^2\bar{\sigma}_2 - 2)^2}{\bar{\lambda}^2(\bar{\lambda}^2\bar{\sigma}_2 - 1)^2}\varepsilon^3. \tag{4.48}$$

Symmetric waves

Following the same procedure, we obtain the asymptotic expansion of phase speed

$$\bar{v}^2 = \bar{\lambda}^2 + \frac{(\Lambda_1^s)^2}{\bar{\lambda}^2}\varepsilon^2 - \frac{2(\Lambda_1^s)^2(\bar{\lambda}^2\bar{\sigma}_2 - 2)^2}{\bar{\lambda}^2(\bar{\lambda}^2\bar{\sigma}_2 - 1)^2}\varepsilon^3. \tag{4.49}$$

Both the anti-symmetric and symmetric approximations (4.48) and (4.49) are shown to provide excellent short wave agreement with the numerical solution in Figure 4.7.

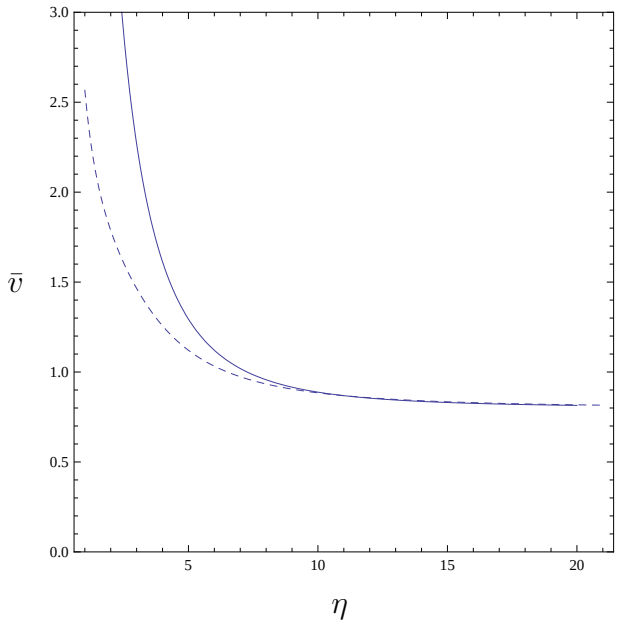

(a)

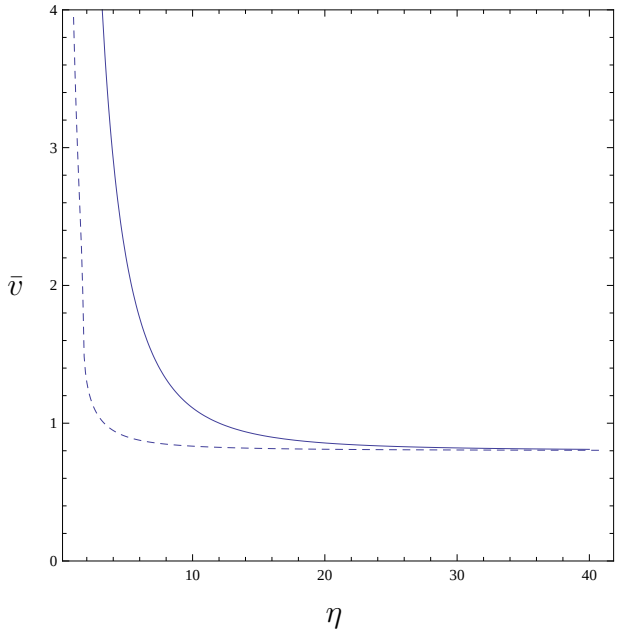

(b)

Figure 4.7: Comparison of the asymptotic solutions with the numerical solutions (dashed lines) for first harmonic of anti-symmetric (a) and symmetric (b) waves when $\delta = 10^{-4}$, $\bar{\lambda} = 0.8$ and $\bar{\sigma}_2 = 1$.

References

Achenbach, J. D. (1969) An asymptotic method to analyze the vibration of an elastic layer. *ASME J. Appl. Mech.* **36**, 65-72.

Adams, S. D. M., Craster, R. V. and Williams, D. P. (2007) Rayleigh waves guided by topography. *Proc. R. Soc.* A **463**, 531-550.

Barnett, D. M. and Lothe, J. (1973) Synthesis of the sextic and the integral formalism for dislocations, Greens function and surface waves in anisotropic elastic solids. *Phys. Norv.* **7**, 13-19.

Barnett, D. M. and Lothe, J. (1974) Consideration of the existence of surface wave (Rayleigh wave) solutions in anisotropic elastic crystals. *J. Phys.* F **4**, 671-686.

Barnett, D. M. and Lothe, J. (1985) Free surface (Rayleigh) waves in anisotropic elastic half-

spaces: the surface impedance method. *Proc. R. Soc.* A **402**, 135-152.

Biot, M. A. (1965) *Mechanics of incremental deformations: theory of elasticity and viscoelasticity of initially stressed solids and fluids, including thermodynamic foundations and applications to finite strain.* New York, London, Sydney, John Wiley and Sons Inc.

Bonnet-Ben Dhia, A. S., Duterte, J. and Joly, P. (1999) Mathematical analysis of elastic surface waves in topographic waveguides. *Math. Models Appl. Sci.* **9**, 755-798.

Burridge, R. and Sabina, F. J. (1972a) The propagation of elastic surface waves guided by ridges. *Proc. R. Soc.* A **330**, 417-441.

Burridge, R. and Sabina, F. J. (1972b) Theoretical computations on ridge acoustic surface waves using the finite element method. *Elect. Lett.* **7**, 720-722.

Chadwick, P. (1997) The application of the Stroh formalism to prestressed elastic media. *Math. Mech. Solids.* **2**, 379403.

Chadwick, P. (1999) *Continuum mechanics: concise theory and problems*. Dover books.

Chadwick, P. and Smith, G. D. (1977) Foundations of the theory of surface waves in anisotropic elastic materials. *Adv. Appl. Mech.* **17**, 303-376.

Connor, P. and Ogden, R. W. (1995) The effect of shear on the propagation of elastic surface waves. *Int. J. Engng Sci.* **33**, 973-982.

Connor, P. and Ogden, R. W. (1996) The influence of shear strain and hydrostatic stress on stability and elastic waves in a layer. *Int. J. Engng Sci.* **34 (1996)**, 375-397.

Crawford, R. J. (1985) *Plastics and rubbers: engineering design and applications.* London: Mechanical Engineering Publications Ltd.

Drazin, P. G. and Johnson, R. S. (1989) *Solitons: an introduction*. Cambridge University Press.

Duterte, J. and Joly, P. (1999) A numerical method for surface waves in a cylindrically perturbed elastic half-space part I:construction and analysis. *SIAM J. Appl. Math.* **59**, 1599-1635.

Edmondson, R. T. and Fu, Y. B. (2009) Stroh formulation for a generally constrained and prestressed elastic material. *Int. J. Non-linear Mech.*, **44**(5), 530-537.

Farnell, G. W. (1970) Property of elastic surface waves. In *Physical Acoustics* (ed. W.P. Mason and R.N. Thurston), Academic Press, New York, Vol. VI, pp.109-166.

Fu, Y. B. and Mielke, A. (2002) A new identity for the surface-impedance matrix and its application to the determination of surface-wave speeds. *Proc. R. Soc. Lond.* A **458**, 2523-2543.

Fu, Y. B. and Brookes, D.W. (2006) Edge waves in asymmetrically laminated plates. *J. Mech. Phys. Solids* **54**, 1-21.

Fu, Y. B., Rogerson, G. A. and Wang, W. F. (2012) Surface waves guided by topography in an anisotropic elastic half-space. *Proc. R. Soc.* A **469** no. 2149.

Fu, Y. B. (2007) Hamiltonian interpretation of the Stroh formalism in anisotropic elasticity. *Proc. R. Soc.* A **463**, 3073-3087.

Graff, K. F. (1991) *Wave Motion in Elastic Solids.* New York: Dover Publications, Inc.

Green, A. E. and Adkins, J. E. (1960) *Large elastic deformations*. Oxford, Clarendon Press.

Green, A. E., Rivlin, R. S. and Shield, R. T. (1952) General theory of small elastic deforma-

tions superimposed on finite elastic deformations. *Proc. R. Soc. Lond.* A **211**, 128-154.

Green, A. E. and Zerna, W. (1954) *Theoretical Elasticity*. Oxford, Clarendon Press.

Gridin, D., Craster, R. V. and Adamou, A. T. I. (2005a) Trapped modes in curved elastic plates. *Proc. R. Soc.* A **461**, 1181-1197.

Gridin, D., Craster, R. V. and Adamou, A. T. I. (2005b) Trapped modes in bent elastic rods. *Wave Motion* **42**, 352-366.

Hirst, A. J. (1969) Rubber suspensions in transport. In L. R. Mernagh, ed., *Rubbers handbook*, 79-86. West Wickham: Morgan-Grampian (Publishers) Ltd.

Kaplunov, J. D., (1995) Long-wave vibrations of a thin-walled body with fixed faces, *Quarterly Journal of Mechanics and Applied Mathematics* **48 (3)**, 311-327.

Kaplunov, J. D., Kossovich, L. Y. and Nolde, E. V. (1997) *dynamics of thin walled elastic bodies*. Academic Press.

Kaplunov, J. D., Kossovich, L. Y. and Rogerson, G. A. (2000a) Direct asymptotic integration of

the equations of transversely isotropic elasticity for a plate near cut-off frequencies, *Q. J. Mech. Appl. Math.* **53 (2)**, 323-341.

Kaplunov, J. D., Nolde, E. V., Rogerson, G. A. (2000b) A low-frequency model for dynamic motion in pre-stressed incompressible elastic structures. *Proc. R. Soc. Lond.* A **456(2003)**, 2589-2610.

Kaplunov, J. D., Nolde, E. V., Rogerson, G. A. (2001a) An asymptotically consistent model for long-wave high frequency motion in a pre-stressed elastic plate. *Mech. Math. Solids* **7**, 581-606.

Kaplunov, J. D., Nolde, E. V., Rogerson, G. A. (2001b) Short wave motion in a pre-stressed elastic plate. *IMA J. Appl. Math.* **67**, 383-399.

Kaplunov, J. D. and Nolde, E. V. (2002) Long-wave vibrations of a nearly incompressible isotropic plate with fixed faces. *Q. J. Mech. Appl. Math.* **55)**, 345-356.

Kaplunov, J. D., Rogerson, G. A. and Tovstik, P. E. (2005) Localized vibration in elastic structures with slowly varying thickness. *Q. J. Mech. Appl. Math.* **58**, 645-664.

Karpman, V. I. (1973) Non-linear waves and dispersive media. Nauka (In Russian).

Klaus, M. (1977) On the bound state of Schrödinger operators in one dimension. *Ann. Phys.* **108**, 288-300.

Konenkov, Yu. K. (1960) A Rayleigh-type flexural wave. *Sov. Phys. Acoust.* **6**, 122-123.

Lamb, H. (1917) On Waves in an Elastic Plate. *Proc. R. Soc. Lond.* A **93 (648)**, 114?28.

Lamb, G. L. (1980) *Elements of soliton theory*. John Wiley and Sons, New York.

Lawrie, J. B. and Kaplunov, J. D. (2012) Edge waves and resonance on elastic structures: An overview. *Math. Mech. Solids* **17**, 4-16.

Liang, C., Lippmann, H. and Najar, J. (1993) Effects of artificially induced vibrations on the prevention of coal mine bumps. In R. P. Young, ed., *Proceedings of the 3rd International Symposium on Rockbursts and Seismicity in Mines* 91-94. Balkema.

Lothe, J. and Barnett, D. M. (1976) On the existence of surface wave solutions for anisotropic half-spaces with free surface. *J. Appl. Phys.* **47**, 428-433.

Love, A. E. H. (1944) *A treatise on the mathematical theory of elasticity*, 4th edition (Dover, New York).

Mielke, A. and Fu, Y. B. (2003) Uniqueness of surface-wave speed: a proof that is independent of the Stroh formalism. *Math. Mech. Solids* **9**, 5-16.

Mindlin, R. D. (1960) Waves and vibrations in isotropic, elastic plates. In J. N. Goodier and N. J. Hoff, eds., *Structural Mechanics*, Pergamon Press, Oxford, 199-232.

Moukhomodiarov, R. R., Pichugin, A. V. and Rogerson, G. A. (2010) The transition between Neumann and Dirichlet boundary conditions in isotropic elastic plates. *Math. Mech. Solids* **15 (4)**, 462-490.

Nolde, E. V., Rogerson, G. A. (2002) Long wave asymptotic integration of the governing equations for a pre-stressed incompressible elastic layer with fixed faces. *Wave motion*, **36**, 287-304.

Nolde, E. V., Prikazchikova, L. A. and Rogerson, G. A. (2004) Dispersion of small amplitude waves in a pre-stressed, compressible elastic plate. *J. Elasticity* **75 (1)**, 1-29.

Norris, A. N., Krylov, V. V. and Abrahams, I. D. (2000) Flexural edge waves and comments

on ’A new bending wave solution for the classical plate equation’ (J. Acoust. Soc. Am. 104, 2220-2222). *J. Acoust. Soc. Am.* **107**, 1781-1784.

Ogden, R. W. (1984) *Non-linear elastic deformations*. New York: Ellis Horwood.

Ogden, R. W. and Roxburgh, D. G. (1993) The effect of pre-stress on the vibration and stability of elastic plates. *Int. J. Engng Sci.*, **30**, 1611?639.

Pichugin, A. V. and Rogerson, G. A. (2002) An asymptotic membrane-like theory for long-wave motion in a pre-stressed elastic plate. *Proc. R. Soc. Lond.* A **458**, 1447-1468.

Poncelet, O., Shuvalov, A. L., Kaplunov, J. D. (2006) Approximation of the flexural velocity branch in plates. *Int. J. Solids Struct.* **43**, 6329?346.

Postnova, J. and Craster, R. V. (2007) Trapped modes in topographically varying elastic wave guides. *Wave Motion* **44**, 205-221.

Postnova, J. and Craster, R. V. (2008) Trapped modes in elastic plates, ocean and quantum wave guides. *Wave Motion* **45**, 565-579.

Prendergast, J. (1995) Seismic isolation in bridges. *ASCE Civic Engineering*, **65**, 58-61.

Rayleigh, Lord (1885) On waves propagated along the plane surface of an elastic solid. *Proc. Lond. Math. Soc.* **17**, 4-11.

Rayleigh, Lord (1889) On the free vibrations of an infinite plate of homogeneous isotropic elastic matter. *Proc. Lond. Math. Soc.* **20**, 225-234.

Rikards, R., Chatea, A., Steinchenb, W., Kesslerc, A. and Bledzkic, A. K. (1999) Method for identification of elastic properties of laminates based on experiment design. *Composites* B **30**, 279-289.

Rogerson, G. A. (1997) Some asymptotic expansions of the dispersion relation for an incompressible elastic plate. *Int. J. Solids Struct.* **34**, 2785-2802.

Rogerson, G. A. and Fu, Y. B. (1995) An asymptotic analysis of the dispersion relation of a pre-stressed incompressible elastic plate. *Acta mechanica*, **111(1-2)**, 59-74.

Roxburgh, D. G. and Ogden, R. W. (1994) Stability and vibration of prestressed compressible elastic plates. *Int. J. Engng Sci.* **32 (3)**, 427-454.

Sandiford, K. J. and Rogerson, G. A. (2000) Some dynamic properties of a pre-stressed, nearly incompressible (rubber-like) elastic layer. *Int. J. N-lin. Mech.* **35**, 849-868.

Sheridan, P. M., James, F. O. and Miller, T. S. (1992) Design of components. In A. N. Gent, ed., *Engineering with Rubber*, 209-235. Munich: Hanser.

Shuvalov, A. L. (2000) On the theory of wave propagation in anisotropic plates, *Proc. R. Soc. Lond.* A **456**, 2197-2222.

Shuvalov, A. L. and Poncelet, O. (2008) On the backward Lamb waves near thickness resonances in anisotropic plates. *Int. J. Solids Struct.* **45 (11-12)**, 3430-3448.

Simon, B. (1976) The bound state of weakly coupled Schrödinger operators in one and two dimensions. *Ann. Phys.* **97**, 279-288.

Song, Y. Q. and Fu, Y. B. (2007) A note on perturbation formulae for the surface-wave speed due to perturbations in material properties. *J. Elasticity*, **88(3)**, 187-192.

Spencer, A. J. M. (1984) Constitutive theory for strongly anisotropic solids,in: Continuum The-

ory of the Mechanics of Fiber-Reinforced Composites (Ed. A.J.M. Spencer). *CISM Courses and Lectures*, No.**282**, pp.1-32. Springer, Wien.

Stroh, A. N. (1958) Dislocations and cracks in anisotropic elasticity. *Phil. Mag.* **3**, 625-646.

Stroh, A. N. (1962) Steady state problems in anisotropic elasticity. *J. Math. Phys.* **41**, 77-103.

Synge, J. L. (1956) Flux of energy for elastic waves in anisotropic media. *Roy. Irish Acad. A: Mathematical and Physical Sciences* **58**, 13-21.

Ting, T. C. T. (1996) *Anisotropic elasticity: theory and applications*. Oxford University Press, Oxford.

Torr, R. P. (1969) Bridge bearings. In L. R. Mernagh, ed., *Rubbers handbook*, 99-103. West Wickham: Morgan-Grampian (Publishers) Ltd.

Tyler, R. G. (1991) Rubber bearings in base-isolated structures–a summary paper. *Bulletin of the New Zealand National Society for Earthquake Engineering*, **24**, 251-274.

Werby, M. F. and Uberall, H. (2002) The analysis and interpretation of special properties of higher order symmetric Lamb waves: The case for plates. *J. Acoust. Soc. Am.* **111 (6)**, 2686-2691.

Zernov, V., Pichugin, A. V., and Kaplunov, J. (2006) Eigenvalue of a semi-infinite elastic strip. *Proc. R. Soc.* A **462**, 1255-1270.